UNIVERSITY of MODENA and REGGIO EMILIA

Department of Sciences and Methods for Engineering

Doctorate School in

INDUSTRIAL INNOVATION ENGINEERING

Synthesis and characterization of innovative polymeric materials for biomedical applications and analysis of their environmental impact

Student:

Martina Fabbri

Scientific Tutors:

Prof. Ing Rita Gamberini

Prof. Ing. Bianca Rimini

Prof. Nadia Lotti

Prof. Ing. Andrea Munari

XXVIII Period

Alla mia mamma,
sempre così orgogliosa.

Table of Contents

Chapter 1. Introduction

In the last sixty years, polymers had replaced traditional materials such as wood, glass, ceramics and steel in many applications. This is due to the unique characteristics of polymeric materials making them the best available technology: durability, processability, modulable mechanical properties and low costs (Gourmelon, 2015).
The global consumption of plastic was 299 million tons for years in 2013 (Figure 1.1), and, unfortunately, within a short period of time the most of them were disposed to the environment.

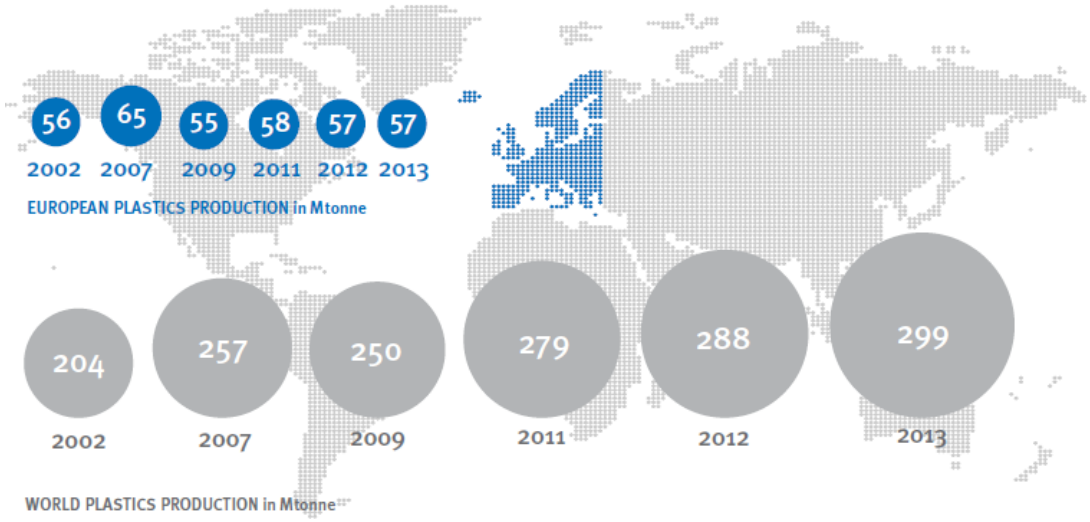

Figure 1.1 World and European plastic production 2002-2013 (source: Plastic Europe, 2014).

Europe produces yearly almost the 20% of the worldwide plastic materials, with packaging as largest application sector (39.6% of the total). Building and construction is the second largest application sector with 20.3% of the total European demand, following by automotive, electrical, electronic and agricultural applications. Other sectors such as appliances, household and consumer products, furniture and medical products comprise a total of 21.7% of the European plastics demand (Figure 1.2).

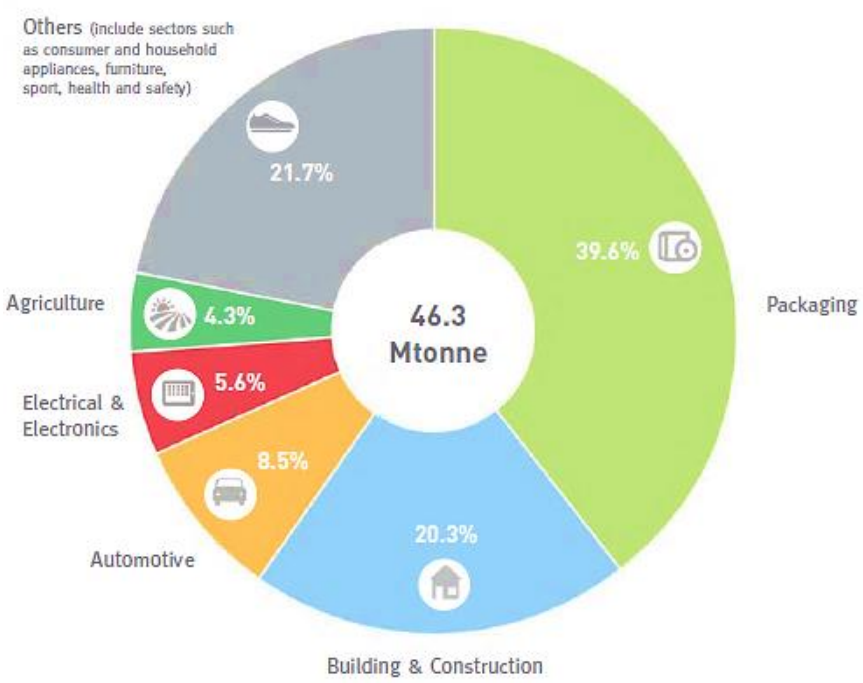

Figure 1.2 European plastics demand in 2013 (source: Plastic Europe, 2014).

To avoid the disposal problems, industrial and academic work to produce materials with controlled life span, designed to be resistant during their use but also having biodegradable properties at the end of their useful life (Lucas *et al.*, 2008). At the same time, materials based on renewable resources are strongly studied.

According to European Bioplastics, a plastic material is defined as a bioplastic if it is either biobased, biodegradable, or features both properties (Figure 1.3). The term "biobased" means that the material or product is derived from biomass, e.g. corn, sugarcane, or cellulose. Biodegradation is a chemical process in which environmental microorganisms convert materials into natural substances such as water, carbon dioxide and compost in specific environmental conditions (e.g. location or temperature). The property of biodegradation does not depend on the resource basis of a material, but is rather linked to its chemical structure. In other words, 100% biobased plastics may be non-biodegradable, and 100% fossil based plastics can biodegrade. For these reason, the family of bioplastics is roughly divided into three main groups:

1. Biobased or partly biobased non-biodegradable plastics, such as biobased polyethylene (PE), polypropanol (PP) or poly(ethylene terephthalate) (PET).

2. Plastics that are both biobased and biodegradable, such as poly(lactic acid) (PLA) and poly(hydroxyl alkanoate) (PHA) or poly(butylene succinate) (PBS).
3. Plastics that are based on fossil resources and are biodegradable, such as poly(butylene adipate terephthalate) (PBAT).

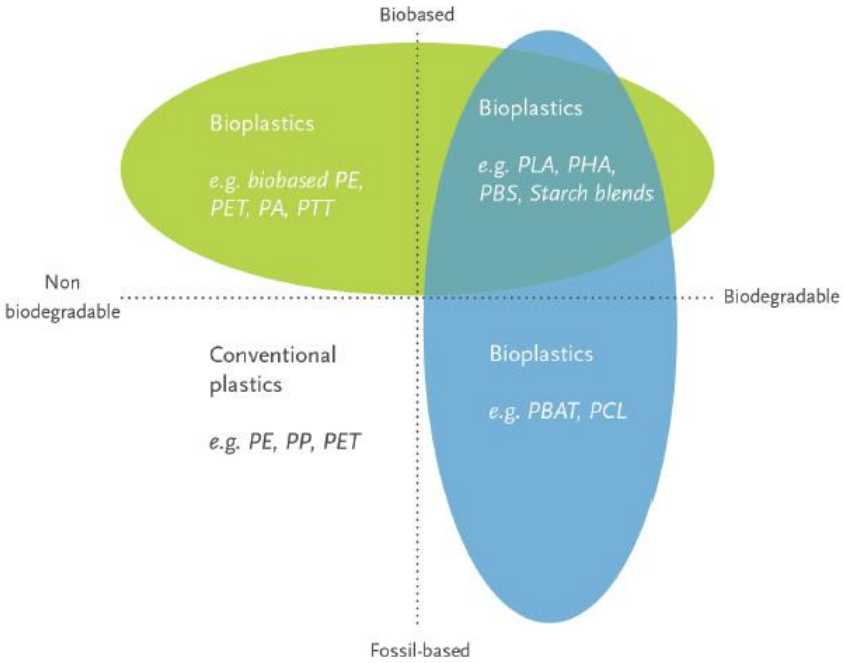

Figure 1.3 Bioplastics categories (source: European Bioplastic, 2015).

At now, the global market is dominated by conventional plastics, the challenge is to widen the range of biodegradable polymer types and possible applications so that they become functionally equivalent to petroplastics. Indeed, according to European Bioplastics, the global production capacity of bioplastics will increase from 1.1 Mt in 2011 (Figure 1.4) to 5.8 Mt in 2016, probably not only due to the intense academic and industrial research, but also to the growing interest of governments and public opinion on this crucial topic.

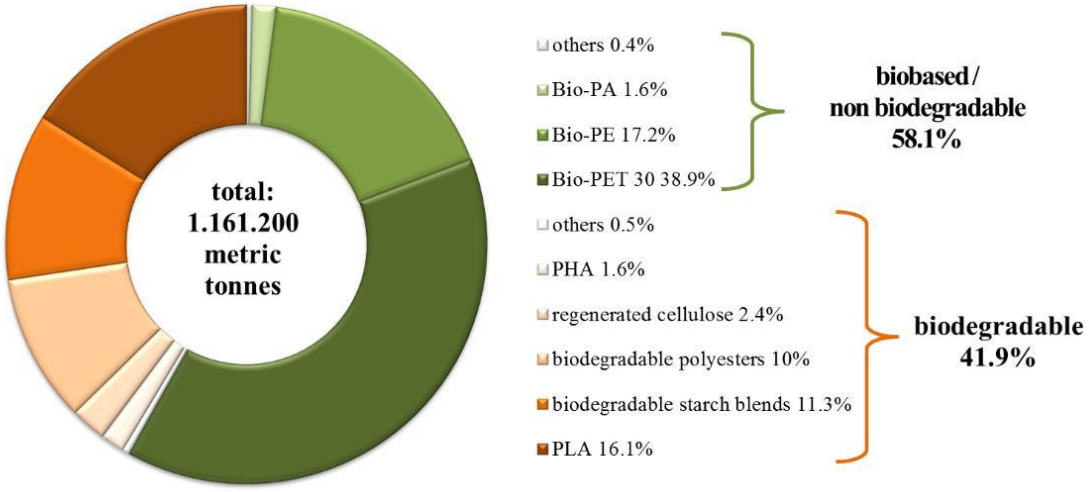

Figure 1.4 Bioplastic production capacity by type.

1.1 Biomaterials

Various definitions of biomaterial are available, probably the most updated being: "A biomaterial is a substance that has been engineered to take a form which, alone or as part of a complex system, is used to direct, by control of interactions with components of living systems, the course of any therapeutic or diagnostic procedure, in human or veterinary medicine" (Nie, 2010).

The research on biomaterials is possible by combining knowledge from different disciplines, such as medicine, biology, chemistry, materials science and engineering. Over the centuries, advancements in synthetic materials, surgical technique and sterilization methods have permitted the use of biomaterials in many ways (Park, 1984). Medical practice today utilized a large numbers of devices (pacemakers, biosensors, artificial hearts) and implants (vascular grafts, heart valves, ligaments, dental implants) to replace and/or restore the function of a traumatized or degenerated tissues or organs, and thus improve the quality of life of the patients (Patel and Gohil, 2012).

Over the last 30 years considerable progress has been made in understanding the interactions between tissues and materials. It was noted that there are profound differences between non-living (avital) and living (vital) materials. Researchers classified biomaterials into several types, such as bionert or bioactive, biostable,

biodegradable and bioresorbable. In broad terms, inert materials prohibited or minimal tissue response, while bioactive materials encourage the natural processes and functions of the surrounding tissue. Biodegradable and resorbable materials are incorporated into the treated tissue, or may even dissolve completely over a period of time. The most important properties of materials employed to medical applications are listed below.

- Biocompatibility, that is the ability to exist in contact with tissue of the human body without causing an unacceptable degree of harm in the body. It refers to a set of properties that a material must have to be used safely in a biological organism. The material should be non-carinogenic, non-pyrogenic, non-toxic, non-allergenic, blood compatible, non-inflamatory (Patel and Gohil, 2012).
- Biofunctionality, that is satisfy the requirements of the desired application, such as transmission and stress distribution, movement of the articulation, control of blood and fluid flow, electrical stimuli, light and sound transmission (Zenz, 2008).
- Toxicology, that is no release from the material of harmful substances.
- Mechanical properties, such as tensile strength, yield strength, elastic modulus, corrosion resistance, creep and hardness, that must be tailored according to the desired application.
- Maintenance of the functional tissue structure.
- Manufacturability, in fact a material must be machinable, moldable, extrudable in function of the desire final form.

1.1.1 Polymers as biomaterials

Polymers are organic materials that form large chain made up of many repeating units (monomers). At now, are the most widely used materials in biomedical applications, because of the combination of different monomers allows to prepare a broad spectrum of new materials with completely diverse physic-mechanical behavior. To be used in contact with human cells and body, polymeric materials must satisfy very strict requirements and, above all, they have to be biocompatible. In addition, another very advantageous property of biomaterials is biodegradability, because the use of surgery to remove the carrier/implant can be avoided since it undergoes degradation and subsequent excretion (or reabsorption) when its useful function has ended. It is worth

mentioning that not only the biomaterial, but the breakdown products as well have to result nontoxic for the host (Williams *et al.*, 2008).

Among polymeric biomaterials, aliphatic polyesters have been widely employed in biomedicine (Ulery *et al.*, 2011), as they combine interesting properties with easy synthetic strategies and acceptable raw material and production costs (Li *et al.*, 2012). The abundance of different monomers employed in their synthesis allow the preparation of a wide spectrum of polymers possessing specific characteristics for the intended application; moreover, different synthetic pathways can be adopted, such as polycondensation, ring opening polymerization (ROP) and in some cases, bacterial synthesis is available as well (Tserki *et al.*, 2006).

Poly(lactic acid) (PLA), poly(glycolic acid) (PGA), poly(ε-caprolactone) (PCL) and their copolymers are the most researched and investigated aliphatic polyesters for biomedical purposes; this is due to their proven biodegradability, biocompatibility and bioresorbability (Vert, 2009).

The use of poly(glycolic acid) and poly(lactic acid) in medicine dates back to the late ‘60s, when bioresorbable sutures based on these materials obtained the FDA approval in 1969 and 1971, respectively (Tian *et al.*, 2012). In the following years the first commercial product, a PGA-based absorbable suture named DEXON®, was marketed. Since then, many items have been developed, comprising screws, suture anchors, and articles for fracture fixation and meniscus repair (Kohn *et al.*, 2007). More recently, also polyesters containing dioxanone (1981) and caprolactone (1997) have been approved by FDA for medical purposes (Kohn *et al.*, 2007). In the last years also poly(butylene succinate) (PBS) has received increasing attention as regards its possible applications in biomedicine, and items in PBS and PBS-based copolymers are available to be employed in tissue engineering and controlled drug delivery.

1.2 Aliphatic polyesters

Aliphatic polyesters are a class of polymers which contain the ester functional group along the main chain (Figure 1.5).

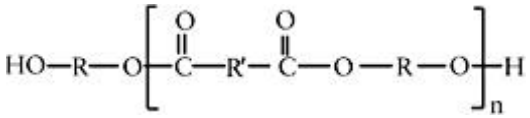

Figure 1.5 Chemical structure of linear aliphatic polyesters.

Linear polyesters were first synthesized by Carothers and coworkers in the early 1930s. Their pioneering studies on polycondensation (including polyesterification) which were commenced at DuPont in 1928, established a firm base for systematic studies of mechanisms of aliphatic polyester formation (Mark and Whitby, 1940). In particular, these included proof of the high molecular weight nature of the polyesterification products, determination of the so called Carothers equation relating the conversion degree of functional groups with the number average degree of polymerization of the resulting linear polyester, and the importance of ring-chain equilibria in the polyester synthesis. Further studies (Flory, 1936, 1939, 1942, 1953) led to the development of the principles of kinetics of polyesterification and of polyester molar mass distribution. Some properties of the aliphatic polyesters, such as hydrolytic instability, low melting temperatures, and solubility in common organic solvents were considered at that time as being detrimental from the practical applications point of view, and this led to a delay in further studies on the synthesis of these polymers.

More recently, aliphatic polyesters are spotlighted because of their peculiar biodegradability, which well adapted to the environmental concerns: indeed, their application as both biomedical and commodity degradable materials is being intensively studied. Effective techniques have been developed to produce high molecular weight polyesters applicable for practical purposes and aliphatic polyesters such as poly(butylene succinate) (PBS), poly(butylene succinate/adipate) (PBSA) and poly(lactic acid) (PLA) have been commercialized as biodegradable plastics (Okada, 2002)

1.2.1 Synthesis

Aliphatic polyesters are synthesized by the polycondensation of difunctional monomers such as the self-condensation of hydroxy acids, diacids with diols, diacid chlorides with

diols or by the ester interchange reaction of diesters and diols, or by ring-opening polymerization (ROP) of lactones and lactides (Nair and Laurencin, 2007).

Nowadays, commercially available biodegradable polyesters are produced by both polycondensation and ROP. The first method can be applicable for a variety of diols and diacids combinations, but it requires, in general, higher temperature, longer reaction time and removal of reaction byproducts to obtain high molecular weight polymers. In addition, polymers obtained do not have controlled chain lengths and polydispersity index (PDI) is usually around two. In contrast, ring-opening polymerization has a restriction on monomers, but it can be carried out under milder conditions to produce high molecular weight polymers in shorter time. Furthermore, recent progress in catalyst and initiators for living polymerization has enabled us to gain polyesters of controlled chain lengths (Okada, 2002). Also enzymes are widely used as catalysts in organic syntheses, being able to be used under moderate conditions. More important, enzymes can easily realize high regiospecificity as well as high stereospecificity that conventional catalysts never achieve (Okada, 2002). For polymer synthesis, in vitro enzyme-catalyzed polymerization has been developed as an effective method to synthesize environmentally benign polymers. Lipases catalyze the ring-opening polymerization of lactones and lactides to produce polyesters, and also the condensation polymerization of hydroxy acid and diacids with diols. Lipase catalyzed polymerization is an eco-friendly technique for the preparation of useful polyesters by polycondensation as well as polyaddition (ring opening) reactions (Varma *et al.*, 2005; Albertsson and Srivastava, 2008; Gross *et al.*, 2010).

1.2.1.1 Polycondensation

Polycondensation is the major technological method of aliphatic-aromatic polyesters production, such as poly(alkylene terephthalate)s, but also fully aliphatic polyesters, such as PBS or PBSA, are industrially synthesized at large scale by polycondensation too. Moreover, this synthetic route is used in the alternative method of polylactic acid (PLA) industrial production.

Polyesterification may be based on two different methods: homo-polycondensation of hydroxycarboxylic acid (Eqn. [1)]) or hetero-polycondensation of a diol with a dicarboxylic acid (Eqn. [2]):

$$n\ HO\text{-}R\text{-}COOH \leftrightarrow HO\text{-}(RCOO)n\text{-}H + (n-1)\ H_2O \quad \textbf{[1]}$$

$$n\ HO\text{-}R^1\text{-}OH + n\ HOOC\text{-}R^2\text{-}COOH \leftrightarrow HO\text{-}(R^1COOR^2COO)n\text{-}H + (2n-1)\ H_2O \quad \textbf{[2]}$$

where R, R^1, and R^2 denote alkylene groups. Polycondensation is a reversible process, and in order to prepare a high molar mass polymer the condensation equilibrium constant (K_C) has to be high enough. As reported by Carothers (1936), generally in the polycondensation of alcohols with carboxylic acids, the equilibrium constant is not sufficiently high (typically $K_C \leq 10$), the condensation side products (usually water or methanol) must be removed from the reaction mixture in order to obtain a reasonably high degree of polymerization (DP_n). This number is related to K_C by a simple equation:

$$DP_n = K_C^{0.5} + 1 \quad \textbf{[3]}$$

Since generally $K_C \approx 10$ for a majority of condensations of simple aliphatic alcohols with carboxylic acids, the number average degree of polymerization $DP_n \approx 4$ would result in the equilibrium polymerization. On the other hand:

$$DP_n = 1/(1 - p) \quad \textbf{[4]}$$

where p is a degree of conversion of the reactive groups (Carothers, 1936). This means that for $K_C = 10$, only 76% of hydroxyl and carboxylic group would react until an equilibrium is reached. For majority of polyesters, $DP_n \geq 100$ is needed in order to obtain the required physical properties; this corresponds to degree of conversion not less than 0.99 and in turn would require $K_C \geq 104$. K_C of this level are observed when acid chlorides (Schotten-Baumann reaction), acid anhydrides or activated carboxylic acids are used.

Shifting the equilibrium to the side of a high molar mass polyester is realized, as mentioned above, by removing from the reaction mixture the low molar mass byproduct of esterification. Eqn. [5], which is derived from Eqn. [3] by assuming $K_C >> 1$, provides a dependence of the degree of polymerization on the extent of removal of the byproduct (q):

$$DP_n = (K_C / q) \cdot 0.5 \quad \textbf{[5]}$$

where $q = N_e/N_0$, i.e., the ratio of the concentration of the byproduct at a given equilibrium to its hypothetical concentration resulting from reactive groups conversion degree related to the required DP_n. For example, in order to prepare polyester having $DP_n = 102$, it is necessary to keep K_C/q above 104. If $K_C = 10$, then q should be below 10-3. This means that only 0.1% of the byproduct of its "normal" equilibrium

concentration is allowed to be left in the reacting mixture. Such a situation creates one of the practical limitations in the syntheses of various polyesters, including PLA, directly by polycondensation. In addition, high viscosity of the system at higher degrees of conversion hampers removal of the low molar mass byproduct, such as water.

Another important factor is related to the stoichiometry of the substrates. Dependence of the number average degree of polymerization of the polyester formed in hetero-polycondensation on the stoichiometric imbalance parameter r is given by:

$$DP_n = (1 + r) / (1 + r - 2p) \quad \textbf{[6]}$$

where $r = N_{OH}/N_{COOH}$ for $N_{OH} < N_{COOH}$ or N_{COOH}/N_{OH} for $N_{OH} > N_{COOH}$ (N_{OH} and N_{COOH} stand for the concentrations of hydroxyl and carboxylic groups, respectively). Thus, for example at $p = 0.99$, and $DP_n = 100$ for the exactly equimolar reacting mixture ($r = 1$), it is sufficient to introduce only 1.0 mol% of imbalance ($r = 0.99$) to reduce DP_n to the value of 67. Even if in the feed the 1:1 stoichiometry is secured, one of the components may be partially lost during the polycondensation process, either because of volatilization, since high reaction temperatures are often used, or reactant losses by side reactions. Therefore, even in the case of homo-polycondensation the internally supplied equimolar stoichiometry may be distorted. In order to minimize this type of difficulty, modification of polycondensation was introduced based on transesterification. At least in one known instance transesterification is at the basis of the large-scale industrial process, i.e. the twostep synthesis of poly(ethylene terephthalate).

The rate of polycondensation only very seldom agrees with simple kinetic expressions throughout the entire polycondensation process. Changes in the reaction mixture properties, such as viscosity or dielectric constant, influence the course of the reaction, even if the most fundamental assumption of equal reactivities of functional groups, independently on the material chain length is obeyed. It is mostly obeyed indeed, because even if at high viscosities the “diffusion in” is slowed down, it is believed to be compensated by equally slowing down of the “diffusion out” (Rabinovitch, 1937).

1.2.1.2 Ring-opening polymerization

Aliphatic polyesters prepared by ring opening polymerization of lactones and lactides, are versatile polymers having good mechanical properties, hydrolyzability, and

biocompatibility (Albertsson and Varma, 2003). Moreover, high molecular weight polyesters can be easily prepared by ROP under mild conditions from lactones of different ring-size, substituted or not by functional groups (Jerome and Lecomte, 2008).

An extensive research effort has been expended in the past few years to refine the technique of ring opening polymerization so that polyesters with controlled architecture and tailor-made properties could be prepared (Albertsson and Varma, 2003). Alternate architectural structures (e.g., linear random or block copolyesters) have been investigated for improving the mechanical properties, hydrophilicity and degradability of these polyesters.

The polymerization of lactones is generally carried out in bulk or in solution (THF, dioxane, toluene, etc.), emulsion, or dispersion. The temperature of bulk polymerization is generally in the range of 100-170 °C, whereas in solution polymerization, low temperatures have been used (0-25 °C) to minimize side reactions (inter- and intramolecular transesterfication) (Albertsson and Varma, 2003). A few lactones polymerize spontaneously on standing or on heating. Most do so in the presence of catalysts or initiators.

Many organometallic compounds, such as oxides, carboxylates, and alkoxides are effective initiators for the controlled synthesis of polyesters using ROP of lactones. Generally speaking, ionic initiators are much reactive and, in case of polyesters, are responsible for detrimental inter- and intra-molecular transesterification reactions lowering the molecular weight and broadening the molecular weight distribution of the polymer. Many organometallic derivatives of metals, such as Al, Sn, Nd, Y, Yb, Sm, La, Fe, Zn, Zr, Ca, Ti and Mg, are imparting control to the polymerization in contrast to their anionic counterpart. In the more favourable cases, the ring-opening polymerization of lactones and lactides is a living/controlled process that leads to polyesters of narrow molecular weight distribution with a molecular weight predetermined by the monomer-to-initiator molar ratio.

The ROP proceeds mainly via two major polymerization mechanisms depending on the used organometallics. Some of them act as catalysts, and activate the monomer by complexation with the carbonyl group. Polymerization is then initiated by any nucleophile, e.g., water or alcohol, present in the polymerization medium as impurities or as compound added on purpose. In the second mechanism, the organometallic plays

the role of initiator and the polymerization proceeds through an ‘insertion–coordination’ mechanism. Metal alkoxides are typical initiators, which first coordinates the carbonyl of the monomer, followed by the cleavage of the acyl–oxygen bond of the monomer and simultaneous insertion into the metal alkoxide bond. An example of ring opening polymerization of lactide is reported on Figure 1.6.

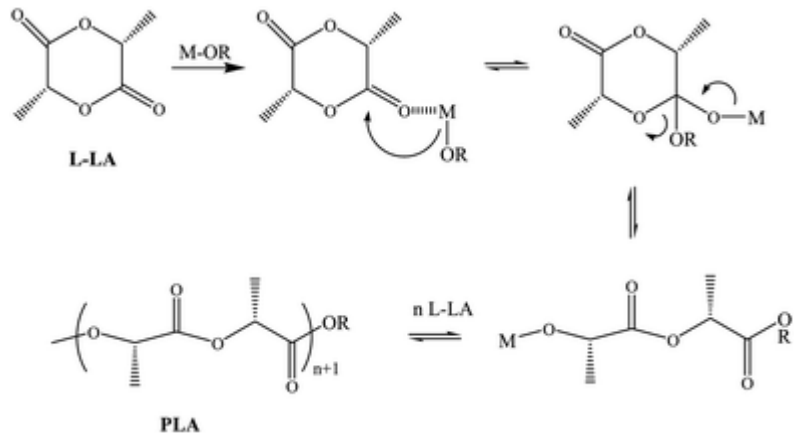

Figura 1.6 ROP of L-lactide.

Probably the most popular polymerization initiator for ROP of aliphatic polyester is tin(II) bis-(2-ethylhexanoate) also referred as tin octoate ($Sn(Oct)_2$) It is accepted as a food additive by the US Food and Drug Administration (FDA) and thus no purification of the polymers is needed for applications such as food packaging. In the most likely proposed polymerization mechanism, $Sn(Oct)_2$ is converted into tin alkoxide, the actual initiator, by reaction with alcohols or other protic impurities.

$Sn(Oct)_2 + ROH \rightarrow Oct–Sn–OR + OctH$ **[7]**

$Oct–Sn–OR + ROH \rightarrow Sn(OR)_2 + OctH$ **[8]**

As a consequence, the polymerization involves a coordination–insertion mechanism.
Again, the deliberate addition of a predetermined amount of alcohol to the polymerization medium is an effective way to control the molecular weight by the monomer-to-alcohol molar ratio. Tin octoate is also efficient in copolymerization of

various lactones. Playing on the composition of such copolymers allows tailoring their properties.

High volumes of PLA are produced via ROP under the name Natureworks™ by the joint venture between Dow and Cargill in a plant built in North America with a capacity of 0.14 million tonnes/year, mainly for commodity market (Jerome and Lecomte, 2008).

1.2.2 Copolymers

Copolymers are macromolecules derived from two or more different species of monomer. The copolymerization process attracts both academically and industrially attention because of the possibility to tailor the properties of the final material. Most commercial copolymers are designed to present synergistic improvements with respect to their parent homopolymers, including better processability, higher mechanical properties and better chemical resistance. In fact, the final properties of the copolymers can be favourably modified, depending on the kind, simply changing the relative amount and distribution of the comonomeric units along the polymeric chain.

To better comprehend the structure of copolymers, different parameters have to be taken into consideration, calculating them on different kinetic and statistical models. These latter permit to describe the comonomeric units linking process and their distribution along the polymer chain. Copolymers classification can be made based on the monomeric units (called to simplify A and B) arrangement along the polymeric chain. There are:

- <u>alternating copolymers</u> with regular alternating of A and **B** units:

  A-**B**-A-**B**-A-**B**-A-**B**-A-**B**-A-**B**

- <u>periodic copolymers</u> with A and **B** units arranged in a repeating sequence:

  (A-**B**-A-**B**-**B**-A-A-A-A-**B**-**B**-**B**)$_n$

- <u>statistical or random copolymers</u> in which the sequence distribution of monomeric units follows Bernoullian statistics:

  A-**B**-A-A-**B**-**B**-A-**B**-A-A-**B**-A

- <u>block copolymers</u> with two or more homopolymer subunits linked by covalent bonds. Block copolymers with two or three distinct blocks are called diblock copolymers and triblock copolymers, respectively:

A-A-A-**B**-**B**-**B**-A-A-A-**B**-**B**-**B**

Copolymers may also be described in terms of the existence of or arrangement of branches in the structure. Linear copolymers consist of a single main chain whereas branched copolymers consist of a single main chain with one or more polymeric side chains. Graft copolymers are a special type of branched copolymers in which the side chains are structurally distinct from the main chain: usually main chain and side chains are composed of two distinct homopolymers. However, the individual chains of a graft copolymer may be homopolymers or copolymers; moreover, different copolymer sequencing is sufficient to define a structural difference, thus an A-B diblock copolymer with A-B alternating copolymer side chains is properly called a graft copolymer. Other special types of branched copolymers include star copolymers, brush copolymers, and comb copolymers.

In the following, the present work will focus on random and block copolymers, i.e. the two copolymer types synthesized during the experimental research.

1.2.2.1 Random copolymers

In amorphous random copolymers, T_g is usually a monotonic function of composition and the most common relationship used to predict T_g as a function of comonomer content is the Fox equation:

$$1/T_g = \omega_A/T_{g,A} + \omega_B/T_{g,B} \quad \textbf{[9]}$$

where $T_{g,A}$ and $T_{g,B}$ are the glass transition temperatures of the pure homopolymers and ω_A and ω_B the respective weight fractions.

A random copolymer can potentially crystallize in two extreme ways. It can form a two phase system in which the crystalline phase is composed entirely of A units and is in equilibrium with a mixed amorphous phase of A units and non crystallizable comonomer B units (comonomer exclusion). Alternatively, the copolymer may form a two phase system in which the crystalline phase is a solid solution of A and B units; the comonomer B units produce defects in the crystalline A lattice and both phases have the same composition (comonomer inclusion). Real copolymer crystals may exhibit a morphology intermediate to the two extremes (Sanchez and Eby, 1973).

As about the crystalline melting point, two models are available: inclusion and exclusion. For the inclusion model the melting point depression is caused by a defective

heat of fusion that accompanies the crystallization, whereas for the exclusion model, the depression is caused by the fact that preferential ordering of the copolymer chains is required for crystallization which raises the entropy of fusion. However, careful crystallinity studies combined with calorimetric determinations of heats of fusion can ascertain which model is more appropriate for a given random copolymer system.

1.2.2.2 Block copolymers: chain extension reaction

The semicrystalline structure development in block copolymers depends on two competing self-organizing mechanisms: microphase separation and crystallization. In general, diblock copolymer present one amorphus block and the other one semicrystalline, which together change the final properties of T_g and T_m of the copolymer. A distinct situation arises in block copolymers where both blocks, or more than one block (typically two) within triblock terpolymers, can crystallize. As it is expected, the crystallization behavior of crystalline-crystalline block copolymers is more complicated; for instance, when the copolymers are quenched from a microphase-separated melt into various temperatures below the melting temperatures of the corresponding blocks, various situations can be observed. When the melting temperatures of both blocks are close enough, a coincident crystallization of both blocks can be obtained by quenching. On the other hand, when the melting temperature of one block is far from the other, one block crystallizes in advance and produces a specific morphology, which can or cannot be modified upon crystallization of the other block. Such modification depends, among other controlling parameters, on segregation strength, crystallization temperature and molecular weight of the block components (Muller *et al.,* 2007).

There are different ways to synthesize a block polymer. In the present work the research was focused on an innovative synthetic route carried out through a chain extension reaction of two or three hydroxyl-terminated low molecular weight subunits (homo- or copolymers).

Chain extension is a well-established synthetic strategy which can help to obtain an high molecular weight. In particular, the use of diisocyanates has been deeply investigated (Shirahama *et al.*, 2001; Cohn *et al.*, 2006; Chen *et al*., 2011). By reacting diisocyanates with hydroxyl-terminated polyesters, high molecular weight poly(ester urethane)s

(PEU), can be easily achieved. Moreover, by selecting the number, chemical structure and relative amount of the hydroxyl-terminated polyesters, it is possible to synthesize a wide plethora of new materials with tailored and more functional properties, according to the intended final use.

A polymer like poly(putylene succinate) could be chose as semicrystalline segment, as it displays $T_g < T_{room} < T_m$. On the other hand, the other subunit need a $T_g > T_{room}$ to confer rigidity to the system or a T_g well below T_{room} and Tm close to T_{room} to increase the flexibility. Finally, a small amount of diisocyanate (in general below 5 wt%) is used with the purpose of coupling together the OH-terminated polyesters and of achieving higher molecular weights. According to this motivations, changing the properties of hydroxyl-terminated polyesters is possible obtain final high weight copolymers with modulated properties depending on the application field.

1.2.3 Physical properties

The physical properties of aliphatic polyesters, such as crystallinity and melting temperature, depend on several factors such as the composition of repeat units, flexibility of the chain, presence of polar groups, molecular mass, degree of branching, crystallinity, orientation, etc. Short-chain branches reduce the degree of crystallinity of polymers while long chain branches lower the melt viscosity and impart elongational viscosity with tension-stiffening behavior (Albertsson and Varma, 2003).

Usually aliphatic polyesters are characterized by a high crystallinity degree, T_m usually in the range 40-90°C (in most cases it is well below 100°C) and T_g between –70 and –30°C. In general, the lower the ratio between methylene and carboxylic groups in the polymer chain, the higher the melting temperature: e.g. poly(butylene adipate) T_m is equal to 47°C, while poly(butylene succinate) and poly(L-lactic acid) show T_m = 116°C and 174°C, respectively (Albertsson and Varma, 2003). At the same time, aliphatic poly(ether-ester)s are more flexible because of the presence of ether linkages: e.g. poly(1,4-dioxan-2-one) is a crystalline polymer with a tensile strength and elasticity similar to those of human tissue (Albertsson and Varma, 2003).

The physical properties of aliphatic polyesters can further be tailored by copolymerization or by a change in the macromolecular architecture. Copolymers of glycolic acid and lactic acid have a T_g higher than body temperature (except for samples

of low molecular weight). This fact and the usually crystalline nature of these copolymers limit their applications as biomedical implant materials. By introducing different biodegradable ether-ester units in the backbone of aliphatic polyesters such as poly(1,4-dioxan-2-one), flexible and more pliable materials can be prepared (Albertsson and Varma, 2003).

1.2.4 Degradation

Polymer degradation and erosion have a crucial role for all plastics. The process of "degradation" correspond to the chain scission process during which polymer chains are cleaved to form oligomers and finally to form monomers; "erosion" is a loss of material owing to monomers and oligomers leaving the polymer (Gopferich, 1996).

The distinction between degradable and non-degradable polymers is, therefore, not clean-cut and is in fact arbitrary, as all polymers degrade. It is the relation between the time-scale of degradation and the time-scale of the application that seems to make the difference between degradable and non-degradable polymers. Usually a material defined 'degradable' is able to degrade during their application, or immediately after it. In the same way, non-degradable polymers are those that require a substantially longer time to degrade than the duration of their application (Gopferich, 1996).

There are different types of polymer degradation such as photo-, thermal-, mechanical and chemical degradation. For polymeric biomaterials, the effects of photo- degradation are of minor importance, unless they are submitted to y-sterilization, after which a significant loss of molecular weight can be observed (Seppala *et al*., 1991). Thermal degradation is important for non-degradable polymers and mechanical degradation affects those biodegradable polymers that are subjected to mechanical stress, such as non-degradable polymer or biodegradable polymers used as fixture or suture material (Brandwood *et al.*, 1992). All biodegradable polymers contain hydrolysable bonds, so the most important degradation mechanism is, therefore, chemical degradation.

For polymers that degrade in biological environments, there are two principal ways by which polymer bonds can be cleaved: passively by hydrolysis or actively by enzymatic reaction. In a strict sense, a polymer that loses its weight over time in a living body should be called absorbable, resorbable or bioabsorbable, regardless of its degradation mode, in other words, for both chemical and enzymatic hydrolysis (Ikada and Tsuji,

2000), but in this work often the term biodegradable to degradation in biological conditions will be used.

As a rule, for most biodegradable materials, especially artificial polymers, passive hydrolysis is the most important mode of degradation. Several factors influence the velocity of this reaction: the type of chemical bond, pH, copolymer composition and water uptake, for example. Chemical and physical changes go along with the degradation of biodegradable polymers, like the crystallization of oligomers and monomers or pH changes. Some of these factors can have a substantial feedback effect on the degradation velocity (Gopferich, 1996).

The degradation can be monitored by measuring molecular weight changes, which arise due to bond cleavage, or by measuring weight loss, which is due to depletion of low molecular weight material (Albertsson and Varma, 2003). Besides loss of molecular weight, other parameters have been proposed as a measure for degradation, like loss of mechanical strength, complete degradation into monomers or monomer release.

1.2.4.1 Chemical hydrolysis

To be degraded by water the polymer must contain hydrolysable covalent bonds such as esters, orthoesters, ethers, anhydrides, amides, carbamides (ureas), ester amides(urethanes) and so forth (Lucas *et al.*, 2008).

The type of bonds in the polymer backbone determine the rate of hydrolysis. Several classifications for ranking the reactivity exist which are either based on hydrolysis kinetics data for polymers or are extrapolated from low-molecular weight compounds containing the same functional group. Anhydride and orthoester bonds are the most reactive ones, followed by esters and amides. In the same way, hydrophobic polymers cannot take up large quantities of water and decrease, thereby, their degradation velocity. Hydrophilic polymers, in contrast, take up large quantities of water and increase degradation rates (Gopferich, 1996). The uptake of water is especially important in drug delivery systems. Hydrogels, for example, may undergo substantial swelling, which for some polymers is the decisive parameter for controlling the release of drugs, and may be more important than polymer degradation.

There are two principal pathways by which polymer bonds can be cleaved: bulk erosion, if the diffusion of water into the polymer is faster than the degradation of polymer

bonds, and degradation confined to the polymer surface, when the degradation of the polymer bonds is faster than the diffusion of water, and the matrix surface will be consumed after the water diffusion into the bulk (Von Burkersroda *et al.*, 2002). For aliphatic polyesters the hydrolytic degradation occurs in bulk: the intrusion of water triggers the chemical polymer degradation, leading to the creation of oligomers and monomers (Gopferich, 1996). Several phenomena are involved: water absorption, ester bond cleavage, neutralization of carboxyl end groups at the surface, autocatalysis inside, diffusion and solubilisation of oligomers (Li, 2006). The reaction is:

$$RCOOR^1 + H_2O \leftrightarrow RCOOH + R^1OH \quad \textbf{[10]}$$

The chemical hydrolysis reaction is catalyzed by acid or basic compounds. The acid byproduct, RCOOH, is able to accelerate the hydrolysis by autocatalysis. From a macroscopic point of view, this hydrolysis occurs in two steps: firstly, a random cleavage of polymer chain backbone with a concomitant substantial decrease in molecular weight, leading to a decrease in mechanical properties such as tensile strength, ultimate elongation and impact strength, while weight losses are negligible (Mochizuki and Hirami, 1997). In the intermediate to the last stage of degradation, the molecular fragments are solubilized and the matter disappears (Grima *et al*., 2000).

1.2.4.2 Enzymatic hydrolysis

The biological hydrolysis reaction, with respect to the chemical hydrolysis, is catalyzed by enzymes. A large number of different enzymes are involved, depending of the type of bond to be hydrolyzed. In general, they are called depolymerases. Glycosidic bonds, peptide bonds, and ester bonds are affected by this kind of reaction. It is well known that the ester bond of aliphatic polyesters is cleaved by lipases and PHA-depolymerases (Suyama *et al.*, 1998). The reaction products of an enzymatic hydrolysis or a chemical hydrolysis are the same.

In a biological system when enzyme is fit into the stereochemical conformation of the substrate molecule the biodegradation is effective. This action is described as analogous to a key fitting into a lock (Figure 1.7), and each enzyme performs one chemical function.

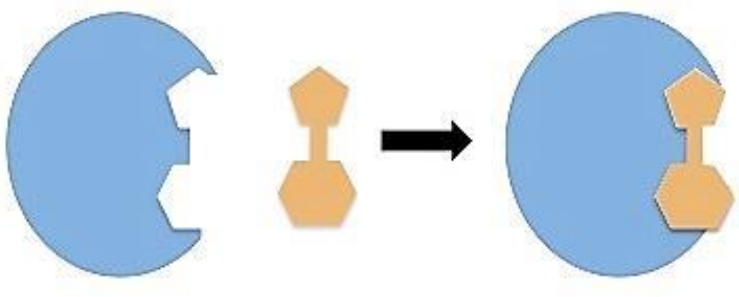

Figure 1.7 Key-lock mechanism of enzyme-substrate fitting.

Enzymatic degradation proceeds only on the surface of the solid substrate accompanying both the surface erosion and weight loss, because the enzyme cannot penetrate polymer matrix. Thus, with an enzymatic hydrolysis, the polymer weight decreases and molar mass and molecular weight distribution barely changes, unlike in chemical hydrolysis (Grima *et al.*, 2000). The low molecular weight degradation products are removed from the substrate by solubilization in the surrounding aqueous medium.

Homogeneous enzymatic reactions are controlled to Michaelis–Menten kinetics, but cannot be applied to heterogeneous enzymatic reactions such as enzymatic hydrolysis of water-insoluble substrates. In the heterogeneous system the enzymes have a hydrophobic domain as a binding site to adhere hydrophobic substrates in addition to a catalytic domain as an active site. The binding domains have been found in other enzymes such as cellulase and chitinase capable of depolymerizing water-insoluble substrates. Also a new kinetic model applicable to heterogeneous enzymatic reactions has been proposed and its usefulness has been confirmed experimentally (Mukai *et al.*, 1993). The heterogeneous enzymatic degradation takes place via two steps of adsorption and hydrolysis. The hydrophobic domains of enzymes adhere to solid substrates by hydrophobic interactions before hydrolysis by catalytic domains.

There are two types of degradation process, in that cleavage occurs either at random points along the polymer chain (the process by an endo-type degradation) or at the ends of the polymer chain (the process by an exo-type degradation). Lipases or PHA depolymerases primarily work with the endo-type scissions, and thus are not dependent on the molecular weight and molecular weight distribution. A very common feature of

depolymerases is a reaction mechanism that uses three aminoacids residues: aspartate, histidine and serine. Aspartate interacts with the histidine ring to form a hydrogen bond. The ring of histidine is thus oriented to interact with serine. Histidine acts as a base, deprotonating the serine to generate a very nucleophilic alkoxide group (-O-). Actually, it is this group that attacks the ester bond (the alkoxide group is a stronger nucleophile than an alcohol group) leading to the formation of an alcohol end group and an acyl-enzyme complex. Subsequently, water attacks the acyl-enzyme bond to produce a carboxyl end group and the free enzyme. This arrangement of serine, histidine and aspartate is termed as catalytic triad (Lucas *et al.*, 2008).

1.2.4.3 Factor influencing hydrolysis

The occurred degradation mechanism depend on both the structure of the polyester and the environment it is subjected to (Albertsson and Varma, 2003). In fact, a wide variety of compositional and property variables controls the degradation process: matrix morphology, chain orientation, chemical composition, stereochemical structure, sequence distribution, molecular weight and molecular weight distribution, the presence of residual monomers, oligomers and other low molecular weight products, size and shape of specimen. Furthermore, the some characteristics of the degradation environment affect the degradation process, e.g. presence of moisture, oxygen, microorganisms, enzymes, pH, temperature and so on.

Crystallinity is the most important factor of solid-state morphology that affects the rate of degradation of solid polymers such as fibers or films. Both enzymatic and non-enzymatic degradations proceed through selective processes with easier degradations of amorphous regions, which allow water and enzymes to diffuse into the substrate, than the crystalline regions, although the crystallites are eventually degraded from the edges inward (Mochizuki and Hirami, 1997). Chain orientation in both crystalline and amorphous regions could also play an important role in the degradation of polymers. In the case of melt-spun fibers, for example, alternative crystalline and amorphous regions arrange in the direction of the fiber axis. Chain orientation along the fiber axis impedes water penetration and enhances the resistance to hydrolytic attack. It is also worthwhile to note that the presence of imperfections and defective crystalline regions has got an effect on degradation rate. If the spherulitic crystallization develops within a matrix

containing impurities, monomers or oligomers, these non-crystallizable species are often concentrated at the inter-spherulitic boundaries. These defects are generally preferentially degraded with the amorphous regions (Li, 2006). Due to the faster erosion of amorphous compared to crystalline polymer regions, the overall crystallinity of samples increases (Gopferich, 1996).

The porosity of polymer matrix is also an important factor. A faster degradation is observed in case of nonporous films as compared with porous ones. This can be assigned to the fact that in the case of porous films, no internal autocatalysis occurred to the ionic exchange facilitated by the porous structure (Li, 2006). On the contrary, when a porous surface is exposed to enzymes, the degradation rate increases due to the enhanced surface/volume ratio, thus higher availability for the enzymatic attack.

The hydrolysis of esters is affected tremendously by pH variations (Von Burkersroda *et al.*, 2002). Ester hydrolysis can be either acid or base catalyzed. After shifts in pH, reaction rates of esters may thereby change some orders of magnitude due to catalysis (Gopferich, 1996). In the case of enzymatic hydrolysis, the pH plays even a greater role, due to the strict and well-known relationship between enzymatic activity and pH.

As far as the molecular weight is concerned, generally the lower the Mw, the faster the degradation rate, in agreement with the presence of more carboxylic acid catalysing groups (Li, 2006). Among the degradable aliphatic polyesters, a polymer having a lower melting point, T_m, is generally more susceptible to biodegradation than one having a higher melting point. In order to a synthetic polymer to be degraded by an enzyme catalyst, the polymer chain must be flexible enough to fit into the active site of the enzyme. This accounts for the above-mentioned fact that the flexible aliphatic polyesters, having also generally lower T_m, are readily degraded by lipases, while the more rigid aromatic polyesters are bioinert (Mochizuki and Hirami, 1997).

As to the relationship between biodegradability and primary structure of aliphatic polyesters, it is generally accepted that enzymatic and microbial degradations of various analogous synthetic polymer series proceed better with balanced hydrophobicity–hydrophilicity ratio in the polymer structure (Mochizuki and Hirami, 1997). Finally, the composition of polymer chains greatly determines the degradation rates of aliphatic polyesters (Li, 2006). By introducing a second monomer into the polymer chain, many properties of the original polymer can be influenced, such as crystallinity degree,

melting point and glass transition temperature. These factors can have additional indirect effects on degradation rates (Gopferich, 1996).

1.3 Poly(butylene succinate)

Polybutylene succinate is a biodegradable aliphatic polyester whit similar properties as polypropylene. Thus, PBS is highly flexible and has heat resistance characteristics. It also covers application areas such as automotive, packaging, consumer goods, electric & electronics (Global Poly(butylene succinate) Market Research Report). Growing demand for innovative packaging from industries such as food and beverage, pharmaceuticals, etc., is contributing to the growth of PBS market. Also, PBS helps to manufacture light weight automotive components; which leads to its growing demand from automotive industry. PBS also remains stable at volatile temperature, due to which it is used to manufacture consumer goods. However, recent consumer trend of preferring bio-based products is hampering the growth of the market (Global Poly(butylene succinate) Market Research Report). Its main uses regard environmental purposes, such as mulching films, compostable bags, nonwoven sheets & textiles, catering products and foams.

1.3.1 Main characteristics of poly(butylene succinate)

The monomers employed in the PBS synthesis are succinic acid (SA) and 1,4-butanediol (BD) (Figure 1.8), which are commonly obtained from fossil resources and are readily available on the market.

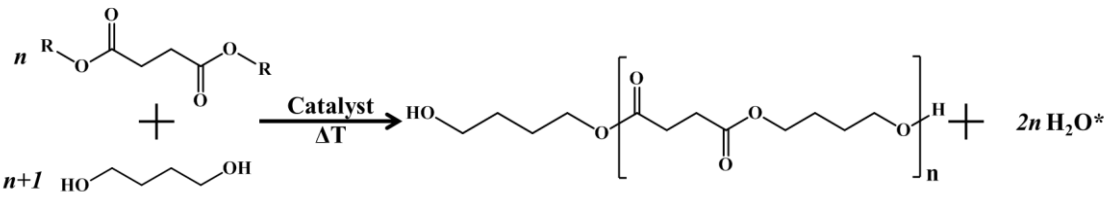

R: H or CH_3
* or CH_3OH if dimethylsuccinate is employed

Figure 1.8 Reaction scheme showing PBS polymerization.

PBS is commonly synthesized by polycondensation in two steps: in the first one, esterification (or transesterification in the case of dimethylsuccinate, DMS) reactions with removal of water (or methanol) occur, while in the second, conducted at higher temperature and under reduced pressure to remove BD (generally an excess of glycol of about 10-20% is used), high molecular weight PBS is obtained.

Different catalysts are traditionally employed for the synthesis of PBS, one of the most common being titanium (IV) butoxide (TBT). Different other types of catalysts, such as organometallic or metal-oxide compounds, have been tested and the results obtained have been fully discussed (Jacquel *et al*., 2011).

Recently, the possibility to obtain PBS by using enzymatic catalysis, in particular with a lipase from *Candida antarctica*, has been explored (Azim *et al.*, 2006; Sugihara *et al.*, 2006; Yagihara and Matsumura, 2012). Two different ways have been tested: direct polycondensation or ROP of cyclic oligomers (firstly obtained by lipase catalysed condensation of DMS and BD). In all cases the ester has been employed, as the use of SA led to unsuccessful polymerizations. Indeed, it seems that the ability of lipases to catalyse the direct polycondensation of a α,ω-linear aliphatic diacid and a diol is strongly related to the monomer chain length; the higher the number of carbon atoms, the better the result (Azim *et al.*, 2006). The positive results achieved have demonstrated the availability of a greener route to the PBS synthesis. However, the issues related to enzyme leaching and inactivation and the use of solvents to avoid polymer precipitation and consequent limitation of the molecular weight growth, hampered the diffusion of this technique.

The success of PBS as thermoplastic materials is closely linked to its properties, which are reported in Table 1.1 and Table 1.2. As a matter of fact, PBS is a semicrystalline polymer with high crystallization ability (χc = 35-45%) (Soccio *et al.*, 2008) and its melting temperature is one of the highest among poly(alkylene dicarboxylate)s (Yoo and Im, 1999; Xu and Guo, 2010). The glass transition temperature is well below room temperature, therefore PBS possesses a broad workability range which allows its processing through extrusion, injection moulding and thermoforming (Miyata and Masuko, 1998; Papageorgiou and Bikiaris, 2005).

Table 1.1PBS properties: lab scale synthesized PBS and commercial BIONOLLE™.

PBS	M_n (g/mol)	PDI	T_g (°C)	T_m (°C)	χ_c (%)
Lab scale without chain extender[a]	51200	2.1	-34	115	41±4
Lab scale without chain extender[b]	64400	n.r.	-18	112	40
Lab scale with chain extender[c]	81200	2.5	-30	112	44±4
Lab scale with chain extender[d]	$[\eta] = 2.72\ dLg^{-1}$		-37	111	n.r.
Bionolle™ [e]	66600	2.2	-32	114	35-45

a source: Gigli *et al*., 2012

b source: Xu and Guo, 2010

c results presented in this work

d source: Wu *et al*., 2014

e source: Siracusa *et al*., 2015

As to the mechanical properties (Table 1.2), they are strictly dependent on the presence of small amounts of diisocyanates, typically hexamethylene diisocyanate, used as chain extenders. High molecular weight PBS synthesized without chain extenders shows a brittle behavior, with very short elongation at break (ε_b) (Gigli *et al.*, 2012) while the use of isocyanates significantly improves its elongation, up to values comparable to those of polyolefins (Fujimaki, 1998)

Table 1.2 PBS mechanical properties: lab scale synthesized PBS and commercial BIONOLLE™.

PBS	E (MPa)	σ_y (%)	σ_b (%)	ε_b (%)
Lab scale without chain extender[a]	337±27	/	31±2	24±4
Lab scale without chain extender[b]	n.r.	35±1	29±2	275±35
Lab scale with chain extender[c]	366±5	/	27±2	303±20
Lab scale with chain extender[d]	372±30	/	45±1	530±10
Bionolle™ [e]	470-540	31	59-62	660-710

a source: Gigli *et al*., 2012

b source: Xu and Guo, 2010

c results presented in this work

d source: Wu *et al*., 2014

e source: Siracusa *et al*., 2015

Poly(butylene succinate) has shown proven biodegradability in the environment, both in compost as well as under natural conditions (soil and water). Hydrolytic degradation and biocompatibility of PBS will be discussed more in detail in the following (Chapter 3).

1.3.2 Industrial development of poly(butylene succinate)

PBS is commercially available since 1993. It is produced under the tradename Bionolle™ by Showa-Denko K.K. and by Mitsubishi Chemical Corporation under the tradename GS Pla™. Both show good processability towards films, sheets, filaments, laminates, molded foam products and injection-molded products. The application fields is currently agriculture but also fishery applications, civil engineering and construction and for common household goods.

Poly(butylene succinate) could be processed on polyolefin processing machines at temperature of 160~200°C, or about 100~230°C under controlled conditions, into various products such as injected, extruded and blown ones (Fujimaki, 1997). Thick films of PBS have properties very similar to LLDPE (linear low-density polyethylene) and relatively high speed biodegradability, and is therefore suitable for a composting bag of kitchen waste. For example, Bionolle™ in compost shows a degradation around 100% in 6 weeks (Showa Denko K.K. Report 2013). At the same time, stretched blown bottles of PBS can be processed either by cold parison method or hot parison method with resin. The permeability values of these bottles to water and alcohol are somewhat high in comparison with PET bottles (Fujimaki, 1997).

At now, fossil PBS capacity-potentially nearly 600 million lb/year, that could be convert quickly to bio succinic acid once bio is available, since it should cost less (It supposedly takes 50% less energy to make bio succinic acid than petro.). Youth Chemical started a 22 million lb/year pilot reactor for bio PBS in 2013 and Mitsubishi Chemical is building a 44 million lb/year bio PBS reactor in Rayong, Thailand, to start in 2015 (Schut, 2014).

1.3.3 Bio-based poly(butylene succinate)

The best way to obtain bio-PBS is to use succinic acid and butanediol deriving from renewable sources.

Interestingly, both SA and BD can be obtained not only from oil, but through fermentation as well. In the last years, various microorganisms have been screened and tested for the production of succinic acid via biotechnological processes, with good yields (Bechtold et al., 2008) The so-obtained succinic acid can then be converted into 1,4-butanediol through hydrogenation (Varadajian and Miller, 1999). This would lead to a complete bio-based PBS.

Various companies such as Succinity® (a joint venture between BASF and Purac), Reverdia, BioAmber and Myriant are operating in the production of biosuccinic acid at industrial scale. At now, different Companies focus the research on bio succinic acid productions (Figure 1.9) or on bio butanediol by direct bacterial fermentation or hydrogenation of SA. For example, BioAmber Inc. has built a 60 million lb/year semi-works fermenter. BioAmber also plans to build two full-scale fermenters, one for 200 million lb/year of bio BD to start in late 2017 with expansion for 140 million lb/year of bio succinic acid, and another for 400 million lb/year of bio succinic acid to start in 2020 (Schut, 2014). At the same time, Myriant Corp. started a 30 million lb/year semi-works fermenter for bio succinic acid in 2013 using corn glucose as feedstock and bacterial fermentation, and Reverdia started a 22 million lb/year semi-works fermenter in 2010. Reverdia uses yeast-based fermentation with starch as feedstock and plans a second 100 million lb/year fermenter by 2016, but hasn’t determined the site (Schut, 2014).

BIO-SUCCINIC ACID PRODUCTION CAPACITY		
Company	**Annual capacity**	**Plant location**
BASF-Purac JV	50,000 tonnes	TBA*
BASF-Purac JV	25,000 tonnes	Barcelona, Spain
BioAmber - ARD	3,000 tonnes capacity	Pomacle, France
BioAmber-Mitsui JV	65,000 tonnes	TBA* (US or Brazil)
BioAmber-Mitsui JV	17,000 tonnes (initial), 34,000 tonnes at full capacity	Sarnia, Ontario, Canada
BioAmber-Mitsui JV	65,000 tonnes	Thailand
Myriant	30m lb (13,600 tonnes)	Lake Providence, Louisiana
Myriant - China National BlueStar	220m lb (110,000 tonnes)	Nanjing, China
Myriant	170m lb (77,110 tonnes)	Lake Providence, Louisiana
Myriant - Uhde (owner and operator)	500 tonnes (first year)	Infraleuna site, Germany
Reverdia (DSM-Roquette)	10,000 tonnes	Cassano Spinola, Italy

*TBA: To be announced SOURCE: ICIS, Company Reports

Figure 1.9 Bio succinic acid production capacity (source ICIS Chemical Business, Guzman, 2012)

1.3.4 Some considerations

At now, the PBS market is restrictes and not yet able to compete with that of other aliphatic polyesters, such as poly(lactic acid), or polyolefins, like polyethylene or polypropylene. But in the last years PBS production had a strong improvement, and thanks to its useful properties together with the possibility to modulate the properties through copolymerization and the opportunity to synthesized PBS from renewable resources, it is assumed that will be more and more used for all those applications in which are required good processability, mechanical resistance, and biodegradation, such as packaging and biomedical applications.

1.4 Biomedical applications

Degradable polymers bought utmost interest because of their ability to be broken down and excreted or resorbed without removal or surgical revision (Ulery *et al.*, 2011). For this reason, in the last forty years, biodegradable or absorbable therapeutic systems replaced currently used biostable (or long lasting) metals, alloys and ceramics, to

provide novel therapeutic solutions, anytime a therapeutic function was required for a limited period of time. Surgery, degradable sutures, bone fracture fixation devices, stents, dental reconstruction, tissue engineering, drug delivery systems, are attractive targets, and some polymers have already received commercial applications.

The host response to both tissue engineering and drug delivery devices depends on the chemical, physical and biological properties of the biomaterials. When these materials are also biodegradable, there exists the additional issue of continuing changes in the material properties induced by degradation over time. These changes can cause long term host responses to these biomaterials to be greatly different than the initial response. In the design of biodegradable biomaterials, many important properties must be considered (Lloyd, 2002):

- not evoke a sustained inflammatory response;
- possess a degradation time coinciding with their function;
- have appropriate mechanical properties for their intended use;
- produce nontoxic degradation products that can be readily resorbed or
- excreted;
- include appropriate permeability and processability for designed application.

These properties are greatly affected by a number of features of degradable polymeric biomaterials including, but not limited to: material chemistry, molecular weight, hydrophobicity, surface charge, water adsorption, degradation and erosion mechanism. Given the complexity and the range of applications polymeric biomaterials are currently used, there is not just one polymeric system available that could be considered as an ideal biomaterial (Nair and Laurencin, 2007). This underlines the need for developing a wide range of biodegradable materials available that can appropriately match the specific and unique requirements of each individual medical application, through the design of the desired chemical, interfacial, mechanical and biological functions. The choice of a specific polymer, in addition to its physico-chemical properties, is dependent on the need for extensive biochemical characterization and specific *in vitro* and *in vivo* preclinical tests to prove its safety (Hoffman, 2008).

Earlier studies on aliphatic homopolyesters and copolyesters in the 1960s were aimed at developing materials for surgical implants and tissue repair. American Cyanamide Co.

first developed resorbable sutures from polyglycolide in 1962 under the trade name of Dexon (Albertsson and Varma, 2003). A copolyester with composition poly(L-lactide-co-glycolide) (PLGA, 8% and 92%, respectively) became available a few years later as a biodegradable suture material under the name Vicryl®. Aliphatic polyesters since then have been considered in a variety of medical applications such as prosthetics, artificial skin, dental implants, vascular grafts, pins, bone screws, stents, and plates for temporary internal fracture fixation.

The use of erodible polymer vehicles for controlled drug delivery was also explored in early 1970s (Yolles *et al.*, 1971). Since then, polyesters have been extensively investigated in drug delivery applications. Systems based on polylactides were investigated for the long-term delivery of antimalarial drugs, contraceptives, and eye drugs (Albertsson and Varma, 2003). A commercially successful drug delivery system is Lupron Depot®, which is intended for endometriosis and prostate cancer therapy. It is based on onemonth injectable microspheres of PLGA containing leuprorelin acetate (Lofgren *et al.*, 1995)

At now, the polyesters of biomedical importance most studied are derived from gycolide (GA), lactide (LA), caprolactone (CL), and 1,5-dioxepan-2-one (DXO). The random copolyesters such as PLGA and block copolyesters lactic acid-*b*-poly(ethylene oxide) (PLA-PEG) have been widely investigated for their degradation behavior and drug delivery applications. In the last years, as said earlier, researchers focused they attention on other polymers, such as PBS and its copolymers (Chapter 3).

1.4.1 Tissue engineering

The term ‘tissue engineering’ was officially coined at a National Science Foundation workshop in 1988 to mean “the application of principles and methods of engineering and life sciences toward the fundamental understanding of structure-function relationships in normal and pathological mammalian tissues and the development of biological substitutes to restore, maintain or improve tissue function”.

The field of tissue engineering is highly multidisciplinary and draws on experts from clinical medicine, mechanical engineering, materials and life science, genetics. Often are used synthetic tissues porous 3D-scaffolds, to provide the appropriate environment for the regeneration of tissues and organs. These scaffolds essentially act as a template

for new tissue formation and are typically seeded with cells and occasionally growth factors, and sometimes subjected to cells mechanical or chemical in a bioreactor (Martin *et al*., 2004). These cell-seeded scaffolds are either cultured *in vitro* to synthesize tissues which can then be implanted into an injured site, or are implanted directly into the injured site, using the own body systems and the regeneration of tissues or organs is induced *in vivo*. Cells, signals and scaffold work in sync to ensure the correct tissue engineering (Figure 1.10).

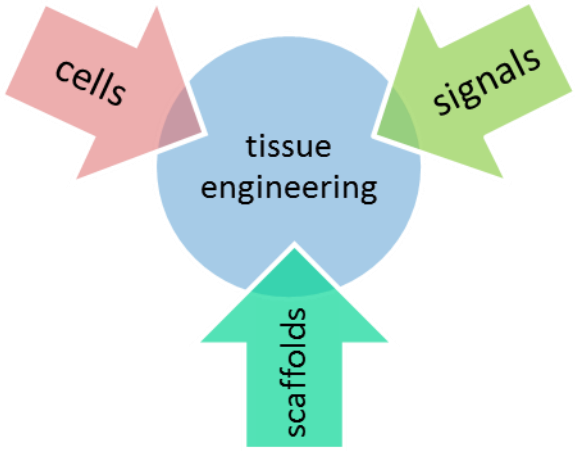

Figure 1.10 Tissue engineering triad of cells, signals and the scaffold.

Numerous scaffolds, produced from a variety of biomaterials and manufactured using different fabrication techniques, have been used in biomedical field to regenerate different tissues and organs in the body. Regardless of the tissue type, different key considerations are to be considered to designing or determining the suitability of a tridimensional support:

- Biocompatibility. The very first criterion of any scaffold for tissue engineering is that it must be biocompatible. Cells must adhere, function normally, and migrate onto the surface and eventually through the scaffold and begin to proliferate before laying down new matrix. After implantation, the scaffold must no elicit a immune reaction in order to prevent a severe inflammatory response that it might reduce healing or cause rejection by the body.

- Biodegradability. The body's own cells, over time, must replace the implanted scaffold or tissue engineered construct, that are not a permanent implants. The by-products of the scaffold degradation should also be non-toxic and able to exit the body without interference with other organs.
- Mechanical properties. Ideally, the scaffold should have mechanical properties consistent with the anatomical site into which it is to be implanted and it must be strong enough to allow surgical handling during implantation. Producing scaffolds with adequate mechanical properties is one of the great challenges in attempting to engineer bone or cartilage. For these tissues, the implanted scaffold must have sufficient mechanical integrity to function from the time of implantation to the completion of the remodelling process (Hutmacher, 2000). A balance between mechanical properties and porous architecture of the scaffolds allow cell infiltration and vascularization together with the support function.
- Scaffold architecture. Scaffolds should have an interconnected pore structure and high porosity to ensure cellular penetration and adequate diffusion of nutrients to cells. At the same time, a porous interconnected structure is required to allow diffusion of waste products out of the scaffold, and the products of scaffold degradation should be able to exit the body without interference with other organs and surrounding tissues (Ko *et al*., 2007).
- Manufacturing technology. In order for tissue engineered scaffolds to become clinically and commercially available, it should be cost effective and it should be possible to scale-up from making one at a time in a research laboratory to small batch production (Hollister, 2009). In addition, the scaffolds must be easily stored.

1.4.1.1 Electrospinning

Electrospinning is currently the only technique that allows the fabrication of continuous fibers with nanometric diameters. The method can be applied to synthetic and natural polymers, polymer alloys, and polymers loaded with chromophores, nanoparticles, or active agents, as well as to metals and ceramics (Greiner and Wendorff, 2007). Fibers with complex architectures, such as core–shell fibers or hollow fibers, can be produced by special electrospinning methods. It is also possible to produce structures ranging

from single fibers to ordered arrangements of fibers (Greiner and Wendorff, 2007). Nanofibers from synthetic or natural polymers can be fabricated in a controlled manner with adjusted dimensions and functionalized by the addition of drugs, or of semiconductor or catalyst nanoparticles.

Electrospinning is not only employed in university laboratories, but is also increasingly being applied in industry for its simplicity and easy adaptability. Electrospun fibers of natural biomaterial or synthetic biocompatible or bioserorbable polymers could be used in different fields: optoelectronics, sensor technology, catalysis, filtration, and biomedical.

The most important processing parameters of nanofibers are: applied voltage, solution flow rate, polymer concentration, molecular weight and distance between the syringe needle tip to ground collection plate (Theron *et al.*, 2004). Also solution viscosity influences fiber diameter: the higher the viscosity of the starting solution, the bigger the diameter of the fibers (Reneker *et al.*, 2000).

The electrospinning apparatus is quite simple. Basically consists of three major components which are (Figure 1.11):

- high voltage power supply with positive or negative polarity;
- syringe pump with capillaries or tubes to carry the solution from the syringe to the spinnerets;
- a grounded collecting plate (usually a metal screen, plate, or rotating mandrel).

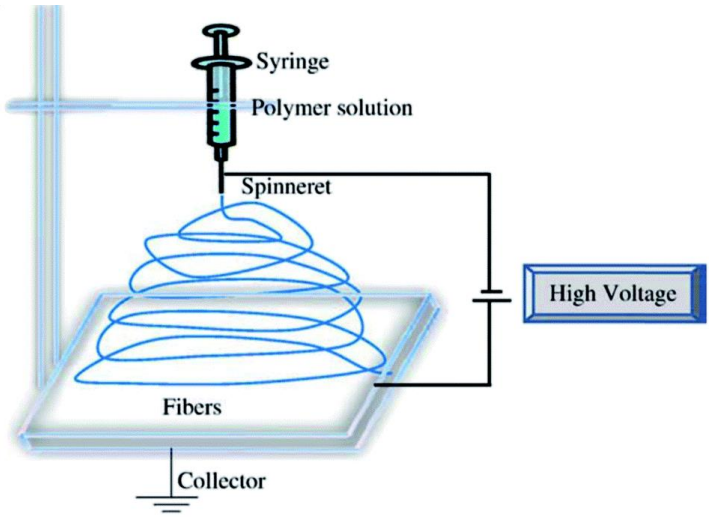

Figure 1.11 Schematic illustration of electrospinning apparatus.

The solution is forced through the syringe pump. At the end of the capillary, the polymer solution held by its surface tension, which is subjected to an electric field and an electric charge, is induced on the liquid surface due to this electric field.

The pendant hemispherical polymer drop takes a cone like projection in the presence of an electric field at the end (Taylor cone). When the applied potential reaches a critical value, the repulsive electrical forces overcome the surface tension forces. At the end, a charged jet of the solution is ejected from the Taylor cone and an unstable and a rapid whipping of the jet between the capillary tip and collector leads to evaporation of the solvent, leaving the polymer behind (Yarin et al., 2001; Adomayiciute and Rimvydas, 2007). The polymer solution must have a concentration high enough to cause polymer entanglements, but not too high that the viscosity prevents polymer motion induced by the electric field. Also the surface tension of the solution must be low enough to prevent the jet from collapsing into droplets before the solvent has evaporated.

1.4.2 Controlled drug release

Delivery systems offer numerous advantages compared to conventional dosage forms including improved efficacy, reduced toxicity, and improved patient compliance and convenience. Such systems often use synthetic polymers as carriers for the drugs (Uhrich *et al*., 1999).

Conventional oral drug administration does not usually provide rate-controlled release or target specificity. In many cases, conventional drug delivery implies sharp increases of drug concentration at potentially toxic levels. Following a relatively short period at the therapeutic level, drug concentration eventually drops off until re-administration. All controlled release systems aim to improve the effectiveness of drug therapy by increasing therapeutic activity compared to the intensity of side effects, reducing the number of drug administrations required during treatment, or eliminating the need for specialized drug administration (e.g., repeated injections) (Uhrich *et al*., 1999).

Controlled drug delivery can be used to reach (Bajpai *et al*., 2008):

- sustained constant concentration of therapeutically active compounds in the blood with minimum fluctuations;
- predictable and reproducible release rates over a long period of time;
- protection of bioactive compounds having a very short half-life;

- elimination of side-effects, waste of drug and frequent dosing;
- optimized therapy and better patient compliance;
- solution of the drug stability problem.

Two types of control over drug release can be achieved, temporal and distribution control. In the first, drug delivery systems aim to deliver the drug over an extended duration or at a specific time during treatment. Controlled release over an extended duration is highly beneficial for drugs that are rapidly metabolized and eliminated from the body after administration. In distribution control, drug delivery systems aim to target the release of the drug to the precise site of activity within the body (Uhrich *et al*., 1999). A large number of classes of drugs can benefit from temporal or distribution controlled release. These classes include chemotherapeutic drugs, immunosuppressants, antiinflammatory agents, antibiotics, opioid antagonists, steroids, hormones, anesthetics, and vaccines.

Today, polymers are the most used materials to construct drug carriers which could perform an increasing of drug availability and selectivity to the target cells. In addition, polymeric carriers could release their drug load only at the site of drug action (or nearby) in response to internal or external stimuli (e.g. pH or temperature changes) or in response to biological signals (e.g. an increase in glucose levels in blood).

1.5 Some other applications of aliphatic polyesters

In addition to biomedical and pharmaceutical sectors to which we have referred so far, aliphatic polyesters are also used to the so-called environmental applications. Indeed, applications such as packaging, mulching films, agricultural staples, coatings to protect seeds, chewing gums, cigarette filters, cartridge and cartridge wax, and so forth can be compared with biomedical implants (Table 1.3; Vert, 2005). In this field the materials are used for a limited period of time, and after use generate wastes. In addition, traditional polymers are not biorecyclable and accumulate in the environment. For this reason degradable polymers are basically necessary to many applications. For example, in agronomy are used polymeric systems to deliver pesticides, insecticides, fertilizers, and so forth, with similar (higher relative efficiency; lower overall toxicity; localization,

time, and rate control of the delivery; etc.) (Vert, 2005). At the same time it is very important the use of biodegradable materials for packaging, because of the big amount of materials that should be deposed after the use. The possibility to degrade this wastes, for example by means of compost, does not generate accumulation.

Table 1.3 Main applications of resorbable and biorecyclable polymers and comparison between the biomedical and the environmental fields.

Biomedical	**Environmental**
surgery	packaging
sutures	washing products
osteosynthesis devices	cartridge for guns
tissue engineering	cartridge wad
wound dressing	cigarette filters
Pharmacology	**Agricolture**
controlled drug delivery	sustained delivery of pesticides, insecticides, pheromones and fertilizers
bioactive macromolecules	seed protection
packaging	mulching films

Obviously, not all polymeric materials may also be suitable for this type of applications: scientists and industrials have developed technologies to take advantage of the outstanding possibility offered by polymeric systems to match material properties and application requirements, namely, copolymerization and formulation with additives.

Taking all the above considerations into due account, aliphatic polyesters are therefore expected to be one of the most economically competitive biodegradable polymers (Tserki *et al.*, 2006). In addition, they have attracted considerable attention as they combine the features of biodegradability and biocompatibility with physical and chemical properties comparable with some of the most extensively used polymers, like LDPE, PP, etc.

1.6 Life Cycle Assessment

Life Cycle Assessment (LCA) provides a comprehensive and quantitative analysis of the environmental impacts of a product or process throughout its entire life cycle, by a cradle-to-grave approach, allowing to evaluate possible low impact improvements and material used during process or product life. In addition, this analytic method is widely used for measuring the sustainability of an enterprise and informing decisions with respect to sustainability and environmental considerations (Hottle *et al.*, 2013). LCAs usually attempt to take every stage of product life cycle into account from raw material acquisition to final disposal. Transparency in the assumptions and methodologies used ensures a reproducible analysis and proper interpretation of results. In addition, take comprehensive consideration of several aspects of the natural environment, human health and resources helps to give a holistic assessment (Guo, 2012). LCA is also a relative approach with all the inputs-outputs and the environmental profile generated being related to the functional unit, allowing to compare different product systems (ISO 2006a). In recent years LCA has attracted the interest of Companies, who are increasingly using to determine the environmental impact of their products and manufacturing processes.

Life Cycle Assessment analysis consists of four phases according to the ISO 14040 (Figure 1.12):

- goal and scope definition;
- life cycle inventory analysis (LCI);
- impact assessment;
- interpretation.

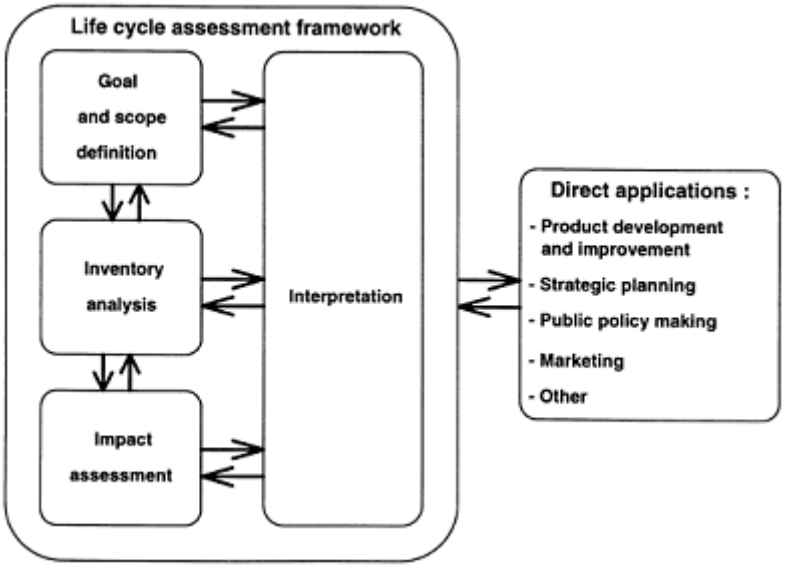

Figure 1.12 ISO-LCA methodology.

The initial step consists of laying out the scope and defining the goals of the study. In this first stage, the boundaries of the study and the functional units should also be made explicit (Duda and Shaw, 1997). The next phase is the inventory analysis. Here, all activities related to the production of one functional unit have to be analysed concerning the following components: raw material extraction, intermediate products, the product or service itself, the use phase and finally the waste removal. Energy, transportation and auxiliary products are included when they are used as inputs. Outputs are co-products, emissions to air, water and soil, waste-heat and solid wastes (Klopffer, 1997). The impact assessment stage attempts to translate the inventory data into effects on human health, ecological health, and resource depletion. The inventory items are classifying into "sets of conditions that may lead to an impact" (Duda and Shaw, 1997). Finally, interpretation aims at a critical evaluation of the whole LCA not only with respect to impact assessment using mathematical tools (sensitivity analysis, dominance analysis) and links the LCA with the applications which are not part of Life Cycle Assessment (Klopffer, 1997). Furthermore, it may be provided an improvement analysis, in which recommendations are made based on the results of the inventory and impact stages and may include modifying a production process, using different raw materials, or choosing one product over another (Duda and Shaw, 1997).

Interpreting the results of an LCA allows to understand the accuracy of the results, and ensuring they meet the goal of the study. A Life Cycle study identifies the data elements that contribute significantly to each impact category, evaluates the sensitivity of these significant data, assesses the completeness and consistency of the study, and draws conclusions and recommendations based on a clear understanding of how the LCA was conducted and the results were developed.

Chapter 2. Aim of the work

Biomedicine is a branch of medical science which synergistically combines different knowledge, such as biochemistry, engineering, genetics, microbiology, toxicology, and so on.

In recent years biomedicine is acquiring great importance for the ever increasing need to identify different treatments and therapies respect traditional medicine, increasing the quality of the health of the human beings. By the mid-1980s bioactive materials started to be clinically employed in a variety of orthopedic and dental applications, including various compositions of bioactive glasses, ceramics, glass-ceramics, and composites (Hench and Polak, 2002). Afterward, resorbable biomaterials were developed. These materials exhibited clinically relevant controlled chemical breakdown and resorption. In this manner, the problem of removing is resolved, because the foreign material is ultimately replaced by regenerating tissues, and there is no discernible difference between the implant site and the host tissue (Hench and Polak, 2002). In most cases, these materials have polymeric nature.

For these reasons, bioplastics are nowadays widely used in biomedical field, but have to fulfil strict requirements. They must be biocompatible and biodegrade in the human body with an appropriate rate, producing non-toxic metabolites. Among other biopolymers, aliphatic polyesters represent one of the most economically competitive solutions (Tserki et al., 2006), and are widely employed for their ability to combine interesting properties with easy synthetic strategies and acceptable raw material and production costs. The abundance of different monomers employable for the synthesis allows for the preparation of a wide spectrum of polymers by realizing materials showing tailored characteristics for the intended application. In recent years, poly(butylene succinate) (PBS) has attracted considerable attention due to its good mechanical properties and thermal stability, although it exhibits a slow biodegradation rate due to its high crystallinity degree (Papageorgiou and Bikiaris, 2007). It is also already commercialized, for example by Showa Denko K.K., under the trademark Bionolle®.

In this framework, the present work has been focused on the synthesis of new biocompatible fully aliphatic PBS-based polyesters. Different copolymers have been designed and realized to improve the physical/chemical and mechanical properties and the degradation rate of PBS homopolymer. The synthetic strategies adopted are the melt polycondensation (to obtain random copolymers), the chain extension reaction of hydroxyl terminated prepolymers (to obtain multiblock poly(ester urethane) copolymers), or the ring-opening polymerization of lactide using an hydroxyl-terminated PBS-based oligomer as initiator (to obtain ABA triblocks). Random copolymers by polycondensation show improved properties with respect the reference homopolymer, tipically with a decreasing in the crystallinity degree and a subsequent mild increase in the flexibility and a faster degradation rate. In multiblock poly(ester urethane), instead, the urethane linkages as connection between the polymeric chains allow to obtain highly flexible materials, able to be stretched a number of times and return to the initial dimension. These polyesters are named thermoplastic elastomers, and are the best for applications where is needed tissue resistance to mechanical stress. ABA triblocks are obtained through a more long and laborious synthetic strategy, but also in this case modifying poly(lactic acid) blackbone with more amorphous and flexible blocks and afterward link them by a chain extender allow to greatly reduce the crystallinity, by implementing the mechanical and thermal properties and the hydrolytic degradation.

All the obtained materials have been characterized by the molecular, thermal and mechanical point of view. Moreover, their hydrolytic degradation profile under physiological conditions and their biocompatibility have been studied to prove their suitability for biomedical applications, like tissue engineering, sutures and prosthesis.

During, the abroad experience at the Spanish National Research Council (CSIC) of Madrid as a visiting PhD student, three-dimensional cells supports with controlled geometry (scaffolds) and nanoparticle delivery systems starting from PBS-based copolymers have been developed and characterized, to further investigate their applicability in biomedicine.

Besides the synthesis of novel polymeric systems, Life Cycle Assessment methodology (LCA) was employed to better analyse the lab scale realization process of PBS scaffolds for applications in soft tissue engineering. Indeed, LCA provides a comprehensive and

quantitative analysis of the environmental impacts of a product or a process throughout its entire life cycle, allowing to evaluate possible low impact improvements and material used during process or product life. In this specific case, it was possible to evaluate, mainly starting from primary data obtained in the laboratory or secondary data from the literature, the critical points of the production process and their optimization, as well as the impact of a scaffold obtained starting from fossil sources. Thanks to this approach we will be able to compare this impact with that generated by scaffolds obtained by renewable resources.

Chapter 3. Analysis of state of art of poly(butylene succinate) and its copolymers for biomedical applications

Before starting the experimental activities of the research project an analysis of the current state of art of poly(butylene succinate) and its copolymers was carried out. It was focused on the biomedical applications of these polymers, specifically on tissue engineering and drug delivery systems. This analysis allowed to better understand already studied materials, most used synthetic routes and characterization techniques, and final applications available, in order to define the priorities for the development of innovative PBS-based polymeric materials for the desired applications.

Literature analysis shows that the most studied biomedical application of PBS and PBS-based copolymers is tissue engineering, where these polymers have been employed both in the form of films (Wu *et al.*, 2014; Wang *et al.*, 2009; Fujimaki 1998; Yang *et al.*, 2004; *Han et al.*, 2005; Li *et al.*, 2005; Correlo *et al.*, 2005; Wang *et al.*, 2010; Coutinho *et al.*, 2008; Lim and Kim, 2009; Coutinho *et al.*, 2012; Gigli *et al.*, 2012, 2013; Soccio *et al.*, 2012; Gualandi *et al.*, 2012; Kun *et al.*, 2012; Guo *et al.*, 2013; Zhang *et al.*, 2013; Hao *et al.*, 2014; Grigoriadou *et al.*, 2014; Arphavasin *et al.*, 2013; Tallawi *et al.*, 2013; Ngamviriyavong *et al.*, 2013; Fan *et al.*, 2014; Tan *et al.*, 2014; Niu *et al.*, 2014; Patntirapong *et al.*, 2015; Wu *et al.*, 2014) as well as scaffolds, obtained by salt leaching (Wang *et al.*, 2004; Correlo *et al.*, 2008; Oliveira *et al.*, 2008; Hariraksapitak *et al.*, 2008; Alves de Silva *et al.*, 2010; Costa-Pinto *et al.*, 2008, 2012, 2014), electrospinning (Tang and Wu, 2006; Zhan *et al.*, 2008; Pinho *et al.*, 2009; Kosorn *et al.*, 2010; Sutthiphong *et al.*, 2009; Oliveira *et al.*, 2011; Gualandi *et al.*, 2012; Kaewkong *et al.*, 2012; Almeida *et al.*, 2013; Uppanan *et al.*, 2013; Stoyanova *et al.*, 2014; Tallawi *et al.*, 2014), or extrusion (Costa-Pinto *et al.*, 2014; Ribeiro *et al.*, 2013). In some cases, realization of microspheres (Park *et al.*, 2006; Liu *et al.*, 2009; Meesap *et al.*, 2010) or nanocarriers (Jager *et al.*, 2012, 2013) as drug delivery systems has been also reported. PBS has been employed as homopolymer with or without the use of isocyanates (Wu *et* al., 2014; Han *et al.*, 2005; Li *et al.*, 2005; Wang *et al.*, 2010; Lim *et al.*, 2009; Coutinho *et al.*, 2012; Hao *et al.*, 2014; Grigoriadou *et al.*, 2014; Hariraksapitak *et al.*, 2008; Pinho *et al.*, 2009; Sutthiphong *et al.*, 2009; Almeida *et al.*, 2013; Ribeiro *et al.*,

2013; Mohanraj *et al.*, 2013), as a blend with PLA (Kun *et al.*, 2012; Stoyanova *et al.*, 2014), poly(L-lysine) (Tan *et al.*, 2014), poly(3-hydroxybotyrate-co-valerate) (Tang and Wu, 2006), PCL (Park *et al.*, 2006) or in copolymeric systems.

3.1 PBS copolymers currently available in literature

PBS-based copolymers have been prepared with the main purpose of modifying and tuning the PBS properties, such as thermal and mechanical behavior or biodegradability rate. From the literature analysis emerge that the two main synthetic strategies adopted to obtain PBS-based copolymers are copolycondensation and reactive blending.

Different comonomeric units have been introduced along the PBS macromolecular chain such as dilinoleic acid (Tallawi *et al.*, 2013, 2014; Jager *et al.*, 2012), ω-pentadecalactone (Liu *et al.*, 2009), itaconic acid (Gowsika and Nanthini, 2014) cyclic carbonates Recently, the introduction of sugar-based subunits, namely 2,4:3,5-di-O-methylene-D-mannitol (Yang *et al.*, 2004) and diethanolamine (Wu *et al.*, 2014). Aliphatic/aromatic copolyesters have been also synthesized (i.e. poly(butylene terephthalate/succinate)s) (Wang *et al.*, 2004). To these last, poly(ethylene glycol) subunits have been also added (Wang *et al.*, 2004). In addition, by reactive blending, it has been possible to obtain multiblock copolymers with different block lengths by simply varying the mixing time. To this purpose, PBS has been copolymerized with other aliphatic polyesters bearing ether and thioether-linkages, such as poly(butylene thiodiglycolate) (Gigli *et al.*, 2012), poly(thiodiethylene succinate) (Soccio *et al.*, 2012), poly(triethylene succinate) (Gualandi *et al.*, 2012), poly(diethylene glycol succinate) (Gualandi *et al.*, 2012), and poly(butylene diglycolate) (Gigli *et al.*, 2013). Last but not least, PBS ionomers containing dimethyl 5-sodium sulfoisophthalate (Han *et al.*, 2005) or sulfonated succinate units (Bautista *et al.*, 2015; Bautista *et al.*, 2015) have been synthesized and characterized.

In the same way, also the realization of composite materials allows to modify the original characteristics of a material: PBS was blended with organic materials, like chitosan (Correlo *et al.*, 2005, 2008; Coutinho *et al.*, 2008; Oliveira *et al.*, 2008, 2011; Costa-Pinto *et al.*, 2008, 2012, 2014, 2014; Alves de Silva *et al.*, 2010), collagen

(Kosorn *et al.*, 2010), and chestnut fibers (CSF) (Wu *et al.*, 2014) or inorganic ones such as calcium phosphate (Arphavasin *et al.*, 2013; Ngamviriyavong *et al.*, 2013; Fan *et al.*, 2014; Patntirapong *et al.*, 2015), hydroxyapatite (HA) (Correlo *et al.*, 2005; Guo *et al.*, 2013; Kosorn *et al.*, 2010; Kaewkong *et al.*, 2012; Uppanan *et al.*, 2013), fluoroapatite (Niu *et al.*, 2014) and wollastonite apatite (Zhan *et al.*, 2008). In one case PBS has been also incorporated in carboxymethylchitosan scaffolds (Meesap *et al.*, 2010). As it can be seen, chitosan (C) and hydroxyapatite were the most used compounds, unfortunately in both cases the final material presents poor mechanical properties that render it non suitable for particular applications (Suchanek and Yoshumura, 1998; White and Best, 2007; Jager *et al.*, 2013).

3.2 Literature analysis considerations

3.2.1 Thermal properties and wettability

As expected, the properties of PBS-based polymeric systems were significantly affected by the synthetic strategy adopted (copolycondensation, reactive blending, physical blending, etc...) and on the kind of comonomer/copolymer employed. Among other properties, the degree of crystallinity and wettability are very important parameters that can influence both biodegradation rate and biocompatibility of the material. In particular, it is well-known that the higher the degree of crystallinity the lower the hydrolytic and enzymatic degradation rate, since the less organized and packed amorphous domains are more easily attacked (Gigli *et al*., 2012, 2013, 2013). Similarly, the higher the hydrophilicity, the higher the hydrolysis rate, due to a greater water adsorption. On the other hand, enzymatic degradation is faster for a balanced hydrophobicity–hydrophilicity ratio, as the interaction of enzymes with the polymer surface is controlled by this parameter (Mochizuki and Hirami, 1997).

3.2..1.1 Random or block copolymers and composited materials

As about random or blocks copolymers, the results strongly depends on the crystallization ability of the two (or more) comonomeric units and eventual michrophase separation (Wang *et al.*, 2004; Liu *et al.*, 2009). In case of

heteroatom.containing multiblock copolymers, the crystallinity and the melting temperature are influenced by the block length of the crystalline PBS co-units: the shorter the length, the lower both the χ_c and T_m because of the formation of less and less perfect crystals due to increased difficulty of PBS chain folding (Gigli *et al.*, 2012, 2013; Soccio *et al.*, 2012; Gualandi *et al.*, 2012). The introduction of polar, ether or thioether groups along the PBS blackbone enhanced its surface hydrophilicity, increasing the degradation rate (Han *et al.*, 2005; Soccio *et al.*, 2012; Gualandi *et al.*, 2012; Kaewkong *et al.*, 2012). The same effect is achieved by incorporating urethane ionic groups (Wu *et al.*, 2014).

In the same way, for the composites is generally noted a T_m decrement and an crystallinity degree increment (Correlo *et al*,. 2005), which, however, tends to decrease with the increasing of the loading filler (Grigoriadou *et al.*, 2014; Tan *et al.*, 2014). In all these cases, an increment in the χ_c determines a decreasing in the wettability of the surface. This effect is also in part due to the increase of the surface roughness for the presence of the filler (Arphavasin *et al.*, 2013; Ngamviriyavong *et al.*, 2013).

3.2.1.2 Fibers and surface modifications

It is demonstrated that the morphology has a great importance for polymer hydrophilicity: Sutthipong *et al*. (2009) and Tallawi *et al.* (2013) demonstrated that for PBS and PBS-copolymers electrospun fibers or rough films there was a decreasing in surface wettability. In the same way, surface modification of materials, such as alkaline hydrolysis or plasma treatments improve the wettability. In fact, through plasma technique new polar functional groups (OH and NH_2) can be inserted at the specimen surface and the wettability can be significantly enhanced (Wang *et al.*, 2009). The effect of plasma treatment also on polymer fibers or composites determine a significant increasing in the wettability of the material (Ribeiro *et al.*, 2013; Coutinho *et al.*, 2008).

3.2.2 Mechanical properties

The mechanical properties are of crucial interest to evaluate the applicability of new synthesized polymers and composites as biomaterials, as similarity between the properties of the polymeric matrix with a specific tissue can not only favour cell

proliferation (Baker *et al.*, 2009), but also induce stem cells differentiation (Engler *et al.*, 2006; Reilly and Engler, 2010).

3.2.2.1 Random or block copolymers and composited materials

For multiblock copolymeric systems containing ether and thioether linkages the mechanical properties shown a reduction of elastic modulus (E) and stress at break (σb) and an increase of elongation at break (εb) with the decrease of block leght (Gigli *et al.*, 2012, 2013; Soccio *et al.*, 2012; Gualandi *et al.*, 2012). This was mainly due to the reduction of crystallinity degree. In addition, Wang *et al*. (2004) demonstred that using PBS to modified poli(ethylene terephthalate) there is a χc reduction and a consequent b increasing. In case of blending copolymers, a decreasing in the mechanical properties was reported (Tallawi *et al*., 2013).

In general, the addition of organic or inorganic filler had a significant impact on the PBS properties: elastic modulus and elongation at break respectively increased and decreased with the increasing filler content. This is probably due to the compisites stiffness and for the presence of inorganic nanofiller, micropores, poor dispersion and agglomeration of the filler into the polymeric matrix (Pinho *et al.*, 2009; Fan *et al.*, 2014; Wu *et al.*, 2014; Guo *et al*., 2013; Correlo *et al.*, 2005; Grigoriadou *et al.*, 2014; Niu *et al.*, 2014; Fan *et al*., 2014; Wu *et al.*, 2014).

3.2.2.2 Fibers and surface modifications

In salt-leaching scaffolds compression and tensile tests revealed a strict relationship between porosity and mechanical properties: increasing the pore size the mechanical properties decrease (Hariraksapitak *et al.*, 2008; Oliveira *et al.*, 2008; Costa-Pinto *et al.*, 2014). For electrospun scaffolds it is well known that the higher the fibers alignment, the better the mechanical strength, specifically with an higher elongation at break (Rizvi *et al.*, 2012; Stoyanova *et al.*, 2014; Ribeiro *et al*., 2013). Lastly, comparing the mechanical properties of films and scaffolds obtained from the same polymers could be noted a considerable increasing in scaffolds σ_b. This result is due to the porous structure of the electrospun scaffolds and its lower crystallinity degree (Sutthipong *et al.*, 2009; Almeida *et al.*, 2013; Tallawi *et al.*, 2014).

3.2.3 Hydrolytic and enzymatic degradation

Polymers used for temporary biomedical applications have to satisfy an important prerequisite: biodegradability. In this particular field the studies are preferably conducted under physiological conditions (37°C, pH 7.4, phosphate-buffered saline) or under enzymatic conditions.

3.2.3.1 Hydrolytic degradation

The *in vitro* hydrolysis of aliphatic polyesters proceeds in bulk in two steps, and it is affected by differents factors, such as chemical structure, hydrolphilic-hydrophobic balance, molecular weight and molecular weight distribution, solid-state morphology and degree of crystallinity (Gigli *et al.*, 2012, 2013). To analyse the degradation profile the molecular weight changes and the weight losses as a function of incubation time are the easiest and extensively used techniques. It is well known that PBS homopolymer hydrolytically degrade very slowly in physiological conditions, due to its high crystallinity and hydrophobicity: its weight remains relatively constant for several weeks and only a decreasing in molecular weight is detected (Han *et al.*, 2005; Li *et al.*, 2005; Gualandi *et al.*, 2012, 2012; Almeida *et al.*, 2013). On the other hand, random or blend copolymerization of PBS with hydrophilic sequences has a notable effect on its hydrolysis rate (Soccio *et al.*, 2012; Correlo *et al.*, 2008; Gualandi *et al.*, 2012; Kosorn *et al.*, 2010), specifically with the introduction of etheroatom subunits (Wang *et al.*, 2004), ionic or urethane ionones groups (Pedroso and Rosa, 2005; Wu *et al.*, 2014), and increasing the block length (Soccio *et al.*, 2012). The same as for PBS-based nanoparticles (Jager *et al.*, 2013).

By a comparison between copolymeric films and scaffolds it can be evicted that the film underwent faster degradation (Gualandi *et al.*, 2012). The reason seems to be linked to the carboxylic end-groups produced during hydrolysis, which could display an autocatalytic effect on the degradation kinetic. In polymer films, the diffusion of the acidic polymeric fragments is much lower with respect to the scaffolds due to size and morphology reasons. Therefore, they accumulate in the sample core, catalysing the hydrolysis of the macromolecular chains (Gopferich, 1996).

3.2.3.2 Enzymatic degradation

Various enzymatic degradation studies have been conducted on PBS-based polymeric systems in the presence of different kind of lipases (Yang *et al.*, 2004; Niu *et al.*, 2014; Grigoriadou *et al.*, 2014; Costa-Pinto *et al.*, 2014). Lipases are in fact well-known enzymes capable of catalysing the hydrolysis of aliphatic polyesters (Mochizuki and Hirami, 1997). Enzymatic hydrolysis is a surface eroding process, while degradation kinetic depends on the same factors mentioned above in the case of simple hydrolysis, i.e. chemical structure, hydrophilic–hydrophobic balance, molecular weight, solid-state morphology and degree of crystallinity. Also, in general, enzymatic degradation is faster (Costa-Pinto *et al.*, 2014).

In all the literature analyzed cases, copolymerisation (Yang *et al.*, 2004; Tan *et al.*, 2014) or blending (Niu *et al.*, 2014) favoured the enzymatic biodegradation, for the reduction of crystallinity degree. Also, composites with hydrophilic nanofillers, contributed to the enzymatic degradation behavior of PBS, not only because of the presence of hydroxyl groups on the surface, but of the formation of holes on the polymers due to the removal of the nanofiller (Grigoriadou *et al.*, 2014) that facilitate the lipase diffusion and accelerate degradation.

3.2.4 Biocompatibility evaluation

The study of polymer cytotoxicity is of a primary importance to assess their potential as substitutes of organic tissues or as drug carriers. Most of the studies available have been conducted *in vitro* by employing different kind of animal or human cells and, in few cases *in vivo*.

The most important factors to be taken into account to assess the cell adhesion and proliferation, thus the biocompatibility, are surface chemistry, wettability and roughness (Ranella *et al.*, 2010). Results demonstrated that adhesion is favoured on hydrophilic substrates (Arima and Iwata, 2007). As regards the surface roughness, it has been observed that the cells better spread on low-rough substrates, confirming that the cell attachment and proliferation are enhanced by a certain surface topography (Ranella *et al.*, 2010). This is because, for substrates displaying a suitable roughness, the cells would modify their shape accordingly to the surface topography, increasing the contact area and, consequently, the interfacial force Ranella *et al.*, 2010). This would result in

higher cell attachment and proliferation. At the same time, some studies carried out on PBS-based substrates have demonstrated that surface modifications that generate a certain degree of surface roughness pronouncedly promote osteoconductive property of scaffold materials (Arphavasin *et al.*, 2013; Patntirapong *et al.*, 2015; Uppanan *et al.*, 2013).

3.2.4.1 In vitro cytotoxicity tests

The cellular types most commonly used for *in vitro* studies are fibroblasts (i.e. NIH 3T3 and L929), osteoblast (i.e. MC3T3-E1, hFOBs 1.19), chondorcytes (i.e. BAC), cardiomyocytes (i.e. H9c2, C2Cl2) and splenocytes (i.e. C57B/6, Balb/c).

In all cases of random or block copolymers and blends it was highlighted an high compatibility and good adhesion with the creation of a cell monolayer on polymers with all the studied cell lines (Yang *et al.*, 2004; Gualandi *et al.*, 2012, 2012; Kun *et al.*, 2012; Zhang *et al.*, 2013; Wang *et al.*, 2004; Soccio *et al.*, 2012; Tallawi *et al.*, 2013; Han *et al,*. 2005; Wu *et al.*, 2014; Mohanraj *et al.*, 2013). Comparable results were obtained for polymer microspheres (Meesap *et al.*, 2010) and composites (Uppanan *et al.*, 2013). In the same way, polymers with surface treatment showed improved biological properties (Ribeiro *et al.*, 2013; Wang *et al.*, 2010; Kosorn *et al.*, 2010; Wang *et al.*, 2009).

Many studies have focused on scaffolds, being the 3D constructs commonly used for tissue engineering. Pore structure and size is a crucial factor in tissue regeneration, as the cell attachment and proliferation is depend on optimal pore size and geometry (Alves de Silva *et al.*, 2010). The results highlighted a good viability and biocompatibility with many different cells (Correlo *et al.*, 2008; Oliveira *et al.*, 2008, 2011; Ribeiro *et al.*, 2013; Sutthipong *et al.*, 2009; Costa-Pinto *et al.*, 2012; Hariraksapitak *et al.*, 2008; Tallawi *et al.*, 2014). The better results were showed when cell monolayer is already observed but no pore occlusion was present, indicating the adequacy of scaffolds pore size (250-500 μm) (Costa-Pinto *et al.*, 2008; Keawkong *et al.*, 2012). Furthermore, dynamic culture conditions may support higher seeding densities and therefore facilitate cell growth, proliferation and production of extracellular matrix.

3.2.4.2 In vitro stem cells tests

Natural tissues and extracellular matrix (ECM) are composed of micro- and nanoscaled elements, which arrange in specific architectures. Their replication, while developing an engineered tissue, is of crucial importance to modulate the tissue function and to determine the success of the implant (Coutinho *et al.*, 2012). Indeed, immediately after implantation, the substrate gets covered by a layer of proteins. Besides the material chemistry, the adsorptive behavior of these proteins is linked to the surface proteins of the substrate (e.g. its micro- and nanostructure) (Coutinho *et al.*, 2012). For this reason several studies have been performed using stem cells to verify how the material nature influences cells differentiation.

Composites materials promote stem cells adhesion and proliferation, thanks to its hydrophilicity and surface roughness (Ngamviriyavong *et al.*, 2013; Atphavasin *et al.*, 2013; Patntinapong *et al.*, 2015; Niu *et al.*, 2014; Zhu *et al.*, 2004). Same results are obtained for salt-leaching composites polymers scaffolds (Costa-Pinto *et al.*, 2012, 2014) and plasma treated PBS scaffolds (Ribeiro *et al.*, 2013).

3.2.4.3 In vivo studies

The *in vivo* experiments have been conducted through subcutaneous implantation in rats (Kun *et al.*, 2012; Wang *et al.*, 2004), in mice calvaria (Costa-Pinto *et al.*, 2012), in cranial defect and iliac submuscular region of Wistar rats (Costa-Pinto *et al.*, 2014, 2014) and in femoral bone of rabbits (Niu *et al.*, 2014).

In all experiments in a first time an acute inflammatory response after surgical procedures was observed, but during time the inflammatory response decrease, indicatind good biocompatibility of the sample (Oliveira *et al.*, 2008). On the other hand, in all cases it is clear a tissue regeneratio, in different times depending on the polymers used, and it is observed the formation of new blood vessels, indicating a good compatibility between the implant and the existing tissue.

3.2.5 Final considerations after literature analysis

The use of poly(butylene succinate) in biomedicine as an alternative to the well-established products is attracting considerable attention as documented by the growing number of publications on this topic.

PBS possesses interesting physic-mechanical properties and it can be easily synthesized by melt polycondensation at moderate costs. Additional value is given by the possibility to obtain both succinic acid and 1,4-butanediol from renewable resources, that makes PBS a fully bio-based and biodegradable polymer.

PBS itself displays a quite slow hydrolysis rate and low flexibility that could hamper its uses for certain applications, but blending and/or copolymerization could be used to tailor the PBS characteristics in order to satisfy many different requirements. Surface wettability, degree of crystallinity, mechanical properties and biodegradation rate have been tuned by acting on the molecular architecture and/or on the nature of comonomeric unit. The addition of organic or inorganic fillers, mainly chitosan or hydroxyapatite, played also a significant role in this respect.

Different techniques, such as salt leaching or electrospinning have been employed to realize scaffolds for tissue engineering. On the other hand, micro- and nanoparticles for controlled drug release applications have been successfully prepared.

Biocompatibility evaluations, conducted under different experimental conditions and with the use of various cell lines, highlighted the good in vitro and in vivo biocompatibility of the PBS-based copolymers and composites.

With respect to the final application, the studies demonstrated the potentiality of PBS to be employed in different areas of tissue engineering ranging from myocardial, thanks to the introduction of soft co-units, to the bone tissue replacement, through the realisation of composites.

Chapter 4. Materials and Methods

All the reagents (Figure 4.1) were purchased from Sigma Aldrich (Milan, Italy). Dimethylsuccinate (DMS), succinic acid (SA), adipic acid (AA), diglycolic acid (DGA), thiodiglycolic acid (TDGA), 1,4-butanediol (BD), 1,4-cyclohexanedicarboxylic acid (CHDA), neopentyl glycol (NPG), 1,4-cyclohexanedimethanol (CHDM), dimethyl azelate (DMAz), 1,6-hexamethylene diisocyanate (HDI) were reagent grade products and were used without any further purification. The catalyst employed, titanium tetrabutoxide ($Ti(OBu)_4$, TBT) and Tin(II)-2-ethylhexanoate ($Sn[CH_3(CH_2)_3CH(C_2H_5)CO_2]_2$, SnOct) (Sigma-Aldrich), was on the contrary distilled before use. L-lactide and pure poly(L-lactic acid) (PLLA) were kindly provided by CORBION.

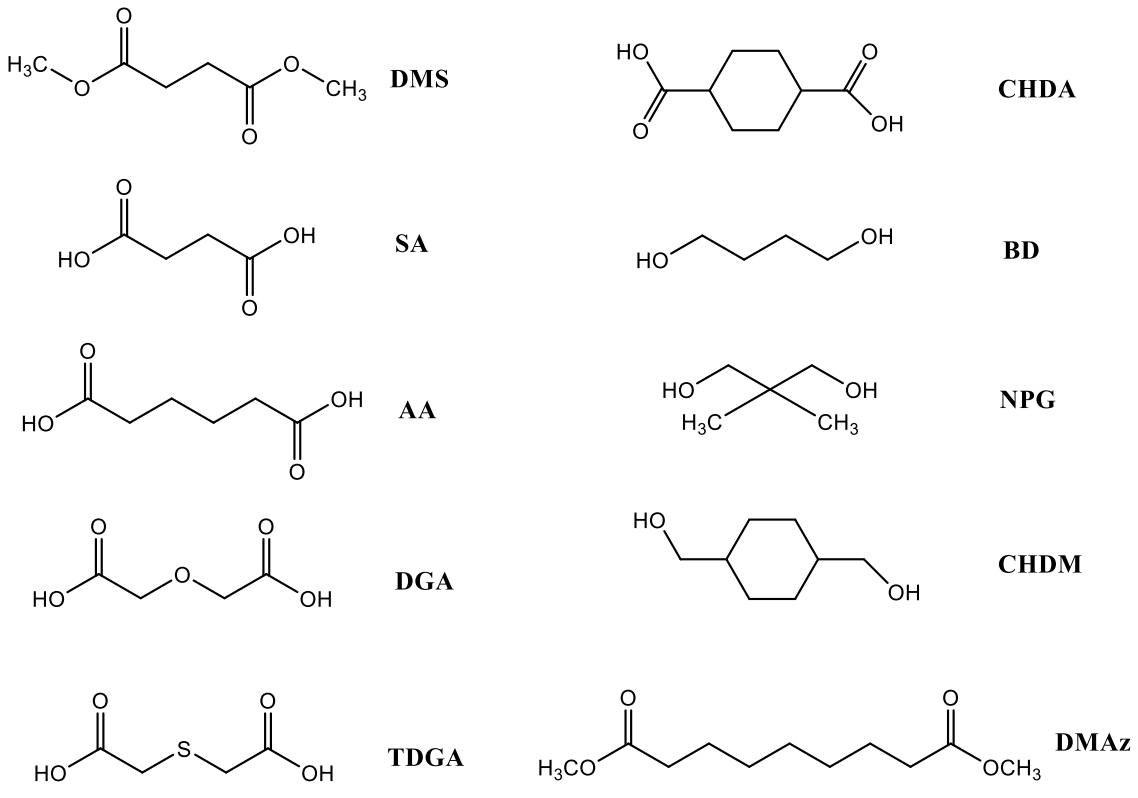

Figure 4.1 Reagents employed in the polymer syntheses.

4.1 Synthesis of homopolymers

Two different kind of homopolymers was prepared: high weight homopolymer and hydroxyl-terminated (low weight) homopolymers. The seconds were subsequently chain extended to obtain high weight homo- and copolymers.

4.1.1 Homopolymer

Poly(butylene succinate) homopolymer with high weight was synthesized in bulk starting from DMS and BD (using 15-20% mol excess of the glycol with respect to dimethylester/dicarboxylic acid), employing $Ti(OBu)_4$ as catalyst (about 150 ppm of Ti/g of theoretical polymer). The syntheses was carried out in a 250 ml stirred glass reactor, with a thermostated silicon oil bath; temperature and torque were continuously recorded during the polymerization.

The polymer was prepared according to the usual two-stage polymerization procedure. In the first stage, under pure nitrogen flow, the temperature was raised to 180°C and maintained there for until more than 90% of the theoretical amount of methanol was distilled off (about 2 hours). In the second stage the pressure was reduced to about 0.1 mbar, in order to facilitate the removal of the glycol in excess and the temperature was risen to 230°; the polymerization was carried out until a torque constant value was measured.

4.1.2 Hydroxyl-terminated homopolymer

Hydroxyl-terminated homopolymers (or prepolymers) were synthesized starting from the appropriate monomers. To ensure the obtaining of an OH-terminated polyesters, a glycol excess of 50-80%, compared to the dicarboxylic acid, was used.

The polycondensations reaction were carried out in bulk employing $Ti(OBu)_4$ as catalyst (about 150 ppm of Ti/g of polymer) in a 250 ml stilled glass reactor, with a thermostated silicon oil bath; temperature and torque were continuously recorded during the polymerization. The prepolymers were obtained according to the usual two-stage polymerization procedure. In the first stage, under pure nitrogen flow, the temperature was set at 170-180°C and kept constant until more than 90% of the theoretical amount

of water was distilled off (about 2 hours). In the second stage, the pressure was progressively reduced to 0.1 mbar, in order to facilitate the removal of the glycol excess, and the temperature was risen to 220-230°C. The syntheses were stopped after two additional hours (Torque increase of 2–3 N·cm with respect to the value measured at the beginning of the second stage).

Table 4.1 Reagents and operating conditions employed for hydroxyl-terminated homopolymer syntheses.

Polymer	Dimethylester/ dicarboxylic acid	Glycol	T_1 st stage (°C)	T_2 nd stage (°C)
Poly(butylene succinate) (PBS-OH)	SA	BD	180	230
Poly(1,4-cyclohexylenedimethylene-1,4-cyclohexanedicarboxylate) (PCCE-OH),	CHDA	CHDM	180	220
Poly(neopentyl glycol adipate) (PNA-OH)	AA	NPG	180	220

The prepolymers obtained were carefully purified by dissolution in chloroform and precipitation in methanol. The samples were then kept under vacuum at room temperature for one week to remove the residual solvent.

The details on operative conditions of hydroxyl-terminated polymers are reported in Table 4.1, while the chemical structures are reported in Figure 4.2.

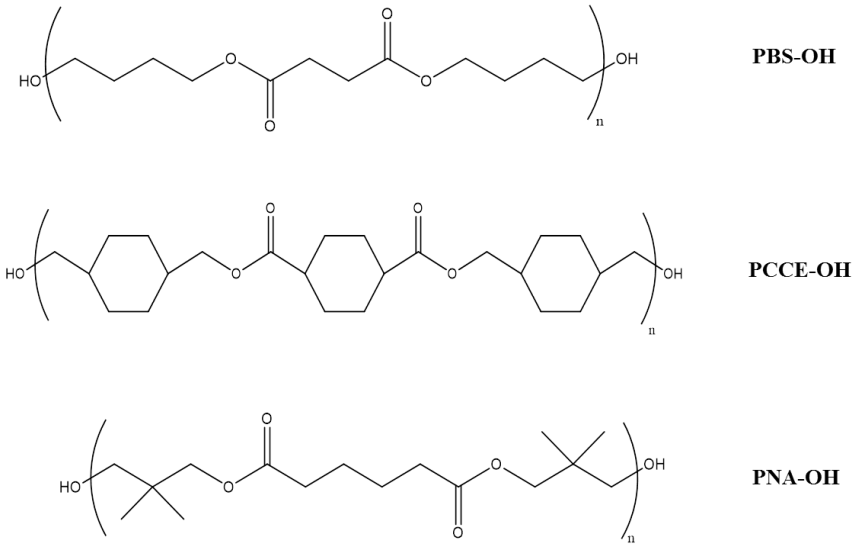

Figure 4.2 Chemical structure of hydroxyl-terminated homopolymers.

4.2 Synthesis of copolymers

4.2.1 Copolymers by polycondensation

Random copolymers were synthesized by polycondensation in bulk starting from the appropriate monomers (using 20% mol excess of the glycol with respect to dimethylester/dicarboxylic acid), employing $Ti(OBu)_4$ as catalyst (about 150 ppm of Ti/g of theoretical polymer). The syntheses were carried according to the procedure described above for homopolymers (Chapter 4.1.1). Depending on the synthesized copolymers, different ratios of the two dimethylesters have been employed in order to obtain copolymers of variable compositions.

A class of random copolymers was synthesized:

- poly(butylene succinate/diglycolate)s (P(BSxBDGy));

where x and y represent the mol% of the two different comonomeric units. The details on operative conditions of copolymers are reported in Table 4.2, while the chemical structure is reported in Figure 4.3.

Table 4.2 Reagents and operating conditions employed for copolymers syntheses.

Polymer	Dimethylester/ dicarboxylic acid	Glycol	$T_1^{st\ stage}$ (°C)	$T_2^{nd\ stage}$ (°C)
Poly(butylene succinate/diglycolate)s (P(BSxBTDGy))	DMS/TDGA	BD	180	230

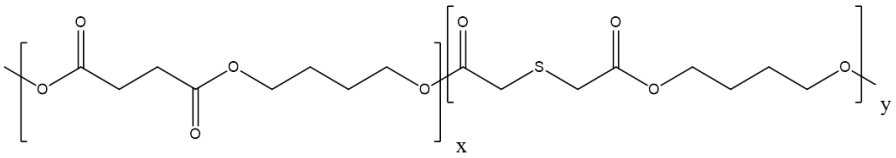

P(BSxBTDGy)

Figure 4.3 Chemical structure of copolymers.

4.2.2 Hydroxyl-terminated copolymers

Hydroxyl-terminated random copolymers were synthesized by polycondensation in bulk starting from the appropriate monomers (using 50-80% mol excess of the glycol with respect to dimethylester/dicarboxylic acid), employing $Ti(OBu)_4$ as catalyst (about 150 ppm of Ti/g of theoretical polymer). The syntheses were carried according to the

procedure described above for hydroxyl-terminated homopolymers (Chapter 4.1.2). Depending on the synthesized copolymers, different ratios of the two diols or dimethylesters/dicarboxylic acids have been employed in order to obtain copolymers of variable compositions.

Two different classes of OH-terminated random copolymers were synthesized:

- poly(butylene adipate/diglycolate)s (P(BAxBDGy)-OH);
- poly(butylene succinate/azelate) (P(BSxBAzy)-OH);

where x and y represent the mol% of the two different comonomeric units. The details on operative conditions of copolymers are reported in Table 4.3, while the chemical structures are reported in Figure 4.4.

Table 4.3 Reagents and operating conditions employed for hydroxyl-terminated homopolymer syntheses.

Polymer	**Dimethylester/ dicarboxylic acid**	**Glycol**	**T_1 st stage (°C)**	**T_2 nd stage (°C)**
Poly(butylene adipate/diglycolate) (P(BAxBDGy)-OH)	AA/DGA	BD	180	230
Poly(butylene succinate/azelate) (P(BSxBAzy)-OH)	DMS/DMAz	BD	170	225

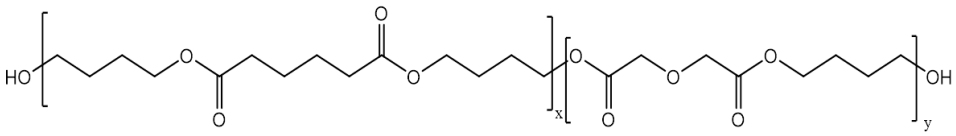

P(BAxBDGy)-OH

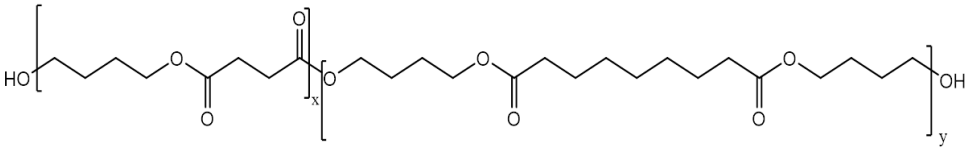

P(BSxBAzy)-OH

Figure 4.4 Chemical structure of hydroxyl-terminated copolymers.

4.3 Synthesis of poly(ester urethane)s (PEUs)

4.3.1 Triblock copolymers by chain extension reaction

Synthesis of triblock copolymers A-B-A, where A indicates the hard segments and B refers to soft segments, starting from hydroxyl-terminated homopolymers or copolymers were carried out by chain extension.

Chain extension reactions were accomplished in bulk at 160-170°C, under nitrogen atmosphere, by adding hexamethylene diisocyanate (HDI) to the molten prepolymers. The reactions were carried out until a constant torque was measured (about 60 minuts). An equimolar amount of isocyanate groups with respect to the OH-terminal groups concentration in the prepolymers was considered. During the chain extension stage a sudden increase of the torque value was detected, demonstrating the formation of urethane links between the triblocks. There were no traces of unreacted HDI after 45 min. After the chain extension process, the PEUs have been purified by dissolution in chloroform and precipitation in methanol.

Block copolymers were prepared by chain extending PBS-OH with different mass percentages of hydroxyl-terminated homopolymers (PCCE-OH and PNA-OH) or hydroxyl-terminated random copolymers (P(BAxBDGy)-OH and P(BSxBAzy)-OH). Chain extended PBS homopolymer was also considered for sake of comparison. The different multiblock copolymers obtained are reported in Table 4.4.

Table 4.4 Operating conditions and mass percentage employed for the syntheses of triblock copolymers.

Triblock copolymer	OH-terminated prepolymer 1	OH-terminated prepolymer 2	OH-terminated prepolymer 3	T (°C)
$PBS_mP(BAxBDGy)_n$	PBS-OH	-	P(BAxBDGy)-OH	160
$PBS_xPCCE_yPNA_z$	PBS-OH	PCCE-OH	PNA-OH	170

4.3.2 Triblock copolymers by ROP of L-lactide and chain extension reaction

An innovative synthesis of triblock copolymers A-B-A, where A indicates the hard segments and B refers to soft segments, starting from hydroxyl-terminated copolymers and L-lactide was studied.

This new synthetic route involves two stages. In the first step, hydroxyl-terminated prepolymers previously synthesized and purified (P(BSxBAzy)-OH), was charged into the polymerization reactor, heated to 170°C and held under inert atmosphere. Once the desired temperature was reached, the indicated amount of L-lactide was added together with the catalyst, Sn(II)-2-ethylhexanoate (about 100 ppm Sn/g of polymer). During this phase, which lasted about 3 hours, the in situ ring opening polymerization (ROP) of L-lactide by the terminal OH groups of the prepolymers took place, with the consequent formation of PLLA blocks (named *hard segments*). In the second stage, to promote the growth of the molecular weight, hexamethylene diisocyanate (HDI) has been employed as chain extender. Isocyanate groups of HDI react with terminal hydroxyl groups of PLLA leading to the formation of copoly(esters-urethanes) (PEUs). An equimolar amount of HDI with respect to the -OH groups was used. Their amount was determined by NMR analysis on the prepolymer. During the chain extension stage a sudden increase of the torque value was detected, demonstrating the formation of urethane links between the triblocks. There were no traces of unreacted HDI after 45 min. After the chain extension process, the PEUs have been purified by dissolution in chloroform and precipitation in methanol.

4.4 Film preparation

Films (0.2 mm thick) of the various semicrystalline polymers were obtained by compression moulding. The polymeric powders were placed between thin Teflon plates (0.3 mm thick), with an appropriate spacer, and heated at $T = T_m + 40°C$ for 2 minutes under a pressure of 2 ton/m^2. Hot-pressed films were cooled down to room temperature by cooling water.

Prior to characterization and degradation tests, films were kept under ambient temperature for at least 2 weeks in order to attain equilibrium crystallinity.

4.5 Scaffold fabrication

The triblock $PLLA_m(PBSxBAzy)_n$ copolymers were subjected to electrospinning in order to realize 3D-scaffolds to be employed in tissue engineering. In particular, two compositions have been taken into consideration ($PLLA_{32}(BS80BAz20)_{68}$ and $PLLA_{61}(BS80BAz20)_{39}$).

The copolymers were dissolved in DCM ($25\%_{w/w}$). Electrospinning was performed using a vertical spinning apparatus (Figure 4.5). The copolymer solution was first loaded into a 5 mL BD plastic syringe with a stainless-steel blunt-ended needle (inner diameter 0.60 mm). A syringe pump (Harvard Apparatus 70-2208) was used to pump the copolymer solution out of the syringe at a rate of 0.015 mL/min. A high voltage power supply (Slass,am High Voltage Inc. Series EL) set at 15 kV was used to confer a constant positive charge to the syringe needle. In order to obtain a 3D distribution of the fibers an aluminum collector with a polyethylene terephthalate mesh was used (Figure 4.5). The mesh guarantees two different geometries to the fibers, depending on where they were located after the electrospinning procedure, if in the hole or on the ridges of the mesh. In fact, fibers deposited in the holes of the mesh show a random architecture, while fibers filed on the ridges of the mesh were aligned perpendicular to ridges.

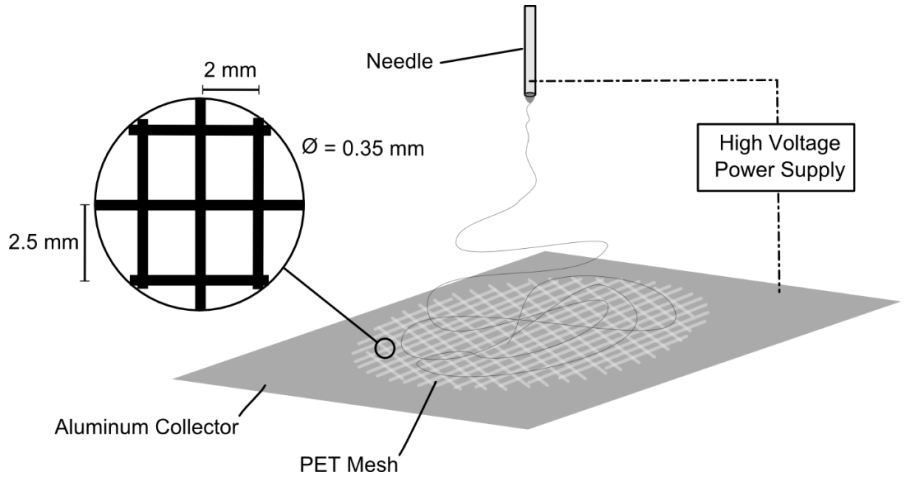

Figure 4.5 Scheme of the electrospinning process.

Dexamethasone is a corticosteroid widely used to treat diseases that are accompanied by inflammation processes. In determine cases, it would be interesting to have a tridimensional support loaded with the drug that can be applied directly into the treated tissue to avoid an inflammatory response, and at the same time, to contribute to the regeneration of the damaged tissue.

3D scaffolds of $PLLA_m(BS80BAz20)_n$ copolymers loaded with dexamethasone were prepared by electrospinning technique. The copolymers were dissolved in DCM ($25\%_{w/w}$) in presence of dexamethasone (5% respect polymer weight) in order to obtain a dexamethasone loaded system ($PLLA_m(BS80BAz20)_n$-Dex) in the same operative conditions.

Electrospun mats were fabricated in the labs of Institute of Polymer Science and Technology, Spanish National Research Council (CSIC), thanks to the scientific collaborations with Professor Julio San Roman.

4.6 Nanoparticles preparation

5 mg of two PEU copolymers ($PLLA_m(PBSxBAzy)_n$) were solved in 1 ml of THF, forming the organic phase. The aqueous phase was water enriched with PVA surfactant, with optimized concentration for the used polymer (0.5-1 wt%). The nanoparticles (NPs) were obtained by nanoprecipitation: the organic solution was added dropwise into the water solution using ultrasound (40 % amplitude dial setting) and stirring bar to homogenize, at room temperature. After adding the polymer solution, agitation was kept for 2/4 hours. Then, the final dispersion was dialyzed (M_{WCO}=3500, Spectrum Laboratories Inc.). The particle size distributions of the obtained NPs were measured by DLS.

4.7 Molecular and thermal characterization

4.7.1 Nuclear magnetic resonance (NMR)

The polymer structure and actual copolymer composition were determined by means of ^{1}H-NMR spectroscopy.

The samples were dissolved in chloroform-d solvent with 0.03% (v/v) tetramethylsilane (TMS) added as an internal standard. ^{1}H-NMR spectra at room temperature for solutions with a polymer concentration of 0.5 wt% (a relaxation delay of 0 s, an acquisition time of 1 s and up to 100 repetitions) employing a Varian INOVA 400 MHz instrument.

4.7.2 Gel permeation chromatography (GPC)

Molecular weight data were obtained by gel-permeation chromatography at 30°C using a 1100 Hewlett Packard system (Palo Alto, US) equipped with PL gel 5 m MiniMIX-C column (250/4.6 length/i.d., in mm) and a refractive index detector. In all cases, chloroform was used as an eluent at a 0.3 ml/min flow and sample concentrations were adjusted to about 2 mg/ml. A molecular weight calibration curve was obtained by means of several polystyrene standards in the molecular weight range of 2000-100,000.

4.7.3 Thermogravimetric analysis (TGA)

Thermogravimetric analysis was carried out under nitrogen atmosphere using a Perkin Elmer TGA7 apparatus (gas flow: 30 ml/min) at 10°C/min heating rate up to 800°C. The procedure suggested by the supplier was followed for the temperature calibration of equipment. This method is based on the change of the magnetic properties of two metal samples (Nickel and Perkalloy) at their Curie points (354.0 and 596.0°C, respectively).

4.7.4 Differential scanning calorimetry (DSC)

Calorimetric measurements were carried out by means of a Perkin Elmer DSC7 instrument equipped with a liquid sub ambient accessory and calibrated with high purity standards (indium and cyclohexane).

With the aim of measuring the glass transition and the melting temperatures of the polymers under investigation, the external block temperature control was set at -120°C and weighed samples of c.a. 10 mg were encapsulated in aluminium pans and heated to about 40°C above fusion temperature at a rate of 20°C/min (first scan), held there for 5 min, and then rapidly quenched (about 100°C/min) to -80°C. Finally, they were reheated from -80°C to a temperature well above the melting point of the sample at a

heating rate of 20°C/min (second scan). The glass-transition temperature (T_g) was taken as the midpoint of the heat capacity increment Δc_p associated with the glass-to-rubber transition. The melting temperature (T_m) and the crystallization temperature (T_c) were determined as the peak value of the endothermal and the exothermal phenomena in the DSC curve, respectively. The specific heat increment Δc_p, associated with the glass transition of the amorphous phase, was calculated from the vertical distance between the two extrapolated baselines at the glass transition temperature. The heat of fusion (ΔH_m) and the heat of crystallization (ΔH_c) of the crystal phase were calculated from the total areas of the DSC endotherm and exotherm, respectively.

4.8 Wide-angle X-ray diffraction

X-Ray diffraction (XRD) patterns of polymeric films were carried out in the wide angle region by using a PANalytical X'PertPro diffractometer equipped with a fast solid state X'Celerator detector and a copper target (λ = 0.15418 nm). Data were acquired in the 5 – 60° 2θ interval, by collecting data for 100 s at each 0.10° step. The indices of crystallinity (χ_C) were evaluated from the XRD profiles by the ratio between the crystalline diffraction area (A_C) and the total area of the diffraction profile (A_t), $\chi_C = A_C/A_t$. The crystalline diffraction area has been obtained from the total area of the diffraction profile by subtracting the amorphous halo. The amorphous was modelled as bell shaped peak baseline. The non-coherent scattering was taken into consideration. The crystal sizes were calculated by using the Scherrer method from the broadening at half the maximum intensity of an appropriate peak for each crystalline phase under investigation. The shape factor was chosen 1.0 and the instrumental broadening was taken in the due account.

4.9 Mechanical characterization

Stress-strain measurements were performed using an Instron 4465 tensile testing machine equipped with a 100N load cell, on rectangular films (5 mm wide and 0.2 mm thick). The gauge length was 20 mm and the cross-head speed was 5.0 mm/min. Load-

displacement curves were obtained and converted to stress-strain curves. Tensile elastic modulus was determined from the initial linear slope of the stress-strain curve. At least six replicate specimens were run for each sample and the results were provided as the average value ± standard deviation.

Only for $PLLA_m(PBSxBAzy)_n$ triblock copolymers the tensile testing of the copolymers was performed using a Zwick Roell Texture machine, equipped with a rubber grip and controlled by a computer. A pre-load of 1MPa was used with a pre-load speed of 5 mm/min. A 500N load cell was used. Stress-strain tests measurements were performed on rectangular films, of 5 mm wide and 50 mm high, with an initial grip separation of 23 mm. The tensile stress-strain measurements were performed with a crosshead speed of 50 mm/min. Five different samples from the same film were tested for each copolymer composition and the results were provided as the average value ± standard deviation. All test were carried out in accordance with ASTM D638 for film thickness below 100 micron and with ASTM D882 for film thickness over 100 micron.

4.10 Surface wettability

Static contact angle measurements were performed on polymer films by using a KSV CAM101 instrument at ambient conditions by recording the side profiles of deionized water drops for image analysis. Five drops were observed on different area for each film and contact angles were reported as the average value ± standard deviation.

4.11 Dynamic light scattering (DLS)

The particle size distribution and the zeta potential of the NPs suspensions were determined by dynamic light scattering (DLS) using a Malvern Nanosizer Nano ZS Instrument equipped with a 4 mW He-Ne laser (λ= 633 nm) at an angle of 173º. Measurements of NP suspensions varying in concentration between 1.00 and 0.05 mg/ml were performed in square polystyrene cuvettes (SARSTEDT). The particle size distributions and the apparent hydrodynamic diameter (D_h) were obtained in terms of intensity. The zeta potential was determined for suspensions of NPs at 0.1 mg/mL

concentration containing 2 mM NaCl and using laser Dopper electrophoresis (LDE) with 30 runs per measurement. The temperature was kept constant at 25 ºC during size and zeta potential measurements. The zeta potentials were automatically calculated from the electrophoretic mobility using the Smoluchowski´s approximation.

4.12 Plasma treatment

A scheme of the reactor used to generate the discharge is sketched in Figure 4.6. Two glass slabs of 160x160x2 mm have been used as dielectrics. This material has been chosen because it is inert to both the plasma and reactive species. A copper sheath (150x150 mm) has been attached to the outermost faces of the slabs, acting as electrodes. These sheaths have been connected to High Voltage (HV) and Ground (GND) terminals of the supply voltage system. Glass slabs have been faced leaving an air gap of 1mm in between them.

When the electrodes are fed with a proper sinusoidal voltage waveform, the air volume within the gap is ionized, generating a DBD plasma.

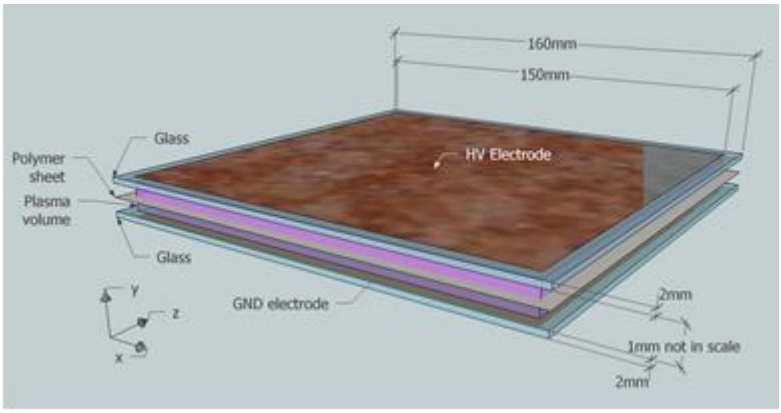

Figure 4.6 Scheme of the plasma reactor. Air gap has been fixed to 1mm and it is not in scale in the sketch.

Polymeric sheets to be treated are positioned in the middle of the inter-electrodic gap as showed in Figure 4.6. This way, both faces of the polymer sheet are treated at the same time.

The supply system is constituted by the following devices. An HP-Agilent 33120A signal source produces a low amplitude sinusoidal voltage waveform, which is delivered to an ELGAR 400-3001 amplifier. The amplifier can provide voltages up to 260 V with a maximal power of 3 kVA. A high voltage ferrite transformer has been used to increase the voltage amplitude to the desired peak value. Time resolved signals of the voltage applied to electrodes v(t) and of the discharge current i(t) have been measured with a Tektronix P6015A capacitive compensated high voltage probe (up to 75 MHz bandwidth) and a Tektronix TCP312 Hall current probe (up to 100 MHz bandwidth) respectively. Instantaneous power values p(t) = v(t)i(t) have been derived and the average power P over one period of the AC supply voltage has been calculated. In the present work, voltage has been set to 9 kV peak and frequency has been fixed to 5 kHz. In this supply condition, active power feeding the discharge has been found to be 85 W.

Voltage and current time behavior are shown in Figure S1. As widely reported in literature, when a sinusoidal waveform is used to supply a DBD reactor, the time behavior of the current follows the periodic behavior of the voltage. During a sinusoidal period there are two time intervals with several current pulses, overlapped to the sinusoidal current. Those current peaks appear during the phases in which the plasma is generated.

In order to avoid any possible damage of the polymer sheet due to thermal effects, the supply system has been operated in an on-off condition, with a duty cycle of 50% and an on-off frequency of 5Hz. This way, the supplying voltage waveform at 5 kHz is applied with on/off cycles lasting 100 ms each. The total treatment time has been set to 30s. In this supply condition an overall energy dose of 1275J has been delivered to the polymer surfaces.

4.13 Hydrolytic degradation tests

Hydrolytic degradation studies of homo-, co- and block- polymers were carried out on rectangular hot-pressed polymer films (10 35 mm, 0.2 mm thick). Films were individually immersed in phosphate buffered solution (0.1 M, pH 7.4) and incubated in

an SW22 Julabo shaking water bath at 37 °C and 50 rpm. The buffer solution was periodically changed to keep the pH at a constant value during the entire time scale of the degradation experiments.

Prior to degradation experiments, each specimen was dried over P_2O_5 under vacuum at room temperature to constant weight, then weighed to obtain the sample initial mass. At different time intervals, duplicate sacrificial specimens of each sample were repeatedly washed with deionized water and dried over P_2O_5 under vacuum for 2 days to constant weight. The mass loss was determined gravimetrically by comparing the residual dry weight with the initial value, and the decreasing of molecular weight was monitored by GPC analysis.

In vitro degradation studies of $PLLA_mP(BSxBAzy)_n$ and $PLLA_mP(BSxBAzy)_n$-Dex were performed by placing discs in 5 mL of phosphate buffer solution (PBS) under physiological conditions (37ºC, pH 7.4). After 2, 7, 15, and 30 days, the corresponding sample was removed, exhaustively washed with distilled water, dried under vacuum and weighed.

4.14 Release experiments

An in vitro elution method was used to determine the release behavior of loaded formulations. PLLAmP(BS80BAz20)n-Dex samples were immersed in vials containing 10 ml of phosphate salt buffer (PBS, pH 7.4) and incubated at Release experiments were carried out in PBS of pH 7.4 at 37ºC without stirring. Aliquots were taken at different periods of time and the dissolution medium was totally changed by fresh PBS solution. The aliquot was lyophilized and dissolved in a mixture of ethanol/aqueous solution.

The release measurements were determined by the amount of dexamethasone released was determined by UV-Vis detector (Lambda 35, Perkin Elmer) analysis at 239 nm. All samples were assayed in triplicate. The calibration curve was made a calibration curve was previously done by using known concentrations of the drug in ethanol.

4.15 Biocompatibility evaluation

Biocompatibility studies have been conducted in the laboratories of Health Sciences and Technologies, Interdepartmental Center for Industrial Research (HST-ICIR) of the University of Bologna and of Institute of Polymer Science and Technology, Spanish National Research Council (CSIC), thanks to the fruitful collaboration with Dr. Emanuele Giordano and Prof. Julio San Roman, respectively.

4.15.1 P(BSxBTDGy) biocompatibility studies

4.15.1.1 Cell culture

Cardiomyoblast H9c2 cell line were cultured in Dulbecco's Modified Eagle Medium (DMEM, Sigma), supplemented with 10% fetal bovine serum (FBS), 1% nonessential amino acids, 1% antibiotic.

Cell culture was cultured at 37°C with 5% CO2, routinely trypsinized after confluence, counted, and seeded onto each film. The polymeric films were placed inside standard 96-well-plates, sterilized with a solution of ethanol 70% for 20 minutes, washed several times with a solution containing 1% antibiotics and at the end with cell culture medium in order to remove possible chemical residues.

4.15.1.2 Indirect citotoxycity

Indirect cytotoxicity evaluations of PBS homopolymer and P(BSxTDGSy) random copolymer, subjected or not to plasma surface treatments, were performed in accordance with the ISO10993-5 international standard for biological evaluation of medical devices, as previous described (Gualandi *et al*., 2012).

H9c2 cells were seeded in a12-well culture plate ($2.5x10^4$ cells/well) in standard Dulbecco's modified Eagle's medium (DMEM) supplemented with 10% heat inactivated fetal bovine serum (FBS), 2 mM of L-glutamine, and 100 U/mL of penicillin/streptomycin, at 37°C in a humidified atmosphere containing 5% CO2 to allow their attachment and were quantified by resazurin (i.e. PrestoBlue®) fluorescence assay (Life Technologies, Monza, Italy). After 24 hours, the culture medium was discarded and polymer-extract media were added to the wells. The cells were further

incubated for 48 hours. At the end of this incubation, PrestoBlue® assay was performed again for cytotoxicity screening. The PrestoBlue® fluorescence (Ex/Em ¼ 540/590 nm) was read in a Tecan Infinite 200 multilabel multiplate reader (Tecan Italia S.r.l.).
Three separate experiments (n = 3), two replicates each, were performed. The signal obtained from cells cultured in DMEM was used as the negative control, while a cytotoxic response (positive control)was obtained by addition of 1mM H_2O_2 for 120 min to cells and readings 48 h after cell seeding. Fluorescence values (mean ± standard error of the mean) were calculated, and the one-way ANOVA with Tukey's as post-test was used to evaluate statistical differences between samples.

4.15.1.3 Cells adhesion and proliferation

Cell adhesion and cell proliferation were assessed in accordance with ISO10993-5 as previous described (Bustin *et al.*, 2009). Cell viability was quantified at day 1, 7, 14, 21 and 28 with the PrestoBlue® fluorescence assay. Control signalwas acquired from H9c2 cells cultured in standard polystyrene substrates (Sarstedt, Numbrecht, Germany).
Three separate experiments (n = 3), two replicates each, were performed. Fluorescence values were expressed as mean ± standard error of the mean. Comparison between groups was performed using the one-way ANOVA with Tukey's as post-test and differences were considered significant for $P < 0.05$.

4.15.1.4 RNA isolation and gene expression profile

Total RNA was extracted from H9c2 seeded on various polymer surfaces using TRIzol® reagent (Life Technologies) and chloroform (Sigma Aldrich, Milan, Italy) as previous described (Hirotsu *et al.*, 2000). For each samples, 500 ng of total RNA was reverse transcribed using SuperScript® VILO™ cDNA synthesis kit (Life Technologies). Myosin heavy chain (MHC) sense and antisense primers, used for DNA amplification in Real-Time PCR were 50-TGGCACCGTGGACTACAATA-30 and 50-TACAGGTGCATCAGCTCCAG-30 , respectively (TIB MOLBIO CBA, Genua, Italy); glyceraldehyde-3-phosphate dehydrogenase (GAPDH) sense and antisense primers were 50-CCTCCTCATTGACCTCAACTAC-30 and 50-CATGGTGGTGAAGACGCCAG-30, respectively (TIB MOLBIO CBA, Genua, Italy). Relative gene expression analysis was performed in a CFX Connect™ Real-Time PCR

Detection System (Bio-Rad, Milan, Italy) using the SYBR Premix Ex Taq II (TaKaRa, Tokyo, Japan) following MIQE guidelines (Zimmerman, 1984). Amplification was performed in a 20 ml final volume including 2 ml of cDNA as template. Specificity of formed products was addressed performing a melting curve analysis. Three separate experiments (n = 3), two replicates each, were performed and data were normalized to GAPDH expression (endogenous control) since the mRNA transcript for this gene was similar among the samples. Fold-changes in gene expression were determined by the 2 DDCq method and are presented relative to levels in H9c2 cultured on PS standard well. Comparison between groups was performed using Student's t-test and differences were considered significant at $P < 0.05$.

4.15.2 $PLLA_m(PBSxBAzy)_n$ biocompatibility studies

4.15.2.1 Cell culture

Cellular toxicity and cell proliferation were evaluated using fibroblast of human embryonic skin (HFB, Innoprot), while inflammatory activity was monitored only on murine RAW 264.7 macrophages (ECACC, Sigma P11). Cells were cultured in Dulbecco's modified Eagle's medium (DMEM) supplemented with HEPES (for HFB cells) or sodium pyruvate (110 mg L−1; for RAW 264.7 cells), and 10% fetal bovine serum (FBS), 100 units mL−1 penicillin, 100 μg mL−1 streptomycin and 200 mM L-glutamine. A humidified atmosphere at 37 °C with 5% CO2 and 95% of air was used for cell cultures growth.

For cell experiments, cells were harvested using 0.25% trypsin and 1 mM EDTA in Hanks buffer.

4.15.2.2 Indirect citotoxycity

The in vitro effects of products released from the electrospun mats on cellular viability was assessed by the 3-(4,5-dimethylthiazol-2-yl)-2,5-diphenyltetrazolium bromide (MTT) assay (Mosmann, 1983; Denizot and Lang, 1986; Yoshii, 1997). Rounded bits of electrospun mats or control PET disks were immersed in 5 mL of FBS-free DMEM at 37 °C. The medium was withdrawn at different time points and replaced with fresh medium. Meanwhile HBF cells were seeded at 2 × 105 cells mL−1 in a sterile 96-well culture plate and grown to confluence. The culture medium was then replaced by the

eluted extracts of each material (100 μL/well), and the plate was incubated at 37 °C, 5% CO_2, and 24 h

Afterwards, cell viability was determined by adding MTT reagent (0.5 mg/mL in PBS) for 4 h at 37 °C. Excess medium and MTT reagent were withdrawn and dimethylsulfoxide was added to solubilize the formazan crystals formed in viable cells. The OD570 (test wavelength) and was determined using a microplate reader (Biotek SYNERGY-HT). Cell viability (CV) was calculated from equation: CV (%) = 100 × (ODS–ODB)/ODC, where ODS, ODB and ODC are, respectively, the optical density of formazan production for the sample, blank (DMEM without cells), and control.

All experiments were performed in triplicate and one-way ANOVA was performed to determine statistical significance.

4.15.2.3 Cellular adhesion and proliferation

Quantitative analysis for cell adhesion and proliferation on copolymers films was carried out by means of the Alamar Blue test (Yildirim et al., 2008). Adhesion and proliferation of cells was also followed by direct analysis by SEM microscopy.

The test was performed using HBF cells at a density of 7 × 104 cells/mL. Determinations were carried out at 24 h and were repeated at 4, 7 and 14 days. Test specimens and TMX control were placed in 24-well sterile culture plate. Alamar Blue dye (1 mL of 10% alamar Alamar blue Blue solution in phenol red free DMEM medium) was added to each specimen. After 4 h of incubation the absorbance was measured at an excitation wavelength of 570 nm. Results were normalized with respect to a negative control (TMX = 100%) and statistically tested with ANOVA.

For the analysis by ESEM, the cells were fixed with 2.5% glutaraldehyde buffered in distilled water for 24 h at room temperature and then washed and dried. The dried samples were sputter-coated with Au/Pd (80/20) before examination under a SEM apparatus (Philips XL 30) at an accelerating voltage of 25 KeV.

All experiments were performed in triplicate and one-way ANOVA was performed to determine statistical significance.

4.15.2.4 Anti inflammatory capacity

The inflammatory activity of polymers was investigated using a nitric oxide inhibitory assay (Wang *et al.*, 2008). Briefly, RAW 264.7 cells were seeded in 96-well plates at a density of 2 × 105 cells mL−1 and incubated at 37 °C for 24 h. After incubation, a bit of electrospun mat were placed on the well and 2 μg/ml of lipopolysaccharides from E.Coli 055:B5 (LPS) were add to any samples and incubated at 37°C for 24 hours. After this time, the nitrite concentration was determined by the Griess reaction (Guevara *et al.*, 1998). Aliquots (100 μL) of the supernatant from RAW 264.7 cells were reacted with 100 μL of Griess reagent [1:1 mixture of 0.1% N-(1-naphthyl) ethylenediamine in water and 1% sulphanilamide in 5% phosphoric acid] in a 96-well plate and the OD548 was recorded. Data were expressed as the percentage of NO production.

All experiments were performed in triplicate and one-way ANOVA was performed to determine statistical significance.

4.16 Collection of inventory data for the final life cycle assessment analysis

The analyzed process consists in catalysed polycondensation of succinic acid (SA) and 1,4-butanediol (BD) to obtain poly(butylene succinate) and subsequent electrospinning for the final product. Also the scaffold sterilization and packaging were considered.

The analysis was conduct with the support of LCA Working Group, Department of Sciences and Methods for Engineering, University of Modena and Reggio Emilia, thanks to the fruitful collaboration with Professor Anna Maria Ferrari and Engineer Paolo Neri.

4.16.1 Scaffold manufacturing process

In Figure 4.7 the flow chart of the considered scaffold manufacturing process is reported.

PBS synthesis

In a first time, the process of succinic acid synthesis was considered starting from maleic anhydride via bimetallic catalysed hydrogenation. At the same time, titanium (IV) tetrabutoxide (TBT), the catalyst necessary for the PBS production, has been derived from titanium tetrachloride and 1-butanol. As about BD, it was already in Econinvent databased. The poly(butylene succinate) synthesis process occurs in two stages: initially the esterification of the alcohol and carboxyl groups of the starting monomers, and subsequently the polycondensation, through loss of water molecules and the increase of molecular weight.

Purification

The obtained PBS was purified by dissolution in chloroforms and further precipitation in methanol (10 volumes), to remove the unreacted monomers, catalyst and low weight holygomers or etherocycles, whose are critical in biomedical field. Polymer shape flocs and is easily recoverable.

Afterwards, purified PBS need to be dried under vacuum at 80°C to remove all the solvent used. As well known, chlorate organic solvent and methanol are dangerous to the human health.

Electrospinning process

Many studies about poly(butylene succinate) electrospinning were reported (Jeong *et al.*, 2005; Liu *et al.*, 2007; Sutthiphong *et al.*, 2009; Gualandi *et al*, 2012). The working principle of electrospinning consist in high voltage provided by a charge flow from a pointed electrode to a collector, allowing a charge aggregation into the polymer solution at the spinneret of syringe. At the exit point of the polymer solution is formed a "Taylor cone", then is drawn out from spinneret as an ideal spiral thinner fiber. The solvent evaporates very quickly and the ultrathin fibers solidify (Li *et al.*, 2010).

Operative conditions used (Gualandi *et al*, 2012):

- 17% polymer concentration;
- mixture dichloromethane/hexane (ratio 80/20);
- flow rate 0.01 ml/min;

- voltage 14 kV;
- air humidity 40%.

In a first time, PBS was dissolved in the mixture of dichloromethane/hexane. Then, the obtained solution was introduced inside the injection syringe of the instrument then the electrospinning process was conducted using the operating conditions described above.

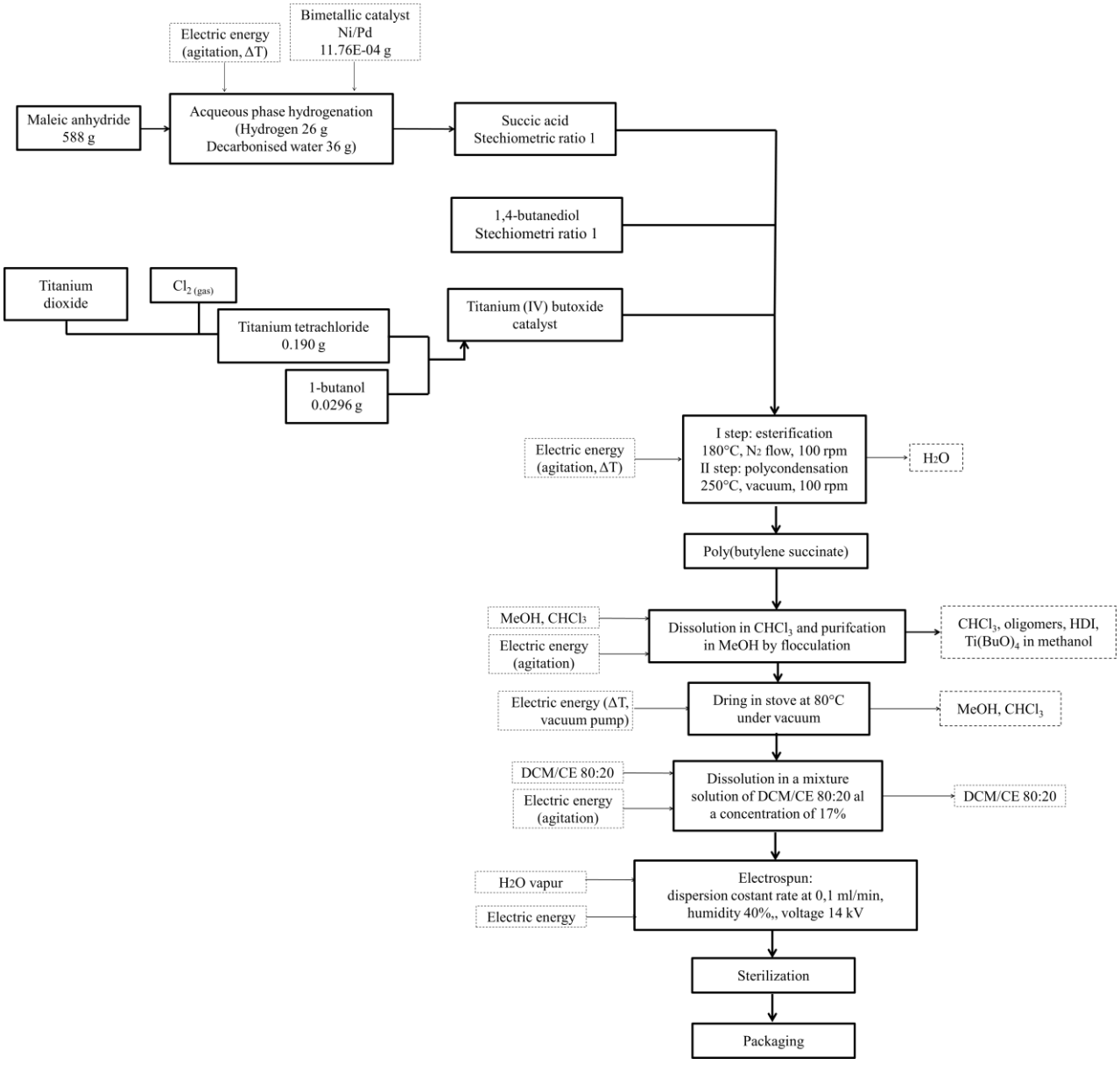

Figure 4.7 Flow chart of the scaffold manufacturing process.

Sterilization

Sterilization is a critical step, because of allows to remove all the possible contaminants that may adhered to the surface of the fibers during processing and make the material suitable to be in contact with the human body. Initially, scaffold was cleaned with ethanol 60% to remove microorganisms and impurities. Later, it was rinsed few times with Phosphate Salt Buffer (8 g NaCl, 0.2 g KCl, 1.44 g Na_2HPO_4, 0.24 g KH_2PO_4 in 1 l of distil water) to remove completely ethanol, that could be harmful for humans.

Packaging

The final product was packed within aluminium and polyethylene bags in an inert atmosphere, and labelled. Now, could be placed on the market.

Some considerations

During the life cycle analysis study some assumptions have been retained in all considerate processes:

- where chemicals were used, an activated carbon filter was forecast to block indoor and outdoor emissions;
- the filter and the exhaust system were designed to 3503.7 Nm^3/h flow;
- emissions were calculated proportionally on the ratio between substance and water boiling points, relaying on an experimental result related to the mass of water evaporated at 30°C.
- emission after filtration were divided into: 99% in atmosphere, 1% in the laboratory. On this latter were considered emission breathe from operator during the processes;
- Indoor emissions damage was calculated on the damage factor of the substance in Eco-indicator99 and IMPACT, dividing the factor to the fate factor and the population density in Eco-indicator99 and after multiplicand to the calculated fate factor and population density of the indoor emission;
- activated carbon of the filters, with a life of 2400 hours, was disposed without considering a possible regeneration;

- any processes consider equipment (including washing), personal protective equipment and systems used;
- the end of life of the substances captured by the filters was considered;
- organic solvents were disposed as hazardous waste to incineration.

The collected data have supposed that:

Goal and scope definition

The aim of this LCA study is the assess meet the environmental impact of the laboratory manufacturing of a scaffold in poly(butylene succinate), in order to identify the hot spot in the synthetic route and evaluate the possible improvements.

Functional unit, function of the system

The functional unit is defined as 50 g of purified poly(butylene succinate) to obtain one scaffold through electrospinning technique. The function of the system is the realization of scaffolds employed in tissue engineering as flexible tridimensional support for cellular growth.

System boundaries

The system boundaries are based on a cradle-to-the-gate approach, starting from the fossil based poly(butylene succinate), till to the final object obtained by electrospinning process. The considered life cycle, shown in Figure 4.7, concern the purification of PBS and the scaffold realization, sterilization and packaging. All these processes take into account production and transportation of chemical materials, facilities and energy consumption, transports and dismantling of waste products, emission into the air and water.

Life cycle inventory

Because of the quality and the credibility of results largely depends on the quality of the data included in the inventory (Pini *et al.*, 2014), primary data used in the study have been collected both directly from the experimental activity (primary data). There are included raw materials and chemicals, synthesis and purification process of PBS and the

used equipments. Secondary data have been obtained from databases to model the background processes (such as land use, material production, transport, fuels and electricity production).

A selection of the most relevant input/output of data used with inventory analysis of the PBS-based scaffold is reported in Table 4.5.

Table 4.5 Collection of input/output data used with inventory analysis.

		Scaffold manufacturing		**Unit**
INPUT	Materials	Succinic acid	52.37E-02	kg
		1,4-Butanediol	47.63E-02	kg
		$Ti(OBu)_4$	81.27E-05	kg
		Liquid nitrogen	36.97E-02	kg
		Chemicals for purification	15.58E+00	kg
		Chemicals for elctrospinning process	24.61E-02	kg
		Chemicals for sterilization	10.75E-02	kg
		Chemicals for phosphate buffer	20.20E-01	kg
		Chemicals for packaging	99.39E-03	kg
	Facilities	Laboratory facilities	25.05E-01	p
	Energies	Electric energy	59.96E+00	kWh
	Transformations	Steel deep grawing	44.11E-06	kg
		Sheet rolling	31.44E-03	kg
		Blow moulding	63.30E-04	kg
	Transports	Facilities transports	58.44E+01	kgkm
		Materials transports	68.75E-01	kgkm
OUTPUT	Emissions to air	Carbon dioxide	21.27E-02	kg
		Water	22.17E-02	kg
		Tetrahydrofuran	72.00E-05	kg
		1,4-Butanediol	21.06E-06	kg
		Butyrolactone	14.40E-05	kg
		Hydrogen chloride	14.58E-04	kg
		Nitrogen	36.97E-05	kg
		Chloroform outdoor	11.11E-04	kg
		Chloroform indoor	34.70E-09	kg
		Methanol outdoor	24.89E-04	kg
		Methanol indoor	91.70E-10	kg
		Dichloromethane outdoor	57.98E-04	kg
		Dichloromethane indoor	25.00E-08	kg
		Hexane outdoor	35.13E-05	kg
		Hexane indoor	12.40E-10	kg
		Ethanol outdoor	58.01E-05	kg
		Ethanol indoor	16.77E-10	kg
	Disposal treatments	Hazardus waste incineration	30.49E+01	kg
		NaCl electrolysis sludge	15.84E-02	kg
		Steel recycling	73.51E-05	kg
		Waste water treatment	20.20E-01	kg
		Aluminium recycling	31.35E-03	kg
		Plastic recycling	63.30E-04	kg
		Paper recycling	25.98E-03	kg
		Shredder fraction treatment	50.00E-04	kg

Chapter 5. Results and Discussion

5.1 Effect of plasma surface modification on the biodegradation rate and biocompatibility of a poly(butylene succinate)-based copolymer

PBS copolymers containing thioether linkages (P(BS85BTDG15)) has been synthesized and characterized from the molecular, thermal and mechanical point of view. The results have been compared to the parent PBS homopolymer. Films obtained by both PBS and P(BS85BTDG15) have been subjected to surface modification by means of non-thermal plasma surface treatment and the effect on physic/mechanical properties has been considered. Hydrolytic degradation rate under physiological conditions and *in vitro* biocompatibility of treated and non-treated polymeric films have been also investigated.

Both the introduction of thioether linkages and the plasma etching enhanced the polymer surface wettability, thus resulting in an increased hydrolytic degradation rate. On the other hand, bulk properties were not significantly affected.

Biocompatibility assays highlighted the absence of potentially cytotoxic products into the culture medium and proved that the investigated polymeric films can support cell adhesion and proliferation.

5.1.1 Synthesis and characterization of the polymers

At room temperature, both the synthesized polyesters appeared as semicrystalline light yellow solids. Tab 5.1 collects the molecular characterization data. PBS_p and P(BS85BTDG15)_p refer to the polymers after plasma treatment. The chemical structure of P(BS85BTDG15) is reported in Figure 4.3.

The two pristine polymers were characterized by relatively high and comparable molecular weights (Table 5.1), indicating that appropriate synthesis conditions and a good polymerization control were achieved. ^{1}H-NMR investigation was performed to verify their chemical structure. The spectra were found to be consistent with the expected structure (Figure S1).

The copolymer composition was calculated from the relative areas of the ^{1}H-NMR resonance peak of the a aliphatic proton of the succinic subunit (located at 2.62 ppm) and of the d protons of the thiodiglycolic subunit (at 4.13 ppm). The actual molar composition is very close to the feed (Table 5.1).

Table 5.1 Molecular characterization data of neat and plasma treated polymers.

Polymer	M_n[a]	PDI[a]	BS[b] (mol%)	WCA (°)
PBS	60200	2.1	100	90 ± 1
PBS_p	60000	2.1	100	79 ± 2
P(BS85BTDG15)	41200	2.3	86	88 ± 1
P(BS85BTDG15)_p	37000	2.3	86	74± 2

a: by GPC

b: by ^{1}H-NMR

Due to the high temperatures involved in the synthesis and the catalyst employed, the comonomeric units along the copolymer macromolecular chain follow a random distribution.

As to PBS_p and P(BS85BTDG15)_p films, no weight losses were observed after the plasma treatment, probably due to the short exposure time (i.e. 30 seconds). It has been in fact reported that weight losses linearly increase with exposure time, and that they are more pronounced for the oxygen plasma due to the oxidative treatment (Hirotsu *et al*., 2000). However, a small decrement of the molecular weight of P(BS85BTDG15) of about 10% was evidenced after treatment, while that of PBS remained unaltered. This can be explained on the basis of the lower bond energy of the C-S bond with respect to the C-C one.

The polymers under study were subjected to thermogravimetric analysis. The temperature corresponding to the onset of the degradation process (T_{onset}) and the temperature corresponding to the maximum weight loss rate (T_{max}) were determined from the thermogravimetic curves (Table 5.2). As evidenced in Figure 5.1 the weight loss takes place in one step. From a comparison between the data reported in Table 5.2, it can be observed that PBS is more thermally stable than P(BS85BTDG15). The result can be attributed to the presence of etheroatoms along the polymeric chain, which reduce the thermal stability of a polymer, since they favour thermo-oxidative processes

(Zimmermann and Grassie, 1984). Both polymers were however characterized by a good thermal stability, above 350°C.

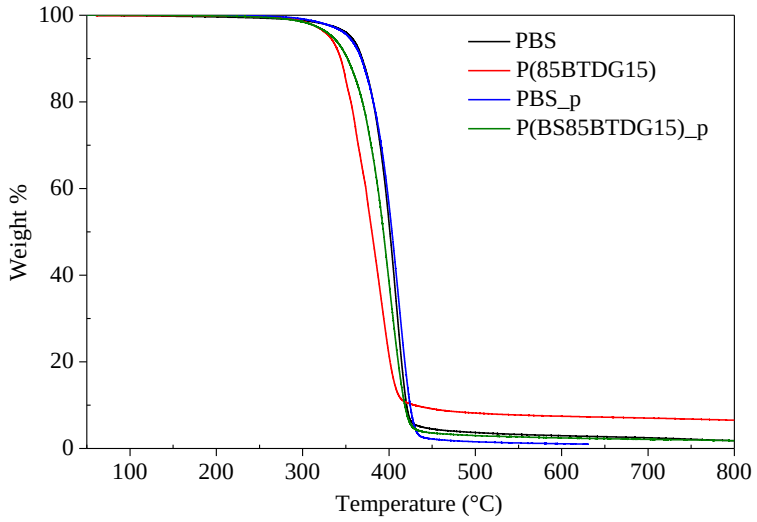

Figure 5.1 Thermogravimetric curves of neat and plasma treated PBS and P(BS85BTDG15).

PBS_p and P(BS85BTDG15)_p showed also a good thermal stability, comparable to the corresponding untreated polymers, although the stability of P(BS85BTDG15) slightly decreased after treatment, probably due to the low molecular weight decrease.

The melting behavior of a polymer is affected by its previous thermal history; therefore, in order to provide the same heat treatment to the samples investigated, prior to thermal analysis each film was kept at room temperature for two weeks. DSC traces of so-treated samples are reported in Figure 5.2a and the data obtained in Table 5.2.

The phase behavior of the two polymers is very similar: both are semicrystalline, being the corresponding calorimetric traces characterized by a conspicuous melting endotherm: the T_m of P(BS85BTDG15) is anyway lower than that of PBS. The perfection of crystalline phase is indeed influenced by the symmetry of the polymeric chain, this latter being reduced in P(BS85BTDG15) because of the introduction of sulphur atoms along the polymer chains.

As far as the glass transition is concerned, the T_gs of the two polyesters are very similar. No significant effect of the presence of the thioether linkages can be observed, because

of the low amount of thiodiglycolic subunit (15 mol%) present along the macromolecular chain.

Table 5.2 Thermal and diffractometric characterization data and water contact angles for PBS and P(BS85BTDG15) random copolymer.

			I scan				*II scan*				
Polymer	T_{onset} **(°C)**	T_{max} **(°C)**	T_m ***(°C)***	T_g ***(°C)***	ΔC_p ***(J/°C g)***	ΔH_m ***(J/g)***	T_g ***(°C)***	ΔC_p ***(J/°C g)***	T_m ***(°C)***	ΔH_m ***(J/g)***	T_{cc} ***(°C)***
PBS	393	409	-35	0.074	114	51	-35	0.085	114	49	81
PBS_p	394	410	-35	0.077	114	50	-35	0.087	114	48	79
P(BS85BTDG15)	354	391	-37	0.088	101	45	-37	0.094	101	43	62
P(BS85BTDG15)_p	349	379	-37	0.117	101	44	-37	0.123	101	42	60

To confirm that in P(BS85BTDG15) the ability of PBS to crystallize decreases, non-isothermal experiments were carried out, subjecting the samples to a controlled cooling rate from the melt. It is worth remembering that the half-time of primary crystallization in isothermal experiments correlates with the temperature of the maximum of the crystallization peaks in non-isothermal experiments (T_{cc}) (Legras *et al.*, 1986), being this latter more easily obtainable. As expected, the temperature of the maximum of the exothermal crystallization peak is lower for P(BS85BTDG15). This fact indicates a decrement of the overall crystallization rate of PBS, due to the presence of co-units which act as obstacles in the regular packing of polymer chains. The exothermic crystallization peaks of the samples under investigation are shown in Figure 5.2b. The second scan after rapid cooling from the melt (at about 100°C min^{-1}) did not highlight any variation with respect to the first scan, indicating that the crystallinity of these samples cannot be hampered by quenching (Table 5.2). No significant differences in the thermal behavior were observed for PBS_p and P(BS85BTDG15)_p as compared to the corresponding neat polymers.

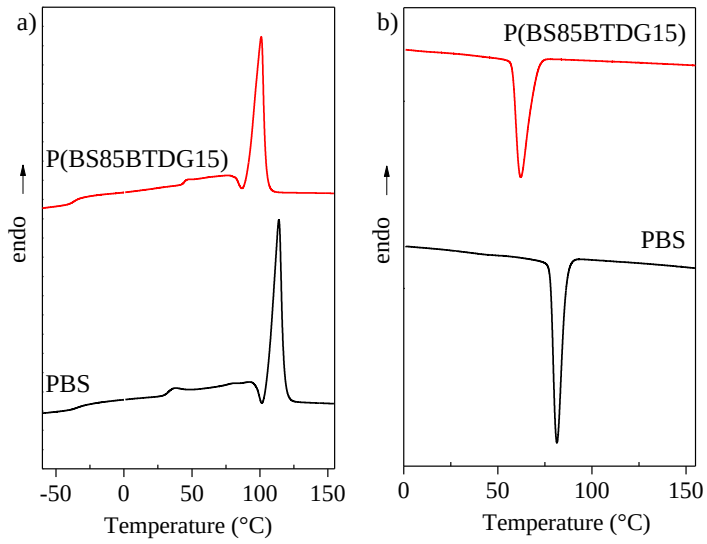

Figure 5.2 Calorimetric curves of PBS and P(BS85BTDG15): (a) I scan, (b) cooling from the melt.

In order to investigate the relative hydrophilicity of PBS and P(BS85BTDG15) films, water contact angle (WCA) measurements were performed. It has to be pointed out that surface wettability reflects surface hydrophilicity but, in the present case, it cannot be directly correlated with bulk material hydrophilicity. Table 5.1 reports the contact angle values for the two polymers, while in Figure 5.3 water drops deposited on the polymer surface are shown.

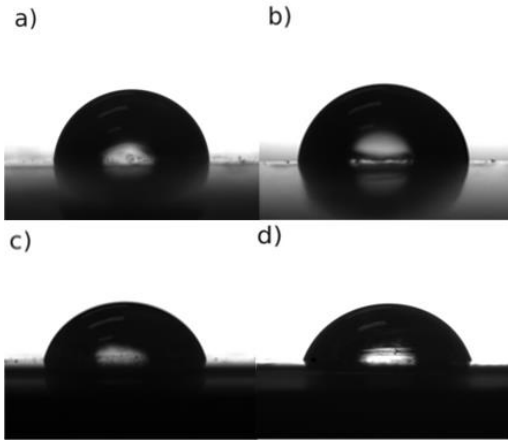

Figure 5.3 Water drops on the polymeric film surface of: a) PBS, b) P(BS85BTDG15), c) PBS_p, d) P(BS85BTDG15)_p.

PBS displayed a more hydrophobic nature with respect to the copolymer: this result, in agreement with previous findings (Soccio *et al.*, 2012), can be explained on the basis of the presence along the polymeric chain of PBS of electronegative sulphur atoms. Interestingly, an increase in the film wettability was displayed after plasma treatment. As a matter of fact, the WCAs of PBS and P(BS85BTDG15) decreased of 12% and 16% respectively, thus evidencing the effectiveness of the plasma etching.

5.1.2 Studies of mechanical properties

The mechanical properties of neat and treated PBS and P(BS85BTDG15) were investigated subjecting the samples to stress-strain measurements. Table 5.3 reports their corresponding mechanical data (elastic modulus, E, stress at break, σb, and deformation at break, εb).

Table 5.3 Mechanical characterization data of neat and treated polymeric films.

Polymer	E (MPa)	σ_b (MPa)	ε_b (%)
PBS	370 ± 6	34 ± 1	42 ± 5
PBS_p	366 ± 3	35 ± 2	37 ± 9
P(BS85BTDG15)	310 ± 8	23 ± 2	60 ± 5
P(BS85BTDG15)_p	290 ± 3	20 ± 3	39 ± 7

As it can be seen, the two polyesters were characterized by similar behavior, even though P(BS85BTDG15) displayed a lower elastic modulus. Since both polymers possess a soft amorphous phase (T_g values are in all cases well below room temperature), the observed trend can be ascribed to two effects: changes in copolymer composition and in crystallinity degree. As reported in Table 5.3, the plasma etching did not affect the PBS tensile behavior, which remained unaltered. On the other hand, a lowering of E, σb and εb was shown by P(BS85BTDG15)_p with respect to the neat polymer, most probably due to the decrease of the molecular weight after treatment.

5.1.3 Hydrolytic degradation studies

Hydrolytic degradation experiments were performed under physiological conditions on the neat and treated polymers in order to evaluate the effect of the introduction of

hydrophilic BTDG units in the PBS macromolecular chains and of the plasma surface etching on the hydrolysis rate. Weight losses are reported in Figure 5.4a as a function of time. Both an effect of the presence of sulphur atoms and of the plasma treatment can be observed.

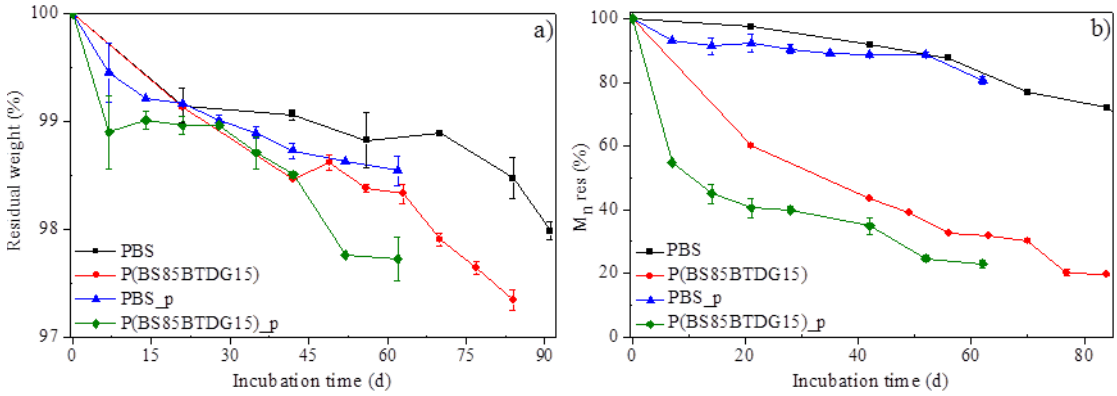

Figure 5.4 Residual weight (a) and residual number molecular weight ($M_{n,res}$) (b), as a function of incubation time.

The weight losses of treated or not P(BS85BTDG15) were higher than those of PBS in the time scale explored. A decrease of only 2-3% of the initial weight was observed for all samples, due to its highly crystalline nature. Monitoring the molecular weight it is clear that the hydrolytic attack was occurred. In Figure 5.4b, which reports the percentage of residual number average molecular weight ($M_{n,res}$%) as a function of incubation time, all the polymers (neat and treated ones) underwent a significant decrease of M_n with time. Moreover, the difference between the PBS and the copolymer was significantly enhanced. On the contrary, the plasma treated samples highlighted only a slight increased hydrolysis rate as compared to the corresponding neat polymer. This result underlines that the introduction of thioether linkages played a greater role to enhance the hydrolysis rate with respect to the plasma treatment. As a matter of fact, the presence of sulphur atoms not only increased the wettability of PBS, but also decreased the crystallinity degree, one of the main factors influencing the polymer biodegradation (Gigli *et al.*, 2012, 2013).

5.1.4 Biocompatibility and gene expression assay

The PrestoBlue® fluorescence assay was used to evaluate the potential indirect cytotoxicity of PBS homopolymer and P(BS85BTDG15) random copolymer on H9c2 cells.

As shown in Figure 5.5, data indicate the absence of potentially cytotoxic products released from both polymers into the culture medium, also when they were subjected to surface plasma treatment. In fact, samples grown for 72 hours in PBS, PBS_p, P(BS85BTDG15) and P(BS85BTDG15)_p extraction medium exhibited comparable fluorescence outputs of the assay and equivalent to the value obtained for the standard DMEM control. Otherwise, when exposed to 1 mM H_2O_2 for 2 hours, as a positive cytotoxicity control, all the cells were killed.

PrestoBlue® fluorescence assay was also used to estimate cell adhesion and proliferation: quantification was performed by fluorescence measurements on aliquots of medium withdrawn up to 4 weeks (1, 7, 14, 21 and 28 days).

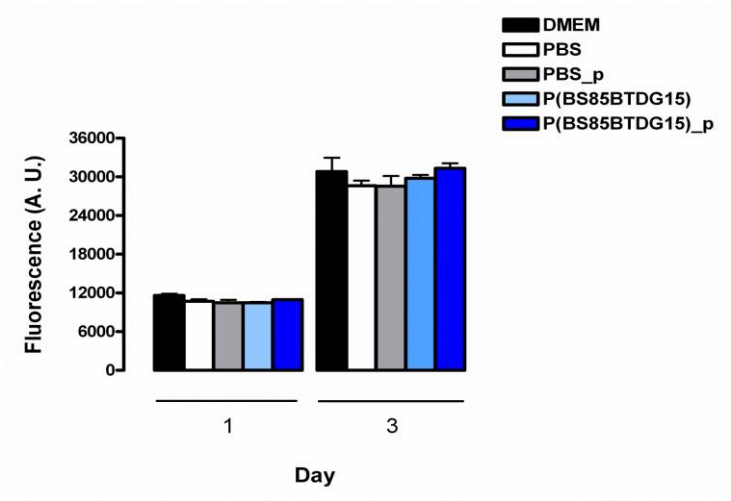

Figure 5.5 Evaluation of indirect cytotoxicity: fluorescence measurements expressed in arbitrary units.

As reported in Figure 5.6, after 24 hours from cell seeding all films harbour about the same number of cells. For all the tested polymers, this is about 40% of the number of H9c2 cells, which adhered to the control polystyrene surface. H9c2 cells continued to grow on the film surfaces up to 28 days in culture highlighting that tested samples,

homopolymer and copolymer, surface plasma treated or not, sustained an equivalent cell adhesion and proliferation.

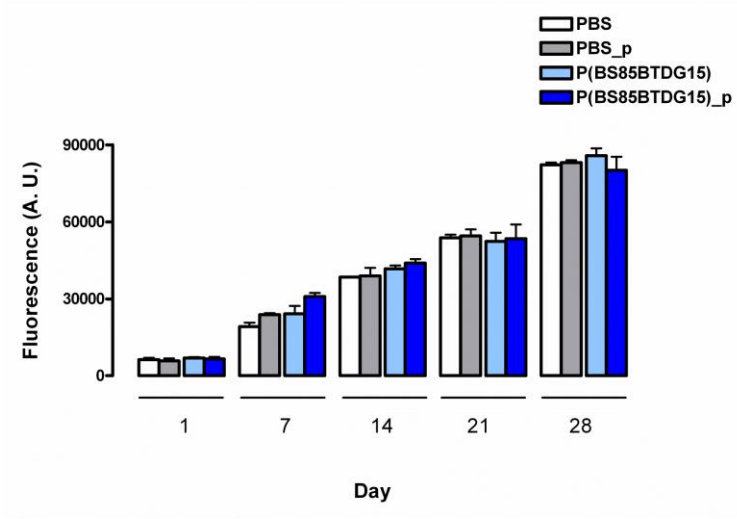

Figure 5.6 Proliferation assay: fluorescence measurements expressed in arbitrary units per day.

Psysicochemical features of polymeric substrates may act as an input for the activation of differentiation patterns specific to cell lineage (Riboldi *et al.*, 2005; Candiani *et al.*, 2010). The level of expression of sarcomeric myosin heavy chain (MHC), a typical marker of muscle differentiation, was thus quantified in H9c2 cells grown over our original polymers. Real time PCR results (Figure 5.7) show that the plasma treatment of our polymeric substrates determines a slight (proximal to the statistical significance limit) increase in this parameter, suggesting that an appropriate tuning of the plasma surface modification might result useful to induce a desirable cell commitment, in addition to impact the physical properties of biomaterials of interest.

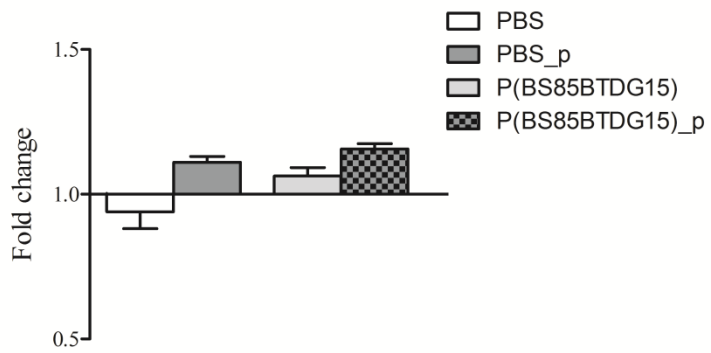

Figure 5.7 Real time PCR data on myosin heavy chain expression. PBS vs. PBS_p: P = 0.0522; P(BS85BTDG15) vs. P(BS85BTDG15)_p: P = 0.0495.

5.1.5 Comment on results obtained

A random PBS-based copolymer containing thioether linkages has been successfully synthesized with good control over the polymerization, as highlighted by the high molecular weight and the actual composition close to the feed. As expected, the introduction of BTDG sequences into the PBS macromolecular chain resulted in an increased surface wettability and a reduced crystallinity and crystallization rate. All these factors affected hydrolytic degradation rate. As a matter of fact, P(BS85BTDG15) showed higher weight losses and larger molecular weight variations with respect to PBS in the time frame explored.

Non-thermal plasma treatment was performed on both polymers under study with promising results, as it permitted to enhance the surface hydrophilicity with respect to the neat polymers. Moreover, it did not significantly affect the bulk properties of the materials, although P(BS85BTDG15) displayed a slight decrease in the molecular weight after the plasma etching, probably due to the breaking of some C-S bonds which possess lower bond energy with respect to the C-C ones.

Biocompatibility assays performed in accordance with the ISO 10993-5 international standard for biological evaluation of medical devices evidenced the absence of potentially cytotoxic products released into the culture medium by the polymers under investigation and demonstrated that the polymeric films can support cell adhesion and proliferation. In addition, myosin heavy chain expression, a marker of a muscle phenotype, showed a tendential increase in cells seeded on plasma treated samples,

suggesting that an appropriate tuning of the surface modification might represent a strategy to initiate a phenotypic cell commitment.

5.2 Hydrolysable PBS-based poly(ester urethane)s thermoplastic elastomers

A new class of aliphatic PBS-based poly(ester urethane)s was synthesized and characterized. To obtain copolymers showing both thermoplastic and elastomeric properties, two hydroxyl-terminated oligomers have been synthesized by melt polycondensation: poly(butylene succinate), as *hard segment*, and two poly(butylene adipate/diglycolate) (P(BAmBDGn) random copolymers as *soft segment*. The introduction of ether-linkages along the PBA chain permitted to depress its crystallinity degree and to enhance the wettability. Multiblock copolymers were finally obtained by chain extending with hexamethylene diisocyanate each P(BAmBDGn) copolymer with two different mass percentages of PBS: 30% and 50%. All copolymers maintained good thermal stability and were characterized by melting temperatures above 100°C. Elastic modulus (E) and stress at break (σb) varied with the chemical composition: the higher the PBS amount, the higher E and σb. No yield and very high elongations at break were observed. Hydrolytic degradation studies highlighted an increase of the degradation rate with the increase of the BDG content.

5.2.1 Synthesis and characterization of the polymers

After the purification process (Chapter 4.1.2 and 4.2.2), the OH-terminated PBS-OH and P(BA70BDG30)-OH copolymer appeared as semicrystalline white floccules, while P(BA50BDG50)-OH as a light yellow coloured rubber. The synthesized prepolymers are listed in Table 5.4, which also collects the data of molecular characterization.

The molecular weight and the chemical structure of PBS-OH and P(BAxBDGy)-OH prepolymers have been determined by ^{1}H-NMR spectroscopy: as an example, ^{1}H-NMR spectra of PBS-OH and P(BA50BDG50)-OH are shown in Figure S2 and Figure S3, together with the chemical shift assignments. In all cases, the spectra were found to be consistent with the expected structure. The copolymer composition was calculated from

the relative areas of the ^{1}H-NMR resonance peak of the **k** aliphatic proton of the adipic subunit (located at 2.33 ppm) and of the e protons of the diglycolic subunit (at 4.24 ppm). From the data of Table 5.4, it can be seen that in all cases the actual molar composition is very close to the feed one.

Table 5.4 Molecular characterization data of PBS-OH and of P(BAxBDGy)-OH copolymers.

Prepolymer	M_n[a] (g/mol)	BDG[a] (mol %)	$OH_{terminal}$ (%)
PBS-OH	5950	-	98.3
P(BA70BDG30)-OH	10950	28	97.8
P(BA50BDG50)-OH	12300	49	97.5

a: by ^{1}H-NMR

Copolymer degree of polymerization (DP) has been calculated from the relative areas of protons of central butandiol at 4.20 (f) and 4.09 (g) ppm and l and m protons of terminal butandiol situated at 3.68 ppm; then the copolymer molecular weight (M_n) has been obtained according to the following formula:

$$M_n = DP\cdot(M_{wDG} + MwA + 56.12) + 89.12\cdot2 \quad \textbf{[11]}$$

where:

M_{wDG} subunit is the molecular weight of the diglycolic subunit in the polymer chain;

M_{wA} subunit is the molecular weight of the adipic subunit in the polymer chain;

BDG content is the actual BDG co-unit content in the polymer;

BA content is the actual BA co-unit content in the polymer;

56.12 is the molecular weight of the butandiol in the polymer chain;

89.12 is the molecular weight of the terminal butandiol (considering 100% of OH terminal groups).

On the other hand, PBS DP was obtained from the relative areas of protons of central butandiol at 4.13 (b) and protons of terminal butandiol situated at 3.68 (d) ppm; its molecular weight was then obtained by:

$$Mn = DP\cdot M_{wPBS} + 89.12\cdot2 \quad \textbf{[12]}$$

where:

M_{wBS} is the molecular weight of BS repeating unit in the polymer chain (174 g/mol).

As to the OH terminal groups content, in all cases it was higher than 97.5%, meaning a high hydroxyl group concentration and therefore that optimized polymerization conditions have been adopted. The molecular weight of the synthesized prepolymers has been also determined from the hydroxyl number using the following equation:

$Mn = (2 \cdot M_{wNaOH} \cdot 1000) / (\text{hydroxyl group number} + \text{carboxyl group number})$ **[13]**

PBS and P(BAxBDGy) copolymers were afterwards examined by differential scanning calorimetry and the resulting data are reported in Table 5.5. PBS and P(BA70BDG30) calorimetric curves displayed both a glass transition and a melting endotherm, while in the case of P(BA50BDG50) only an intense endothermal baseline deviation associated with the glass transition has been observed. Indeed, the increase in the amount of BDG co-units added to PBA, led to a drastic reduction of the heat of fusion, up to the obtainment of a completely amorphous material. It is also worth noting that the higher the BA mol% in P(BAxBDGy) copolymers, the lower the T_g, being the PBA and PBDG T_gs equal to -61 °C (Tserki *et al.*, 2006) and -27 °C (Gigli *et al.*, 2012), respectively. The higher T_g value of PBDG with respect to PBA can be explained on the basis of interchain interactions among PBDG macromolecular chains, due to the electronegativity of ether-oxygen atoms (Eisenberg, 1984).

Table 5.5 Thermal characterization data of PBS-OH and of P(BAxBDGy)-OH copolymers.

Prepolymer	T_g (°C)	ΔCp (J/°C g)	T_m (°C)	ΔH_m (J/g)
PBS-OH	-32	0.087	112	79
P(BA70BDG30)-OH	-51	0.28	39	25
P(BA50BDG50)-OH	-48	0.54	-	-

The multiblock copolymers have been obtained adding an equimolar amount of HDI with respect to the OH group concentration to the molten prepolymers. After the chain extension process, the PBS and the multiblock copolymers appeared as semicrystalline solids, white and light yellow coloured respectively. No unreacted HDI was detected by NMR after one hour of reaction. As an example, the NMR spectrum of the $PBS_{30}P(BA50BDG50)_{70}$ multiblock copolymer is reported in Figure S4: with p, q and r

are indicated the protons of the chain extender (located at 3.30 ppm, 1.34 ppm and 1.25 ppm, respectively). All the spectra are consistent with the expected structure. The actual composition resulted very close to the feed and the HDI content was in all cases below 5% (Table 5.6).

Table 5.6 reports also the molecular weight data obtained by GPC. As expected, the samples show a significant higher molecular weight with respect to the prepolymers and, moreover, a pretty narrow polydispersity was found, indicating a good control over the chain extension process.

Table 5.6 Molecular characterization data of PBS and of $PBS_mP(BAxBDGy)_n$ copolymers.

Polymer	M_n[a] (g/mol)	D[a]	BS[b] (mol%)	BDG[b] (mol%)	%HDI[b] (mol%)	WCA (%)
PBS	81200	2.5	100	-	4.0	92 ± 2
$PBS_{50}P(BA70BDG30)_{50}$	76100	2.3	53	14	3.7	96 ± 1
$PBS_{30}P(BA70BDG30)_{70}$	77000	2.3	33	20	3.3	92 ± 2

a: by GPC

b: by ^{1}H-NMR

The polyesters have been subjected to thermogravimetric analysis under dry nitrogen atmosphere; the temperature corresponding to 5% weight loss ($T_{5\%\ w.loss}$) and the temperature corresponding to the maximum weight loss rate (T_{max}) were determined from the thermogravimetric curves and collected in Table 5.7.

The thermal degradation took place practically in one step. Thermal stability of all the synthesized copolymers was comparable to that of PBS homopolymer; anyway, with the increasing of BDG unit content, the thermal degradation process started at slightly lower temperatures (lower $T_{5\%\ w.loss}$); this is due to the presence of ether-oxygen atoms which favor the thermal oxidation processes.

Table 5.7 Thermal characterization data (I scan) and crystallinity degree of PBS and $PBS_mP(BAxBDGy)_n$ copolymers.

	I scan					
Polymer	**$T_{5\%}$ (°C)**	**T_{max} (°C)**	**T_{mBS} (°C)**	**ΔH_{mBS} (J/g)**	**T_{mBABDG} (°C)**	**ΔH_{mBABDG} (J/g)**
PBS	339	402	112	51	-	-
$PBS_{50}P(BA70BDG30)_{50}$	337	400	106	28	10	5
$PBS_{30}P(BA70BDG30)_{70}$	337	402	104	19	18	10
$PBS_{50}P(BA50BDG50)_{50}$	335	401	105	29	-	-
$PBS_{30}P(BA50BDG50)_{70}$	329	402	101	15	-	-

It is well established that the melting behavior of a polymer is affected by its previous thermal history; therefore, in order to provide the same heat treatment to all the samples investigated prior to thermal analysis each sample was kept at room temperature for two weeks. DSC traces of so-treated samples are reported in Figure 5.8a and the data obtained in Table 5.7.

In all cases, a glass transition and a melting endotherm are evident. In the case of $PBS_{50}P(BA70BDG30)_{50}$ and $PBS_{30}P(BA70BDG30)_{70}$, two well separated melting peaks are observed, whose temperature regularly decreases as the content of P(BA70BDG30) in the multiblock copolymer increases. The main endothermic peak present in all the copolymers located at high temperature is surely due to the fusion of PBS crystalline sequences. The less intense endothermic peak observed only in $PBS_{50}P(BA70BDG30)_{50}$ and $PBS_{30}P(BA70BDG30)_{70}$ multiblock copolymer DSC thermograms is on the contrary reasonably ascribed to the fusion of BA sequences, which in the copolymers under study are present in major amount and are characterized by a higher crystallization rate with respect to BDG ones (Gigli *et al.*, 2012; Tserki *et al.*, 2006). WAXS analysis permitted to verify our hypothesis.

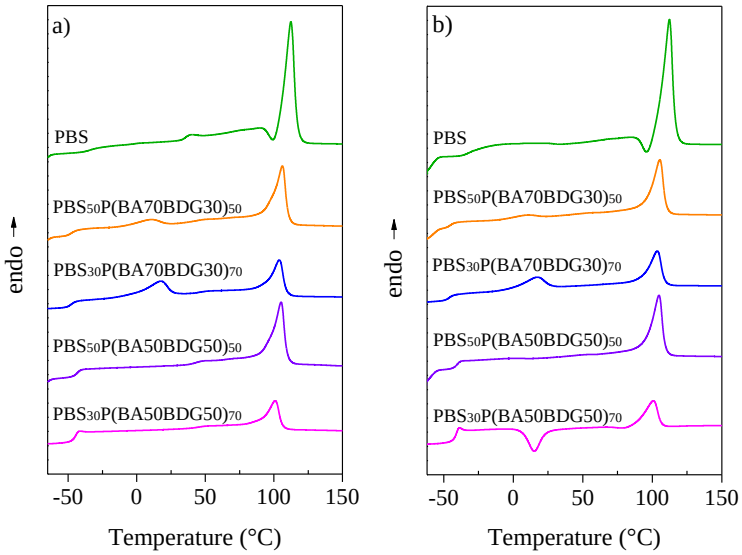

Figure 5.8 Calorimetric curves of $PBS_mP(BAxBDGy)_n$: a) I scan; b) II scan after melt quenching.

As to the PBS, it presented the highest melting temperature (112°C) and heat of fusion (51 J/g). It is worth highlighting that all copolymers are characterized by a melting temperature above 100°C, even if a slight decrease with respect to PBS was observed. On the other hand, the $PBS_mP(BAxBDGy)_n$ copolymers displayed a significant decrease in the heat of fusion in comparison to PBS, indicating a reduced level of crystallinity. This is due to two different effects: i) to the decrease of the PBS content ii) and/or to the decrease of crystallisable BA co-units in the soft segments. In other words, the higher the BDG unit content, the lower the heat of fusion.

In order to clarify the nature of the crystalline phase present in the polymers under investigation, the structural characterization of $PBS_mP(BAxBDGy)_n$ polymers was carried out by wide angle X-ray diffraction: the diffraction patterns of the multiblock copolymers are reported in Figure 5.9 together with that of PBS added for sake of comparison.

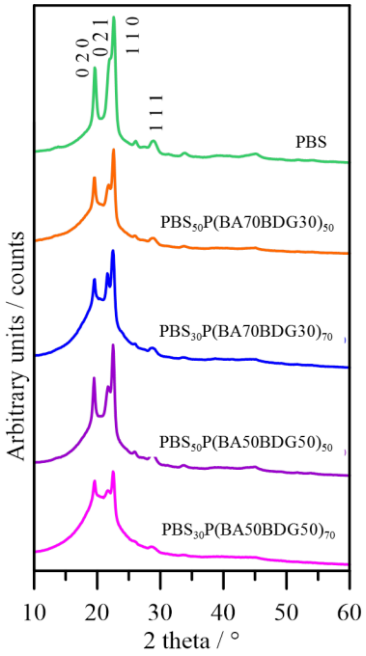

Figure 5.9 X-ray diffraction patterns of PBS and $PBS_mP(BAxBDGy)_n$ copolymers.

As it can be seen, the WAXD patterns of copolymers appeared to be characterized by relatively intense diffraction peaks. All the copolymer samples exhibit the PBS type pattern with the two main peaks *020* and *110* at about 19.6° and 22.8° (2θ, d= 0.45 and 0.39 nm), demonstrating that in all the samples a PBS type crystal phase is present. In addition, a slight enlargement of the interlayer distances is present in the copolymers, the most affected being the *021* reflection. This can be explained on the basis of the difficulty to accommodate both the larger comonomeric units (BA and BDG) in the PBS cell. In $PBS_{30}P(BA70BDG30)_{70}$ sample the *021* reflection shifts significantly, so much so that the *021* reflection can be completely distinguished from the *110* one; the presence of PBA crystal phase in this copolymer is therefore supported also by WAXS analysis. As to the crystallinity degree, it appreciably decreases as the BS unit content decreases, in agreement with calorimetric results (Table 5.8).

Table 5.8 Diffraction data and crystallinity degree of PBS and $PBS_mP(BAxBDGy)_n$ copolymers.

Polymer	*0 2 0*	*0 2 1*	*1 1 0*	*1 1 1*	χ_c (%)
PBS	0.4524	0.4050	0.3935	0.3093	44 ± 4
$PBS_{50}P(BA70BDG30)_{50}$	0.4540	0.4079	0.3940	0.3101	37 ± 3
$PBS_{30}P(BA70BDG30)_{70}$	0.4542	0.4105	0.3957	0.3111	27 ± 3
$PBS_{50}P(BA50BDG50)_{50}$	0.4554	0.4087	0.3950	0.3102	33 ± 3
$PBS_{30}P(BA50BDG50)_{70}$	0.4537	0.4094	0.3949	0.3121	24 ± 3

To confirm that in the copolymers the tendency of PBS to crystallize decreases as the BDG unit content is increased, non-isothermal experiments were carried out, subjecting the samples to a controlled cooling rate from the melt (Figure 5.10).

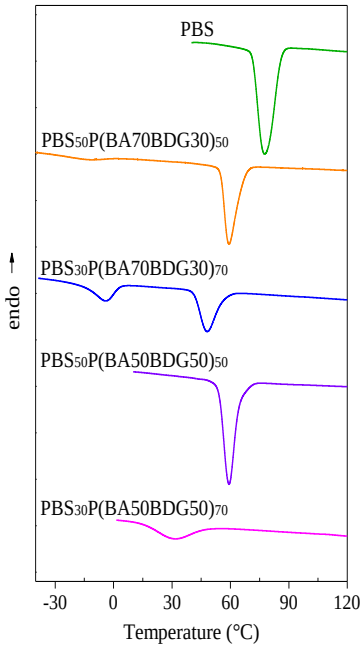

Figure 5.10 DSC crystallization exotherms of PBS and $PBS_m(BAxBDGy)_n$ random copolymers cooled from the melt at 5°C/min.

It is worth remembering that the half-time of primary crystallization in isothermal experiments correlates with the temperature of the maximum of the crystallization peaks in non-isothermal experiments (T_{cc}) (Legras *et al.*, 1986), being this latter more easily obtainable. The exothermic crystallization peaks of the samples under investigation are

shown in Figure 5.10 and the T_{cc} are reported in Table 5.9. In all copolymers, a significant reduction of the PBS crystallization rate can be observed, due to the presence of the P(BAxBDGy) sequences: the lower the PBS content the lower the crystallization rate. This effect is completely independent on the P(BAxBSGy) copolymer composition; as a matter of fact $PBS_{50}P(BA70BDG30)_{50}$ and $PBS_{50}P(BA50BDG50)_{50}$ showed the same T_{cc} (59°C), being the actual PBS content in both copolymers very close, 53 and 55%, respectively. On the other hand, $PBS_{30}P(BA70BDG30)_{70}$ and $PBS_{30}P(BA50BDG50)_{70}$, displayed two T_{cc}s, which are very different from each other, due to the different actual PBS content: 33 and 26%, respectively. In addition, in the multiblock copolymers containing the P(BA70BDG30) sequences, a second crystallization peak can be noted, confirming the presence of the PBA second crystalline phase, besides the PBS one. This is more evident in the $PBS_{30}P(BA70BDG30)_{70}$, as already shown through DSC and WAXS analyses, because of the higher BA unit content.

Furthermore, in order to study the influence of chemical structure on the glass transition of the multiblock copolymers, the phenomenon should be examined in the total absence of crystallinity. In this view, all the samples under investigation were subjected to rapid cooling (quenching) from the melt. The DSC curves after melt quenching are shown in Figure 5.8b and the results are reported in Table 5.9: the calorimetric traces of all the polymers under investigation are typical of semicrystalline polymers. As to the melting phenomenon, the behavior is substantially analogous to that observed in the first scan, with the exception of $PBS_{30}P(BA50BDG50)_{70}$ copolymer.

Table 5.9 Thermal characterization data (II scan after melt quenching) of PBS and $PBS_mP(BAxBDGy)_n$ copolymers.

II scan

Polymer	T_g (°C)	ΔCp (J/°C g)	T_c (°C)	ΔH_c (J/g)	T_{mBS} (°C)	ΔH_{mBS} (J/g)	T_{mBABDG} (°C)	ΔH_{mBABDG} (J/g)	T_{ccBS} (°C)	$T_{ccBABDG}$ (°C)
PBS	-30	0.21	-	-	112	54	-	-	77	-
$PBS_{50}P(BA70BDG30)_{50}$	-45	0.20	-	-	105	26	9	3	59	-
$PBS_{30}P(BA70BDG30)_{70}$	-46	0.29	-	-	104	18	17	11	48	-4
$PBS_{50}P(BA50BDG50)_{50}$	-41	0.32	-	-	105	27	-	-	59	-
$PBS_{30}P(BA50BDG50)_{70}$	-42	0.52	15	-13	101	15	-	-	31	-

In the case of this last sample interestingly, DSC trace evidenced a glass transition followed by an exothermal "cold crystallization" peak and a melting endotherm at higher temperature. The enthalpy of crystallization is very similar to the corresponding heat of fusion, indicating that this copolymer can be frozen into a completely amorphous state by quenching. As mentioned above in the case of the prepolymers, the glass transition temperature is influenced by the amount of BA units in the chain and practically the same trend was found.

In order to investigate the relative hydrophilicity of PBS and $PBS_mP(BAxBDGy)_n$ copolymers, water contact angle (WCA) measurements were performed. It has to be pointed out that surface wettability reflects surface hydrophilicity but, in the present case, it cannot be directly correlated with bulk material hydrophilicity. Table 5.6 reports the contact angle values for each polymer and in Figure 5.11 as an example, the water drops deposited on some of the polymeric films under study are shown.

The copolymer wettability is remarkably affected by the copolymer composition: as expected, hydrophilicity regularly increases with the increasing of the BDG mol%: as a matter of fact $PBS_{50}P(BA70BDG30)_{50}$ displayed the lowest hydrophilicity (96°) and $PBS_{30}P(BA50BDG50)_{70}$ the highest (86°), being the BDG unit content 14 and 34%, respectively. This result can be explained on the basis of the presence along the polymeric chain of highly electronegative ether-oxygen atoms.

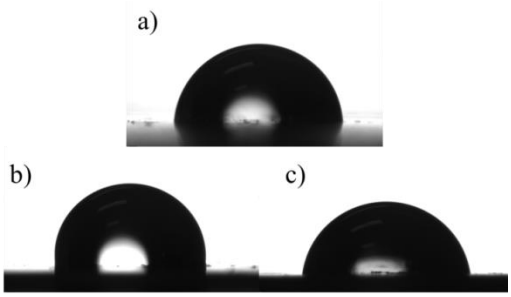

Figure 5.11 Water drops on the polymeric film surface of: a) PBS, b) $PBS_{50}P(BA70BDG30)_{50}$, c) $PBS_{30}P(BA50BDG50)_{70}$.

Interestingly, PBS resulted more hydrophilic than $PBS_{50}P(BA70BDG30)_{50}$, despite the absence of ether-linkages; this is probably due to the longer hydrophobic methylene sequences present in the BA co-units with respect to the BS ones.

5.2.2 Studies of mechanical properties

The mechanical properties of the polymers under investigation were analysed by subjecting the samples to stress-strain measurements. Their tensile behavior of the PBS and multiblock copolymers is shown in Figure 5.12, while Table 5.10 reports the corresponding mechanical data.

Table 5.10 Mechanical data of PBS and $PBS_mP(BAxBDGy)_n$ copolymers.

Polymer	E (MPa)	σ_b (MPa)	ε_b (%)
PBS	366 ± 5	27 ± 2	303 ± 21
$PBS_{50}P(BA70BDG30)_{50}$	111 ± 4	30 ± 2	1085 ± 75
$PBS_{30}P(BA70BDG30)_{70}$	41 ± 5	12 ± 2	942 ± 11
$PBS_{50}P(BA50BDG50)_{50}$	102 ± 2	21 ± 3	939 ± 30
$PBS_{30}P(BA50BDG50)_{70}$	23 ± 3	8 ± 1	1410 ± 107

All the copolymers evidenced the typical behavior of thermoplastic elastomers: no yield, high toughness, and excellent εb (about 1000%).

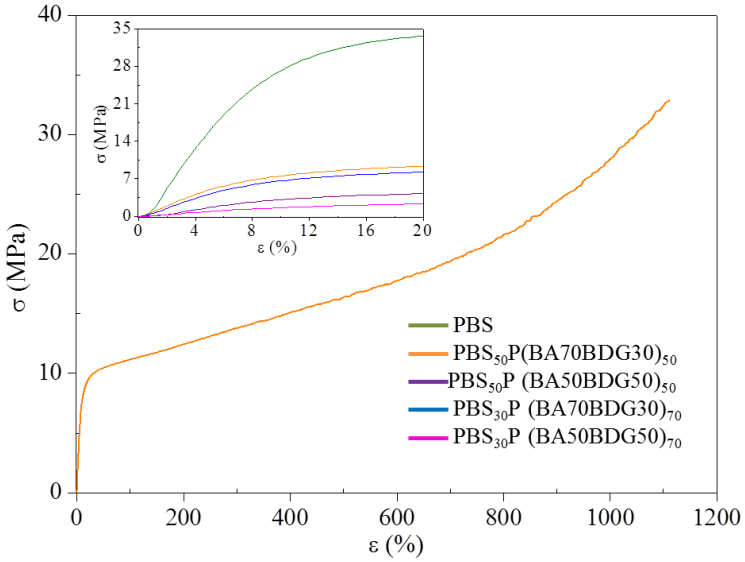

Figure 5.12 Stress-strain curve of $PBS_{50}(BA70BDG30)_{50}$. In the inset, an enlargement of the initial portion of the stress-strain curve of PBS and multiblock copolymers.

As expected, the elastic modulus and stress at break of these materials varied with the crystallinity degree, since all the investigated polymers display a soft amorphous phase (T_g values are in all cases well below RT): the higher the χc, the higher the E and σb.
Overall, mechanical characterization demonstrated that the chain extension of an *hard segment* (PBS) with a *soft* one (P(BAxBDGy) copolymers) resulted in a significant improvement of the homopolymer mechanical properties, which can be properly modulated by varying the mutual amount of the two segments and/or the kind of the soft segment.

5.2.3 Hydrolytic degradations studies

Hydrolytic degradation experiments have been carried out under physiological conditions (37°C, pH 7.4) in phosphate buffer to study the biodegradation kinetic of the synthesized materials in human body mimicking conditions.
In Figure 5.13a the residual weight of PBS and $PBS_mP(BAxBDGy)_n$ is reported as a function of the incubation time.

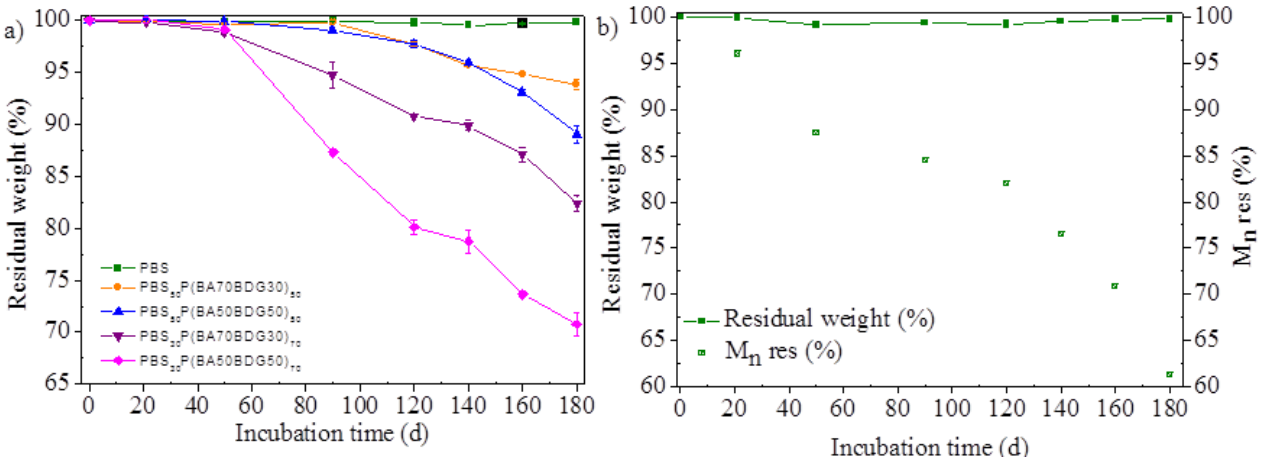

Figure 5.13 a) Residual weight (%) as a function of incubation time for PBS and $PBS_mP(BAxBDGy)_n$ copolymers; b) PBS residual weight (%) and residual number molecular weight as a function of incubation time.

In the time scale explored, PBS did not lose any weight, whereas all copolymers appreciably degraded. As it can be seen from Figure 5.13a, the degradation rate is strongly dependent on the copolymer composition; as a matter of fact the higher the BDG mol%, the higher the degradation rate. After 180 days, $PBS_{30}P(BA50BDG50)_{70}$ lost almost 30% of its initial weight. The slowest degradation rate was on the contrary displayed by $PBS_{50}P(BA70BDG30)_{50}$, which residual weight at the end of the experiments was about 94%.

It is well known (Vert, 2005) that in the first stages of hydrolytic degradation substantial decrease in molecular weight occurs, even if weight losses are still negligible. In this view, PBS incubated samples have been subjected to molecular weight determination to verify the occurrence of the hydrolytic attack. As shown in Figure 5.13b, which reports the percentage of residual number average molecular weight (M_n res%) as a function of incubation time, PBS underwent a significant decrease of M_n with time, confirming the starting of the degradation process. Moreover, as already observed for other polymeric systems (Bikiaris *et al.*, 2006) the polydispersity index decreased with the incubation time from 2.49 (0d) to 2.16 at the end of the experiment (180d). The M_n of multiblock copolymers decreased too, displaying a similar trend with respect to weight loss measurements (results not shown). The results obtained can be explained on the basis of

the different factors affecting the biodegradation rate of a polymer; among all, crystallinity degree, crystal perfection and hydrophilicity. As a matter of fact, the presence of BDG co-units resulted in an enhanced hydrophilicity and reduced crystallinity degree and crystal perfection. In particular, hydrophilicity regularly increased, whereas crystallinity degree and crystal perfection regularly decreased with the increase of BDG mol% (Table 5.6 and Table 5.8). A confirmation that the amorphous regions of the polymer are degraded more quickly than the crystalline ones, was obtained by subjecting the partially degraded copolymer samples to a heating calorimetric scan (20 °C/min).

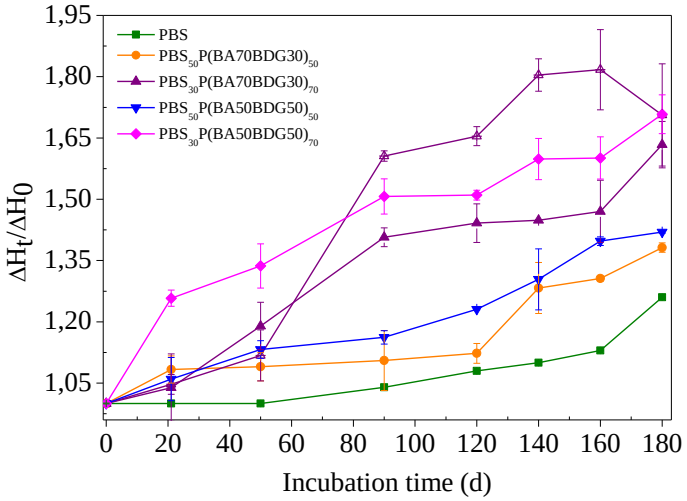

Figure 5.14 Normalized heat of fusion as a function of incubation time for PBS and $PBS_mP(BAxBDGy)_n$ copolymers. Open symbol represent the heat of fusion of the lower melting temperature peak.

It is worth remembering that the increment of the crystalline/amorphous ratio can be also due to an additional process, occurring when a polymer is placed at a temperature comprised between its T_g and T_m (as 37°C is for this class of polyesters). This phenomenon, called annealing, consists in the increase and improvement of the crystalline phase with time. To verify the presence of annealing, all the copolymers under study have been incubated at 37°C under nitrogen atmosphere (to prevent any possible degradation process) and subjected to DSC measurements at the same sampling intervals as the hydrolytic degradation experiments.

All the calorimetric traces were found to be characterized by an endothermic peak associated with the fusion process of crystalline portion of the material (data not shown). The corresponding heat of fusion was normalized with respect to the heat of fusion of non-degraded sample ($\Delta H_t/\Delta H_0$) by having subtracted the annealing contribution. The results obtained are reported in Figure 5.14.

In all the polymers under study the normalized heat of fusion regularly increased with incubation time. Moreover, it can be observed that the higher the degradation rate, the higher the increase in the crystalline/amorphous ratio. As a matter of fact, $PBS_{30}P(BA50BDG50)_{70}$ displayed the highest increase in the normalized heat of fusion, while PBS the lowest. In the $PBS_{30}P(BA70BDG_{30})70$ sample, both crystalline domains were involved in the process. In particular, the crystalline/amorphous ratio of the PBA crystalline phase underwent the highest increase: this is probably due to the preferential attack of the P(BA70BDG30) less crystalline domains with respect to the PBS ones.

5.2.4 Comment on results obtained

A new class of high molecular weight PBS-based poly(ester-urethane)s has been successfully synthesized, and the solid-state properties and the biodegradation rate under physiological conditions have been evaluated.

The chain-extension technique allowed the overcoming of the typical problems of copolymerization; among all, a substantial decrease of the melting temperature when significant amounts of the comonomeric unit are introduced along the homopolymer backbone. The use of two segments (*hard* and *soft*) possessing very different physical properties, permitted to obtain novel thermoplastic elastomers, each displaying peculiar mechanical properties and biodegradation rate, by simply playing with the mutual ratio of the two prepolymers. Moreover, the variation of the *soft segment* chemical composition revealed an additional winning parameter to further tailor the final properties of the synthesized materials.

As a matter of fact, all the poly(ester urethane)s showed high toughness and elongation to break, but the elastic modulus, the wettability, the crystallinity degree, and therefore the biodegradation rate, were found dependent on either the *soft/hard* ratio in the polymers and the chemical composition of the soft prepolymer.

The introduction of ether-linkages in the polyester backbone had a notable and controllable effect on their physico-chemical properties leading to a decrement of chain symmetry and regularity as a result of the presence of co-unit chain segments and to an improvement in the surface wettability related to the presence of highly electronegative oxygen atoms.

5.3 Design of fully aliphatic multiblock poly(ester urethane)s displaying thermoplastic elastomeric properties

Three hydroxyl-terminated fully aliphatic polyesters have been chain extended by the combination of prepolymers with very different physical/chemical properties. Poly(butylene succinate), poly(1,4-cyclohexylenedimethylene-1,4-cyclohexanedicarboxylate), and poly(neopentyl glycol adipate) have been respectively used as *soft-hard*, *hard* and *soft segment*. The obtained multiblock poly(ester urethane)s (PEU) displaying thermoplastic elastomeric characteristics. The evaluation of molecular, thermal, and mechanical properties and hydrolytic degradation profile permitted to correlate the behavior of the so-obtained materials with their molecular structure, and highlighted that it is possible to nicely tune the final characteristics of this class of PEUs by just varying the mutual amount of the three segments.

5.3.1 Synthesis and characterization of the polymers

In a first time OH-terminated prepolymers were synthesized. After purification PBS-OH appeared as semicrystalline white floccules, PNA-OH as a light yellow wax, while PCCE-OH as a glassy colourless material. The synthesized prepolymers are listed in Table 5.11, which also collects the data of molecular characterization.

Table 5.11 Molecular and thermal characterization data of PBS-OH, PCCE-OH and PNA-OH.

				I scan[c]			*II scan*[c]			
Polymer	**M_n[a] (g/mol)**	**M_n[b] (g/mol)**	**D[b]**	**T_m (°C)**	**ΔH_m (J/g)**	**T_g (°C)**	**Δc_p (J/°C g)**	**T_m (°C)**	**ΔH_m (J/g)**	**X_c[d] (%)**
PBS-OH	5000	6200	2.4	115	64	-33	0.150	115	61	46 ± 4
PCCE-OH	4400	7400	2.5	-	-	35	0.190	-	-	-
PNA-OH	15800	15900	2.2	34	35	-47	0.385	-	-	30 ± 5

a: by ^{1}H-NMR

b: by GPC

c: by DSC

d: by WAXS

The molecular weight and the chemical structure of PBS-OH (Figure S2), PNA-OH (Figure S5) and PCCE-OH (Figure S6) prepolymers have been determined by ^{1}H-NMR spectroscopy. In all cases, the spectra were found to be consistent with the expected structure. The degree of polymerization (DP) has been calculated by comparing the areas of the peaks of the glycol subunit in the polymer chain with the area of the signal of terminal glycols, respectively situated at 3.68 ppm (Figure S2, d), at 3.31 (Figure S5, i) and at 3.46 and 3.55 (Figure S6, o) for PBS-OH, PNA-OH and PCCE-OH.

Then, the polymer molecular weight (M_n) has been obtained according to the following formula:

$$M_n = DP \cdot M_{wunit} + X \qquad \textbf{[14]}$$

where:

M_{wunit} is the molecular weight of the repeating unit in the polymer chain (174 g/mol for PBS, 216 g/mol for PNA and 282 g/mol for PCCE);

X is the molecular weight of the terminal glycol (considering 100% of OH terminal groups).

The molecular weight values obtained by NMR are comparable to those measured by GPC analysis (Table 5.11). It is worth underlining that the prepolymer synthesis procedure was optimized to achieve molecular weights as high as possible, nevertheless preserving a high concentration of OH terminal groups, required for the chain extension technique. Moreover, the high molecular weight allows limiting the lowering of the melting temperature in the multiblock copolymers.

The thermal transitions of the prepolymers were afterwards investigated by differential scanning calorimetry (Table 5.11). In the first scan PBS-OH and PNA-OH displayed both a glass transition and a melting endothermic peak, while for PCCE-OH only the glass transition has been observed. These results have been also confirmed by WAXS, where PCCE-OH doesn't show crystallinity degree (Table 5.11). As to the second scan after quenching, PCCE-OH and PBS-OH curves did not display any difference from the first scan, indicating that PBS-OH cannot be frozen into a completely amorphous state by quenching. Interestingly, in the case of PNA-OH only the baseline deviation due to the glass transition phenomenon was found but not melting endothermic peak.

Afterword, the multiblock copolymers have been obtained by adding an equimolar amount of HDI with respect to the concentration of OH groups to the molten prepolymers. After the chain extension process, PEUs appeared as light yellowish semicrystalline solids. No unreacted HDI was detected by NMR after purification. As an example, the ^{1}H-NMR spectrum of the $PBS_{50}PCCE_{10}PNA_{40}$ multiblock copolymer is reported in Figure S7: with z, w and y are indicated the protons of the reacted chain extender (located at 3.30 ppm, 1.34 ppm and 1.25 ppm, respectively). All the spectra are consistent with the expected structure. The actual composition resulted very close to the feed and the HDI content was in all cases below 5 wt% (Table 5.12).

Table 5.12 Molecular characterization data of PBS and of $PBS_xPCCE_yPNA_z$ copolymers.

Polymer	Mn[a] (g/mol)	D[a]	PBS[b] (wt%)	PCCE[b] (wt%)	PNA[b] (wt%)	HDI[b] (wt%)
PBS	65300	2.5	96.5	-	-	3.5
$PBS_{50}PCCE_{50}$	40200	2.7	35.2	61.7	-	3.1
$PBS_{50}PCCE_{30}PNA_{20}$	31000	3.1	40.5	35.4	19.3	4.8
$PBS_{50}PCCE_{10}PNA_{40}$	33400	3.0	39.8	13.4	43.2	3.6
$PBS_{50}PNA_{50}$	40300	2.6	47.1	-	47.9	5.0

a: by GPC

b: by ^{1}H-NMR

Table 5.12 reports the molecular weight data obtained by GPC. As expected, the samples showed a significant increase of molecular weight with respect to the prepolymers.

Prior to further characterization, the compression moulded polymers have been stored at room temperature for two weeks in order to attain equilibrium crystallinity. Subsequently, the PEUs have been subjected to thermogravimetric analysis under dry nitrogen atmosphere. The temperature corresponding to the degradation onset (T_{onset}) and the temperature corresponding to the maximum weight loss rate (T_{max}) were determined from the thermogravimetric curves are collected in Table 5.13.

The thermal degradation took place in one step. The thermal stability of all the synthesized copolymers remained good even though slightly lower than that of PBS homopolymer. $PBS_{50}PCCE_{50}$ displayed a higher stability, due to the presence of aliphatic rings. Although no mass loss has been observed below 370°C, the breaking of the urethane bonds cannot be excluded. Indeed, as previously demonstrated (Hentschel and Münstedt, 2001), urethane bonds break above 200°C, leading to a decrease in the polymer molecular weight. Therefore, the thermogravimetric curves observed could be representative only of the degradation of the polyester prepolymers, while high molecular weight PEUs are not stable already above 200°C.

Table 5.13 Thermal characterization data (I scan) and crystallinity degree of PBS and $PBS_xPCCE_yPNA_z$ copolymers.

				I scan[b]				
Polymer	**T_{onset}[a] (°C)**	**T_{max}[a] (°C)**	**T_g (°C)**	**ΔCp (J/°C g)**	**T_m (°C)**	**ΔH_m (J/g)**	**T_{cc}[b] (°C)**	**Xc[c] (%)**
PBS	373	405	-33	0.139	110	43	80	46 ± 4
$PBS_{50}PCCE_{50}$	390	432	-33 / 35	0.086 / 0.266	111	21	76	16 ± 2
$PBS_{50}PCCE_{30}PNA_{20}$	360	410	-36	0.232	86	18	45	17 ± 2
$PBS_{50}PCCE_{10}PNA_{40}$	360	400	-38	0.356	98	20	50	27 ± 3
$PBS_{50}PNA_{50}$	360	394	-40	0.301	102	23	58	29 ± 3

a: by TGA

b: by DSC

c: by WAXS

DSC traces of PEU samples are reported in Figure 5.15a and the data obtained in Table 5.13. All PEUs showed a melting endotherm, indicating the partially crystalline nature of the samples. PBS and $PBS_{50}PCCE_{50}$ displayed the highest values of T_m, around

110°C, with a well-defined endothermic peak surely due to the fusion of PBS crystalline sequences.

As to the copolymers containing PNA, besides the PBS melting peak at higher temperatures, a small bump is visible at around 35°C. This phenomenon, can be reasonably ascribed to the fusion of the PNA sequences, but may be also due to the melting of less perfect PBS crystalline domains, as already observed in other PBS-based aliphatic copolyesters (Soccio *et al.*, 2012; Gigli *et al.*, 2013).

As expected, PBS displayed the highest heat of fusion (43 J/g), while in the copolymers it was drastically reduced, indicating a lower amount of crystalline phase (Table 5.13). This can be ascribed to two different factors: the reduced amount of PBS and the presence of PNA and PCCE sequences, which may have hampered the PBS crystallization ability.

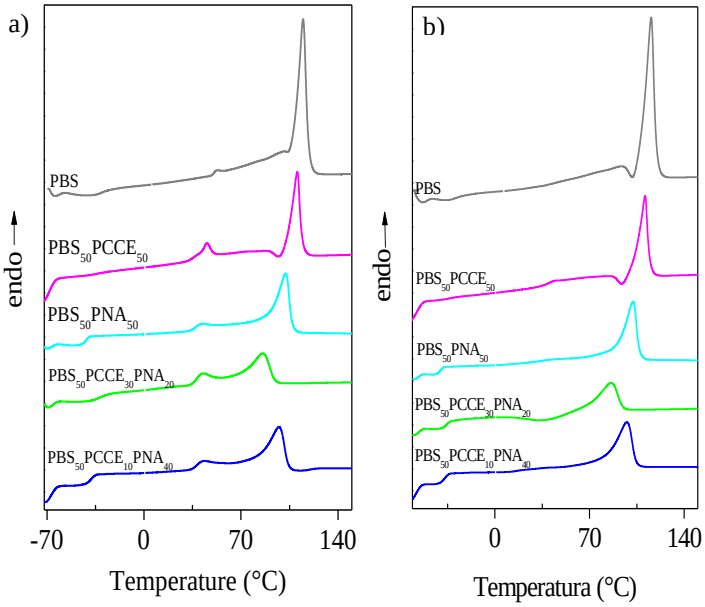

Figure 5.15 Calorimetric curves of $PBS_xPCCE_yPNA_z$: a) 1st scan; b) 2nd scan after melt quenching.

To better understand the nature of the crystalline phase in the polymers under study, wide angle X-ray diffraction experiments have been carried out. The patterns of the prepolymers and chain-extended PEUs are reported in Figure 5.16.

With the exception of PCCE-OH, whose pattern is a bell-shaped curve meaning the completely amorphous status of this polymer, the WAXD patterns of the other polymers appear to be characterized by relatively intense diffraction peaks. In the $PBS_{50}PCCE_{50}$ pattern, the PBS crystalline phase, with the two main peaks *020* and *211* at about 19.6° and 22.9° (2θ, d= 0.45 and 0.39 nm), is partially covered by the bell shaped curve of the PCCE. In the PEUs containing PNA segments, the presence of both the PBS and PNA crystalline phases is well documented (Figure 5.16), thus confirming one of the two hypothesis above formulated on the basis of the calorimetric results.

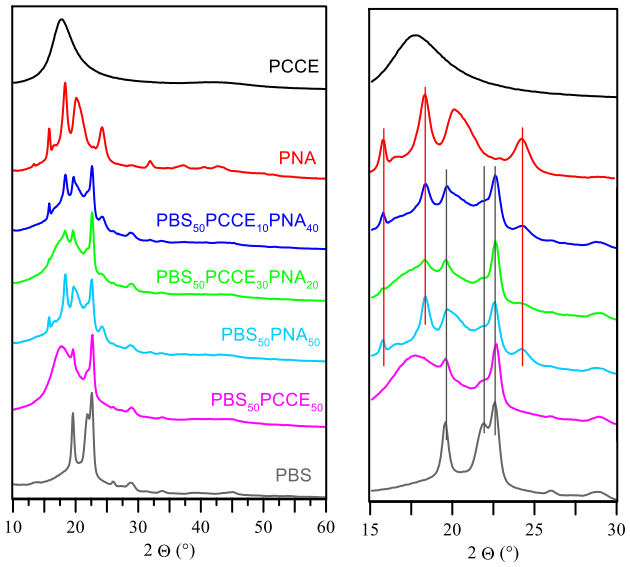

Figure 5.16 X-ray diffraction patterns of $PBS_xPCCE_yPNA_z$ copolymers. In the right side a zoomed view is reported; the vertical lines are eyeguides of the peak position of PBS (black) and PNA (red) phases.

The PNA crystalline phase is characterized by three sharpened peaks at 2θ = 15.9°, 18.4° and 24.1° and a broader one at 20.3°. In the copolymers, no change in the peaks position has been observed, thus meaning the formation of pure crystalline phases. Copolymer patterns displayed a broadening of the peaks and an increase of the interplanar gaps, due to the higher rejection problems of the different comonomeric units from each crystalline phase. As expected, the crystallinity degree is in all cases lower than that of PBS homopolymer. Moreover, a correlation between the amount of PCCE segments and X_c can be noticed: the higher the PCCE content, the lower the

crystallinity degree. To confirm that in the PEU copolymers the tendency of PBS to crystallize decreases, non-isothermal experiments were carried out, subjecting the samples to a controlled cooling rate from the melt.

It is worth remembering that the half-time of primary crystallization in isothermal experiments correlates with the temperature of the maximum of the crystallization peaks in non-isothermal experiments (T_{cc}) (Legras *et al.*, 1986),being this latter more easily obtainable. The exothermic crystallization peaks of the samples under investigation are shown in Figure 5.17 and the T_{cc} are reported in Table 5.13.

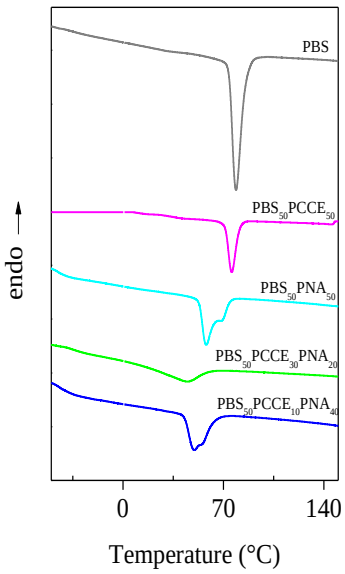

Figure 5.17 DSC crystallization exotherms of $PBS_xPCCE_yPNA_z$ copolymers cooled from the melt at 5°C/min.

In all the copolymers, with the exception of $PBS_{50}PCCE_{50}$, a significant reduction of the PBS crystallization rate can be observed, while in the above mentioned one the presence of the PCCE segment did not dramatically depress the PBS crystallization ability, thus confirming the results observed by 1st DSC scan. The introduction of PNA sequences had on the contrary a remarkable impact. As a matter of fact, T_{cc} decreased from 80 to 58°C, because of the crystallization of the PNA segments, which hampered the regular crystallization process of PBS chains. In addition, the presence of both PNA and PCCE, contributed to an even more pronounced lowering of the T_{cc}. The crystallization of both

PBS and PNA phases is confirmed by the presence of a double crystallization peak (Figure 5.17).

In order to better study the influence of chemical structure on the glass transition of the PEUs, the phenomenon should be examined in the total absence of crystallinity. As it is well known, the miscibility of block copolymers and blends can be evaluated by analysing their glass transition. The presence of a single glass transition at a temperature comprised between those of the pure components, suggests complete miscibility. On the other hand, two T_gs indicate immiscibility or partial miscibility of the components. In particular, the observation of two glass transitions at temperatures corresponding to those of the pure homopolymers, is a clear evidence of no miscibility. In this view, all the samples under investigation were subjected to rapid cooling (quenching) from the melt. The DSC curves after melt quenching are shown in Figure 4b and the results are reported in Table 5.14.

Table 5.14 Thermal characterization data (II scan) and crystallinity degree of PBS and $PBS_xPCCE_yPNA_z$ copolymers.

	II scan					
Polymer	**T_g (°C)**	**ΔCp (J/°C g)**	**T_c (°C)**	**ΔH_c (J/g)**	**T_m (°C)**	**ΔH_m (J/g)**
PBS	-33	0.0832			110	39
$PBS_{50}PCCE_{50}$	-33/35	0.096/0.278			111	21
$PBS_{50}PCCE_{30}PNA_{20}$	-36	0.255	35	4	86	17
$PBS_{50}PCCE_{10}PNA_{40}$	-38	0.352			98	19
$PBS_{50}PNA_{50}$	-40	0.294			102	23
PNA						

$PBS_{50}PCCE_{50}$ copolymer presented two clear and distinct T_gs at -33 and 35°C, relative to the pure PBS and PCCE sequences respectively, thus suggesting the complete immiscibility of the two blocks in the amorphous phase. On the contrary, $PBS_{50}PNA_{50}$ sample was characterized by a single glass transition at -40°C, a temperature in between those of the pure PBS and PNA polymers. Therefore, the miscibility of the two components in the amorphous state can be reasonably considered.

As to the PEUs containing all the three segments, the T_g decreased with the increasing amount of the PNA segment. However, the presence of a second glass transition at 35°C, due to the PCCE sequences, cannot be excluded. As a matter of fact, $PBS_{50}PCCE_{30}PNA_{20}$ DSC curve displayed a cold crystallization phenomenon at 35°C,

which may have hampered the second T_g detection, while in the case of $PBS_{50}PCCE_{10}PNA_{40}$ the amount of PCCE (10%) is probably too low to allow the visualization of its T_g.

As to the melting phenomenon, it can be observed that only the fusion of the PBS crystalline domains is present; therefore the crystallization of the PNA phase did not take place. of $PBS_{50}PCCE_{30}PNA_{20}$ evidenced a glass transition followed by an exothermal "cold crystallization" peak and a melting endotherm at higher temperature (Figure 4.16b). The enthalpy of crystallization is however lower than the corresponding heat of fusion, indicating that this copolymer cannot be frozen into a completely amorphous state by quenching.

5.3.2 Studies of mechanical properties

The mechanical properties of the PEUs under investigation were analysed by stress-strain tests. Their mechanical data (elastic modulus E, stress at yield σy, deformation at yield εy, stress at break σb, and deformation at break εb) are reported in Table 5.15.

The results obtained clearly evidenced that the introduction of flexible and/or rigid segments along the PBS macromolecular chains resulted in significant modification of the PBS mechanical properties. As expected, rigid PCCE sequences permitted to increase the elastic modulus of PBS of about 50%, while the presence of flexible PNA segments drastically lowered E. When both PCCE and PNA segments have been introduced, a conflicting effect can be noticed: E is in both PEUs lower than $PBS_{50}PNA_{50}$, but the higher the PCCE content, the higher the modulus, notwithstanding the much lower crystallinity degree.

Table 5.15 Mechanical data of $PBS_xPCCE_yPNA_z$ copolymers.

Polymer	E (MPa)	σ_y (MPa)	ε_y (%)	σ_b (MPa)	ε_b (%)
PBS	427 ± 34	27 ± 2	14 ± 2	29 ± 2	350 ± 20
$PBS_{50}PCCE_{50}$	660 ± 31	10 ± 2	8 ± 1	37 ± 4	440 ± 20
$PBS_{50}PCCE_{30}PNA_{20}$	68 ± 6	-	-	18 ± 4	660 ± 120
$PBS_{50}PCCE_{10}PNA_{40}$	60 ± 4	-	-	21 ± 4	945 ± 140
$PBS_{50}PNA_{50}$	87 ± 7	-	-	23 ± 5	730 ± 150

All the copolymers containing flexible PNA sequences evidenced the typical behavior of thermoplastic elastomers (Figure 5.18): no yield, high toughness, and excellent εb (higher than 650%).

Overall, mechanical characterization demonstrated that the synthetic strategy adopted permitted to modify the homopolymer mechanical properties by introducing flexible (PNA) or amorphous and rigid (PCCE) segments along the PBS macromolecular main chain

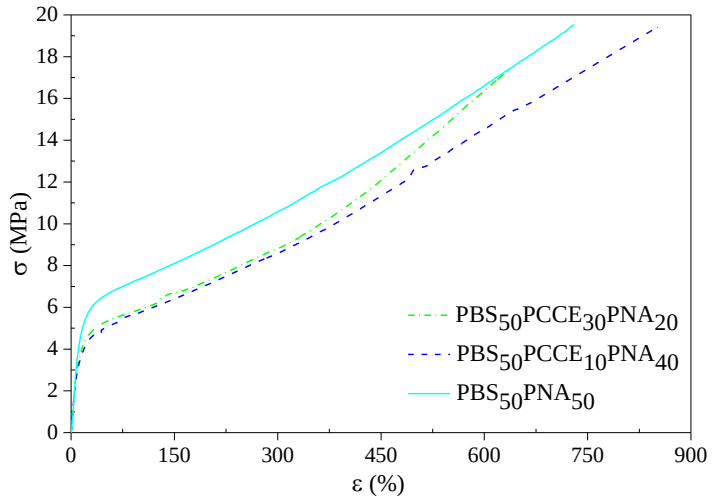

Figure 5.18 Representative stress-strain curves of $PBS_{50}PCCE_{30}PNA_{20}$, $PBS_{50}PCCE_{10}PNA_{40}$ and $PBS_{50}PNA_{50}$.

The copolymers displaying thermoplastic elastomeric behavior, i.e. $PBS_{50}PCCE_{30}PNA_{20}$, $PBS_{50}PCCE_{10}PNA_{40}$ and $PBS_{50}PNA_{50}$, were subjected to cyclic stress-strain tests. The PEUs under investigation displayed high elasticity, even after 25 cycles, even though a certain amount of permanent set could be seen after each loading–unloading cycle (Figure 5.19).

The stress–strain curve in the second cycle is much more compliant than that observed in the first cycle. This behavior, known as softening, can be due to a rearrangement in the crystalline microphase (Soccio *et al.*, 2012). On the other hand, starting from the second cycle, the stress–strain curves stabilized to a fixed trajectory. Moreover, the hysteresis area of the second cycle is much smaller than that of the first cycle. The difference between the ascending curve of the first cycle and that of the second cycle

can be explained on the basis of a reorientation of the macromolecules together with crystallization during straining (Andronova and Albertsson, 2006).

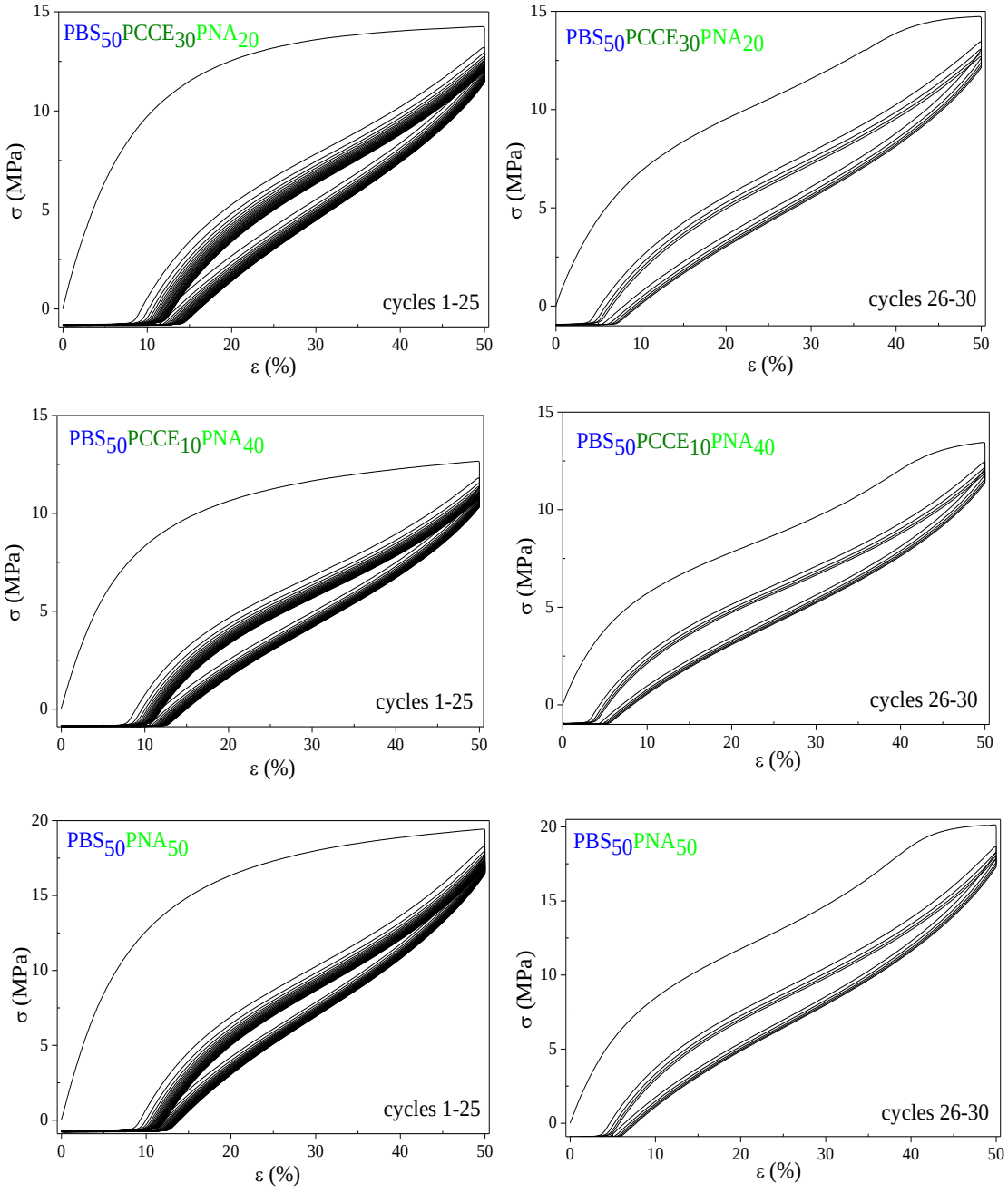

Figure 5.19 Hysteresis behavior of $PBS_{50}PCCE_{30}PNA_{20}$, $PBS_{50}PCCE_{10}PNA_{40}$ and $PBS_{50}PNA_{50}$ upon cyclic loading: left side cycles 1-20, right side cycles 26-30 (after 48 h relaxation).

The unloading paths are relatively independent of cycle number, i.e., the unloading stress–strain behavior is not dependent on the deformation history. The residual strain is also not dependent on the deformation history.

After 48 hours relaxation, a significant reduction of the permanent set produced during the first cycle was observed, while the other cycles followed a similar curve as cycles 2-25 (Figure 5.19).

5.3.3 Hydrolytic degradation studies

Hydrolytic degradation experiments have been carried out under physiological conditions (37 °C, pH 7.4) in phosphate buffer. After 204 days of incubation, all the samples practically did not lose weight (weight losses of about 1-2%, results not shown). PEU samples have therefore been subjected to molecular weight determination to verify the occurrence of the hydrolytic attack. It is in fact well known that in the first stages of hydrolytic degradation a substantial decrease in molecular weight occurs, even if weight losses are still negligible (Mochizuki and Hirami, 1997). As shown in Figure 5.20, which reports the percentage of residual number average molecular weight (M_n res%) as a function of incubation time, all polymers underwent a significant decrease of M_n with time, confirming the occurrence of the degradation process.

In the first 80 days of incubation, no marked differences between the samples can be highlighted. On the contrary, at higher degradation times a clearer trend can be deduced. As to the copolymers, the higher the PNA content, the higher molecular weight decrease, regardless the crystallinity degree and the molecular weight, two well-known factors affecting the degradation behavior of a polymeric material. In this case, the major role is reasonably played by the chemical structure: the presence of a greater amount of flexible and mobile segments facilitates the water penetration into the polymer matrix. On the contrary, the introduction of rigid PCCE segments, that show a T_g of about 35°C, hampers the hydrolysis process.

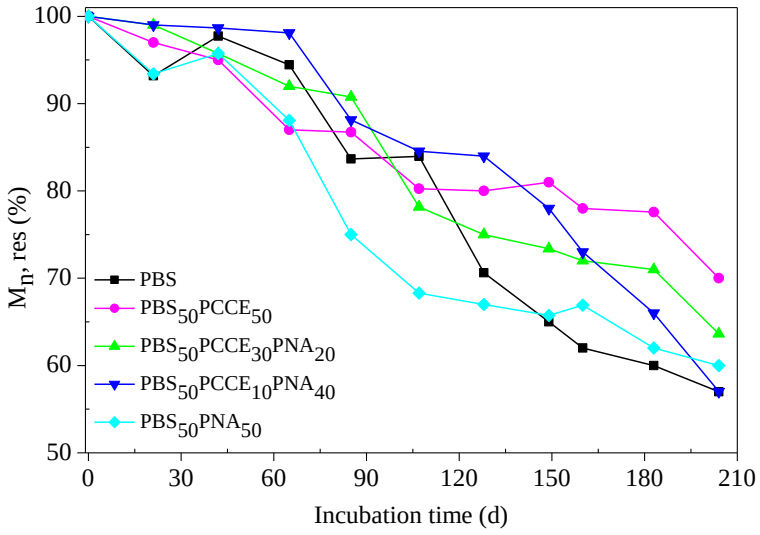

Figure 5.20 Residual molecular weight ($M_{n,\,res\,\%}$) as a function of incubation time for $PBS_xPCCE_yPNA_z$ copolymers.

Interestingly, the PBS molecular weight decrease is similar to that of $PBS_{50}PNA_{50}$, even though it possesses a higher crystallinity degree. This finding could be dictated by two different factors: a) steric hindrance caused by the two methyl groups of the neopentyl glycol; b) lower hydrophilicity of the PNA with respect to PBS due to the methyl groups of NPG and the longer CH_2 chain of adipic acid with respect to succinic acid.

5.3.4 Comment on results obtained

Poly(ester urethane)s containing *soft*, *hard* and *soft-hard* sequences have been prepared by chain extending hydroxyl terminated aliphatic polyesters with hexamethylene diisocyanate. A new class of multiblock copolymers with randomly distributed sequences of PBS, PCCE and PNA have been obtained.

Through this strategy, it has been possible to synthesize high molecular weight semicrystalline polymers. The thermal and mechanical characteristics of the copolymers have been evaluated and correlated to the chemical structure of the materials.

Tensile testing proved that the new PEUs containing PNA sequences displayed a thermoplastic elastomeric behavior: high toughness and elongations to break above 900% have been achieved. Moreover, cyclic loading measurements revealed a highly elastic behavior, even after 25 cycles.

Hydrolytic degradation experiments under physiological conditions showed that the degradation profile is dependent on the chemical composition of the $PBS_xPCCE_yPNA_z$ copolymers. The mechanical properties and hydrolysis profile can be modulated according to the desired application, by just varying the kind and the amount of the prepolymers in the final material.

5.4 New fully bio-based PLLA triblock copolymers as potential candidates for soft tissue engineering

5.4.1 Some initial considerations

Back in 1973, lactic acid and glycolic acid were proposed as degradable matrices for the sustained delivery of bioactive substances (Auras *et al.*, 2004). Likewise, poly(lactic acid) (PLA) has been demonstrated to be a suitable bioabsorbable thermoplastic commonly used in biomedical devices, such as resorbable plates and screws (Cheng *et al.*, 2009), because of their excellent biocompatibility. In the last few years, bioabsorbable fixation devices have been extensively used as dissolvable suture meshes and recently, by orthopedic surgeons. Moreover, because of its significant therapeutic effectiveness, from 2004 the Food and Drug Administration (FDA) approved PLA products for use in the biomedical field (Xiao *et al*., 2012). As added benefit, lactic acid, the PLA precursor, could be produced starting from renewable resources, by fermentation of sugars such as sugarcane. Therefore, PLA can be produced and used in an environmentally friendly cycle (Lasprilla *et al.*, 2012), in agreement with the European directives for the decrease in the use of fossil fuels and the deployment of so-called "green materials".

The stereochemistry and thermal history have direct influence on PLA crystallinity, and therefore, on its properties in general. PLA with L-isomer (PLLA) content higher than 90% tends to be crystalline, while the lower optically pure is amorphous. The melting temperature (T_m), and the glass transition temperature (T_g) of PLA decrease with decreasing amounts of PLLA (Auras *et al.*, 2010). Also physical characteristics such as density, heat capacity, and mechanical and rheological properties of PLA depends on its

transition temperatures. The different properties off PLA polymers are shown in Table 5.16.

Table 5.16 Lactid acid polymers properties (adapted from Nampoothiri *et al.*, 2010)

Lactic acid polymers	T_g (°C)	T_m (°C)	Density (g/m^3)
PLLA	55-80	173-178	1.29
PDLLA	43-53	120-170	1.25
PDLA	40-50	120-150	1.25

PLA also can be tailored by formulation involving co-polymerizing of the lactide with other lactones-type monomers, a hydrophilic macromonomers (polyethylene glycol), or other monomers with functional groups (such as amino and carboxylic groups, etc.), and blending PLA with other materials (Cheng *et al.*, 2009). Blending can radically alter the resultant properties, which depend sensitively on the mechanical properties of the components as well as the blend microstructure and the interface between the phases.

PLA degrades primarily by hydrolysis, after several months exposure to moisture. The degradation occurs in two stages: first random non-enzymatic chain scission of the ester groups leads to a reduction in molecular weight, and in the second stage the molecular weight is reduced until the lactic acid and non-toxic low molecular weight oligomers are eliminated through normal cellular activity or urine. (Lasprilla *et al.*, 2012).

PLA could be synthesized by direct polycondensation of lactic acid or by ring opening polymerization (ROP) starting from lactide. Although there are multiple ways to fabricate PLA, none of them is simple or easy to execute. PLA synthesis requires rigorous control of conditions (temperature, pressure and pH), the use of catalysts and long polymerization times which implies high energy consumption.

In the present work, an innovative fully bio-based poly(lactic acid) copoly(ester-urethane)s have been successfully synthesized starting from L-lactide and OH-terminated PBS-based copolymers. The new system is composed of a series of A-B-A triblock copolymers, where A, *hard block*, is poly(L-lactic acid) (PLLA) and B, *soft block*, is an ad hoc designed random aliphatic copolyester, poly(butylene succinate/azelate) (P(BS80Baz20)), characterized by high flexibility. Triblock units are joined by hexamethylene diisocyanate, known chain extender that allows the obtaining

of polymers with high molecular weights. The samples synthesized were subjected to a detailed molecular, thermal, structural and mechanical characterization.

The results obtained, show that copolymerization leads to better mechanical response with respect to poly(lactic acid) homopolymer. Moreover, the presence of the *soft block* in the main polymer chain facilitates the process of biodegradability. Nanoparticles of selected copolymers fabricated by using the nanoprecipitation method showed rounded morphology and average hydrodynamic diameters around 180 nm. Cellular behavior was assessed using human fibroblasts in vitro assays and results showed absence of cytotoxicity and a good cellular adhesion and proliferation on all the copolymer surfaces.

5.4.2 Synthesis and characterization of the polymers

After the purification process, the OH-terminated P(BS80BAz20) random copolymer appeared as a light yellow colored wax. The chemical structure, the composition and the molecular weight have been determined by ^{1}H-NMR spectroscopy. Figure S8 shown the ^{1}H-NMR spectrum of P(BS80BAz20) together with the chemical shift assignments. The spectrum was found to be consistent with the expected structure. Together with the signals of the aliphatic protons of the inner repetitive units, the peak due to the outer subunits can also be detected: the triplet a' corresponding to the external glycol units. The copolymer composition was calculated from the relative areas of the ^{1}H-NMR resonance peaks related to c singlet of the succinic subunit and d triplet associated with the azelaic part. The actual molar composition was very close to the feed one.

The copolymers degree of polymerization (DP) has been calculated from the relative areas of a protons of central butanediol (I_a) and a' protons of terminal butanediol ($I_{a'}$) as follows:

$$DP = [(I_a /2 + I_{a'}) * 2] / I_{a'} \quad \textbf{[15]}$$

The copolymer molecular weight (M_n) has been obtained according to the following formula:

$$M_n = DP * (MBS * BS + MBAz * BAz) \quad \textbf{[16]}$$

where MBS is the molecular weight of the butylene succinate repeating unit; MBAz is the molecular weight of the butylene azelate repeating unit; BS and BAz are the actual

butylene succinate and butylene azelate percentage contents, respectively. M_n calculated by this procedure was 6400 g/mol.

After calculating the molecular weight and assuming that the chains were mainly OH-terminated, we can also derive the moles of hydroxyl groups per unit mass, and consequently, the amount of hexamethylene diisocyanate to be used during the chain extension reaction.

Chain extended PLLA as well as triblock copolymers appeared as semicrystalline solids, white and light yellow colored, respectively. No unreacted HDI was detected by NMR analysis after 1 hour of reaction. As an example, the ^{1}H-NMR spectrum of $PLLA_{32}P(BS80BAz20)_{68}$ triblock copolymer is reported in Figure S9. All the spectra were consistent with the expected structure. The actual composition was calculated by the relative areas of the singlet corresponding to protons c of the succinic unit (located at 2.62 ppm) and the quadruplet of proton h of the lactic unit (at 5.18 ppm), resulting very close to the feed one (Table 5.17). The HDI content was in all cases below 5%.

Table 5.17 reports also the molecular weight data obtained by GPC. As expected, the samples show a higher molecular weight (M_n) with respect to the prepolymer and, moreover, a pretty narrow polydispersity (D) was found, indicating a good control over both the ring opening polymerization and the chain extension process.

Table 5.17 Molecular characterization data of the synthesized copoly(esters-urethanes) system.

Polymers	**Mn[a] (g/mol)**	**D[a]**	**wt% PLA[b]**	**mol% HDI[b]**
$PLLA_{18}P(BS80BAz20)_{82}$	26800	2.5	18	3
$PLLA_{32}P(BS80BAz20)_{68}$	40500	2.4	32	4
$PLLA_{61}P(BS80BAz20)_{39}$	39800	2.1	61	3
$PLLA_{73}P(BS80BAz20)_{27}$	40300	3.1	73	5
PLLA	40500	1.9	100	4

a: by GPC

b: by NMR

The synthesized triblock copolymers have been subjected to thermogravimetric analysis under dry nitrogen atmosphere; the temperatures corresponding to the initial weight loss (T_{id}) was determined from the thermogravimetric curves and collected in Table 5.18. As

shown in Figure 5.21, PLLA homopolymer appeared to be less thermally stable with respect to the triblock copolymers. This effect could be due to the higher ester groups density per repeating unit in the PLLA chains with respect to the P(BS80BAz20) ones. Regarding the triblock copolymers, the thermal degradation took place in two steps. The relative height of the two steps clearly depends on the composition. The higher the PLLA content, the more intense was the first weight loss step. Anyway, the temperature of the initial degradation in the PLLA-based copolymers was comparable to that of the homopolymer.

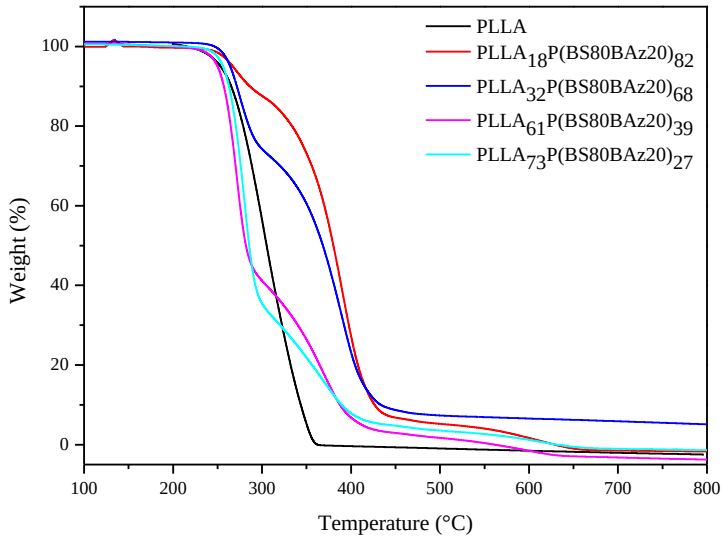

Figure 5.21 Thermogravimetric curves of the copolyester-urethanes, under nitrogen atmosphere (10°C/min).

Prior to further characterization, the compression molded polymers (see the Experimental section for the experimental procedure employed to prepare the polymer films) have been stored at room temperature for one month in order to attain equilibrium crystallinity. A period of 30 days has proven to be appropriate for making uniform the thermal history and reaching the equilibrium crystallinity. DSC traces of these films are reported in Figure 5.22 and the data obtained in Table 5.18 and Table 5.20.

Table 5.18 Thermal characterization data by TGA and DSC (first scan) analysis.

						I scan			
Polymers	**T_{id} (°C)**	**T_g (°C)**	**Δc_p (J/°C g)**	**$T_{m,BS}$ (°C)**	**$\Delta H_{m,BS}$ (J/g)**	**T_c (°C)**	**ΔH_c (J/g)**	**$T_{m,PLA}$ (°C)**	**$\Delta H_{m,PLA}$ (J/g)**
$PLLA_{18}P(BS80BAz20)_{82}$	252	-26 43	0.376 0.171	86	28	--	--	--	--
$PLLA_{32}P(BS80BAz20)_{68}$	258	-5 41	0.201 0.170	81	17	90	4	132	6
$PLLA_{61}P(BS80BAz20)_{39}$	256	44	0.189	--	--	88	12	141	11
$PLLA_{73}P(BS80BAz20)_{27}$	255	53	0.162	--	--	91	10	153	32
PLLA	265	61	0.460	--	--	--	--	170	40

Calorimetric curves of the system under investigation evidence that the thermal behavior of $PLLA_mP(BS80BAz20)_n$ samples deeply depends on the weight ratio between the *hard* and the *soft* blocks. All the triblock copolymers were semicrystalline, showing at least a melting endotherm together with an endothermic baseline change associated with the glass transition. In the case of the samples containing higher amount of *soft* block, $PLLA_{18}P(BS80BAz20)_{82}$ and $PLLA_{32}P(BS80BAz20)_{68}$, two glass transitions can be evidenced. This result indicates a phase separation in the amorphous state of the two components that leads to the formation of a P(BS80BAz20)-rich phase, characterized by the lowest T_g, and a PLLA-rich phase, associated to the highest T_g. For the higher PLLA containing samples just one glass transition temperature, the one related to the PLLA-rich phase, can be detected, probably due to the low amount of P(BS80BAz20) blocks.

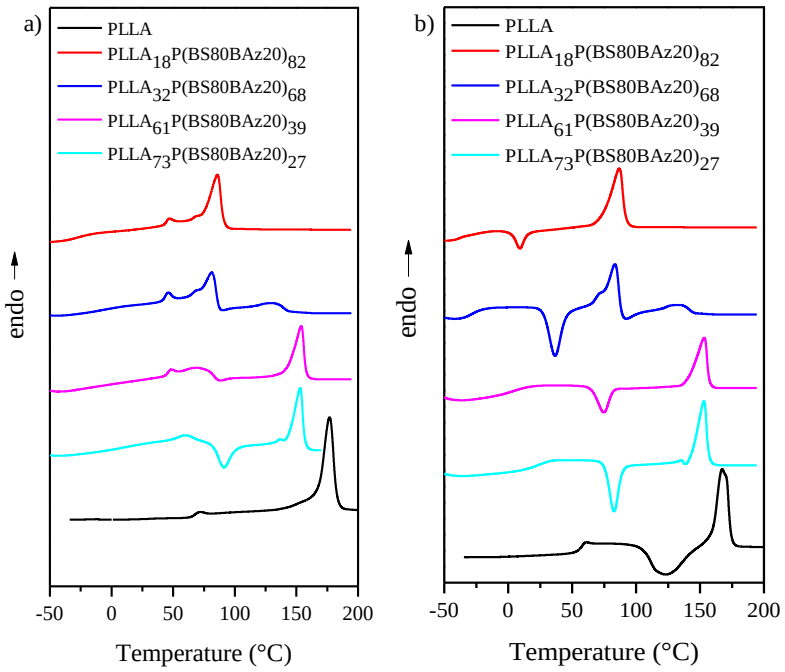

Figure 5.22 Calorimetric curves of chain extended PLLA and $PLLA_mP(BS80BAz20)_n$ triblock copolymers: a) 1st scan; b) 2nd scan after melt quenching.

Concerning the melting phenomenon, in the case of PLLA homopolymer, the melting peak is located at high temperature (170°C) and the heat of fusion associated is consistent, while its copolymers show lower melting temperatures and melting heats. In particular, as the amount of *soft* segment increases, the melting peak shifts towards lower temperatures. In fact, higher content of P(BS80BAz20) block leads to the formation of crystals with a lower degree of perfection. Simultaneously, the decrease of the *hard* phase (PLLA) also involves a reduction in the melting heat value due to a lowering of the crystallinity degree. On the other hand, the DSC curves of $PLLA_{18}P(BS80BAz20)_{82}$ and $PLLA_{32}P(BS80BAz20)_{68}$ another endotherm appears at lower temperature. All the copolymers, except $PLLA_{18}P(BS80BAz20)_{82}$, were able to crystallize during the temperature scan. Nevertheless, the corresponding crystallization heat is significantly lower than the melting one indicating these polymers were semicrystalline.

In order to investigate the nature of the crystalline phase, the samples were submitted to X-ray analysis. In Figure 5.23 the X-ray diffraction patterns of PLLA and its copolymers $PLLA_nP(BS80BAz20)_m$ are reported. The diffractometric profiles are typical of semicrystalline materials showing well defined reflections, characteristic of the ordered portion of the material, superimposed over a bell-shaped baseline due to the amorphous component. As far as concerns the crystal phase, the two higher PLLA containing samples as well as the homopolymer show the typical pattern of α-PLLA crystal phase characterized by the presence of a strong peak at 16.6° and other reflections at 19.0° and 22.2°. The sample $PLLA_{32}P(BS80BAz20)_{68}$ shows peaks of either PLLA and PBS phases while the copolymer $PLLA_{18}P(BS80BAz20)_{82}$ displays essentially the pattern of α-PBS phase (main reflections at 19.5° and 22.5°). As reported in Table 5.19, the highest crystallinity degree values correspond to the samples richest in one of the two components. The peaks position seems not affected by copolymerization, confirming the total exclusion of the co-units from the PLLA and PBS crystals, respectively. The reduction of the perfection of the crystal phase is also suggested by the decrease of the peaks intensity and the disappearance of some reflections. The diffractometric data were in agreement with the calorimetric ones.

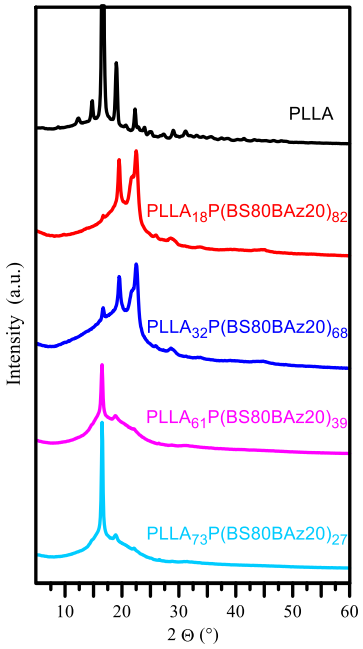

Figure 5.23 X-Ray diffraction patterns of PLLA and of $PLLA_nP(BS80BAz20)_m$ copolymers.

Table 5.19 Diffractometric characterization data: main crystalline phase and percentage crystallinity degree (X_c).

Sample	Main Phase	X_c (%)
PLLA	PLLA	41
$PLLA_{73}P(BS80BAz20)_{27}$	PLLA	28
$PLLA_{61}P(BS80BAz20)_{39}$	PLLA	18
$PLLA_{32}P(BS80BAz20)_{68}$	PBS	22
$PLLA_{18}P(BS80BAz20)_{82}$	PBS	30

Miscibility of the two components in the amorphous phase has been further investigated by analyzing the thermal behavior after melt quenching. In fact, with a cooling rate faster than the crystallization rate, an amorphous material would be obtained and, being the amorphous phase more abundant than in the semicrystalline sample, a more intense glass transition step could be evidenced. Moreover, although in literature different results have been reported, it is commonly accepted that crystallinity acts like crosslinking points reducing the mobility of the amorphous polymer chains and consequently enhancing the T_g value. In Figure 5.22b are reported the calorimetric curves after melt quenching of the system under investigation.

Table 5.20 Thermal characterization data by DSC analysis (second scan after melt quenching).

			II scan					
Polymers	**T_g (°C)**	**Δc_p (J/°C g)**	**T_c (°C)**	**ΔH_c (J/g)**	**$T_{m,BS}$ (°C)**	**$\Delta H_{m,BS}$ (J/g)**	**$T_{m,PLA}$ (°C)**	**$\Delta H_{m,PLA}$ (J/g)**
$PLLA_{18}P(BS80BAz20)_{82}$	-38	0.147	9	8	87	34	--	--
$PLLA_{32}P(BS80BAz20)_{68}$	-27	0.489	37	26	84	31	130	13
$PLLA_{61}P(BS80BAz20)_{39}$	2	0.531	75	13	--	--	153	20
$PLLA_{73}P(BS80BAz20)_{27}$	21	0.462	83	21	--	--	153	26
PLLA	57	0.540	133	20	--	--	167	30

All the samples show one glass transition step and at least one melting peak. For each material, the macromolecular chains, once passed T_g, acquire adequate energy and mobility to crystallize during the temperature scan. Nevertheless, being $\Delta H_c < \Delta H_m$, the samples were not totally vitrified in the amorphous state after rapid cooling from the

melt, but a certain crystalline portion was still present. Anyway, as one can see from Figure 5b and the results collected in Table 5.20, all the copolymers present a single T_g in an intermediate position with respect to those of the two blocks. The presence of one T_g for all the copolyesters in the second scan indicates that the permanence in the molten state for few minutes favors the mixing of the two blocks that become miscible in the amorphous phase. The glass transition temperature depends on the amount of *soft* segment in the chain. In particular, as expected, the copolymers with a higher percentage of *soft* block present a lower T_g value.

5.4.3 Studies of mechanical properties

Mechanical properties of a specific material are of crucial importance for its suitability for a specific application. To provide insight into the mechanical response of the copolymers synthesized, tensile measurements were carried out. The results of tensile testing (elastic modulus E, yield strength σ^y and yield strain ε^y, stress at break σ^B and strain at break ε^B), are summarized in Table 5.21, while in Figure 5.24 are reported the stress-strain curves recorded for the PLLA-based copolymers.

Table 5.21 Mechanical characterization data of PLLA and $PLLA_nP(BS80BAz20)_m$ triblock copolymers.

Polymers	E (MPa)	σ^y (MPa)	ε^y (%)	σ^b (MPa)	ε^b (%)
PLLA	1812±122	-	-	37±4	2.7±0.2
$PLLA_{73}P(BS80BAz20)_{27}$	368±32	16±2	11±2	11±1	102±13
$PLLA_{61}P(BS80BAz20)_{39}$	264±32	12±1	11±2	11±2	233±76
$PLLA_{32}P(BS80BAz20)_{68}$	193±17	12±1	14±1	12±3	607±69
$PLLA_{18}P(BS80BAz20)_{82}$	213±8	12±1	11±1	17±3	547±88

It can be noted that PLLA shows a very high elastic modulus value, confirming the remarkable stiffness of the material. The copolymers have a significantly different mechanical response: as *soft* block content increases, E progressively decreases, with the exception of the copolymer with the lowest PLLA content. The result can be attributed to the low crystallinity degree of these copolymers with respect to PLLA homopolymer. By further increasing the P(BS80BAz20) percentage, the crystallinity degree raises up because of the formation of PBS crystals, leading to an increase of the

elastic modulus. Elastic modulus trend is also due to the rigidity of the repetitive unit. In fact, if we compare $PLLA_{73}P(BS80BAz20)_{27}$ and $PLA_{18}P(BS80BAz20)_{82}$, characterized by similar X_c value, the copolymer with a higher *soft* block content shows a smaller elastic modulus. As to the strain at break (ε^B), it was found to be inversely proportional to the crystalline phase degree and directly related to the *soft* block content, reaching a value of ≈ 600% for the copolymer $PLLA_{32}P(BS80BAz20)_{68}$.

The effect of copolymerization on stress at break (σ^B) is less noticeable: there is a decrease with respect to the homopolymer, but it does not change remarkably with the composition. Moreover, the copolymers present a very similar yield point, being the yield strength (σ^y) and the yield strain (ε^y) comparable for all the materials obtained.

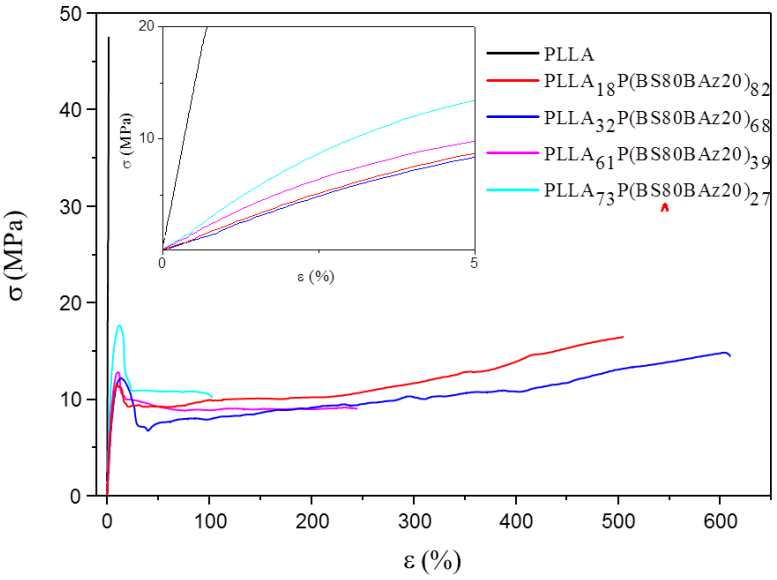

Figure 5.24 Stress-strain curves of $PLLA_mP(BS80BAz20)_n$ copolyester-urethanes synthesized.

5.4.4 Hydrolytic degradation studies

Hydrolytic degradation experiments have been carried out under physiological conditions (37°C, pH 7.4) in phosphate buffer to study the biodegradation kinetic of the synthesized materials in human body mimicking conditions.

In Figure 5.25a the residual weight of PLLA and $PLLA_mP(BS80BAz20)_n$ copolymers is reported as a function of the incubation time. In the time scale explored, PLLA did not

lose any weight, whereas all the copolymers degraded. This evidence indicates the hydrolysis process is faster in the triblock copolymers, but the degradation rate seems to be independent on the copolymer composition, with the exception of $PLLA_{18}P(BS80BAz20)_{82}$, sample.

As well known (Gigli *et al.*, 2012, 2013), there are more factors affecting the degradation rate, such as: molecular weight, crystallinity degree, amorphous phase mobility, ester groups density and steric hindrance. Although the correlation between the different factors and the rate of degradation is quite complex, we can assert that the acceleration of the hydrolysis process in the case of copolymers is mainly due to the lower crystallinity degree and the higher flexibility of the amorphous phase of these last. For the triblock copolymers, after 124 days, a weight loss up to 25% can be evidenced.

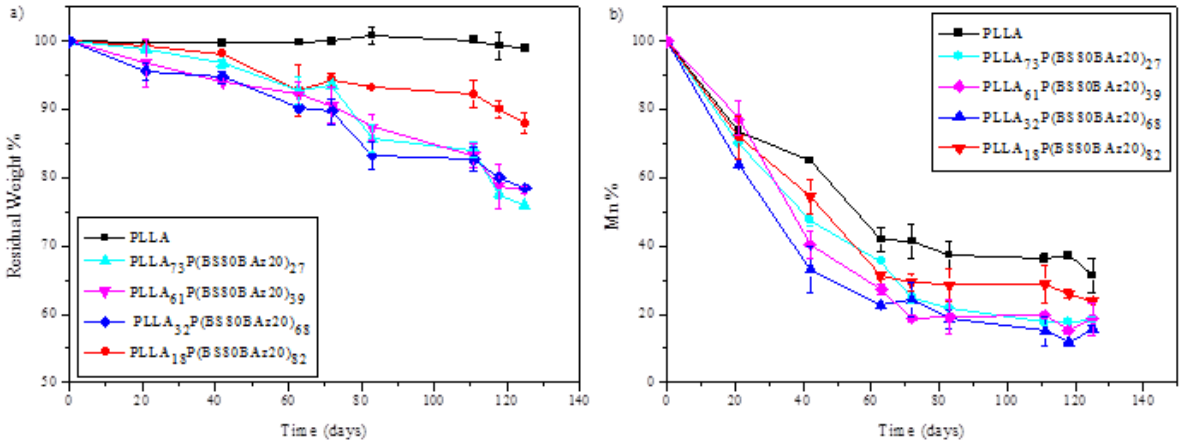

Figure 5.25 Residual gravimetric weight (a) and residual molecular weight (b) as a function of time. Measurements conducted at 37ºC and pH 7.4.

It is well known (Mochizuki and Hirami, 1997) that in the first stages of hydrolytic degradation substantial decrease in molecular weight occurs, even if weight losses are still negligible. In this view, PLLA and $PLLA_mP(BS80BAz20)_n$ samples have been subjected to molecular weight determination to verify the occurrence of the hydrolytic attack. As shown in Figure 8b, which reports the percentage of residual number average molecular weight (M_n) as a function of the incubation time, PLLA underwent a significant decrease of M_n (up to 60%) with time, confirming the starting of the

degradation process. The M_n of multiblock copolymers decreased too, displaying a similar trend with respect to weight loss measurements.

5.4.5 Biocompatibility assay

In vitro tolerance of the copolymers was evaluated by means of cellular viability measurements in presence of extracts of the copolymers taken at different time periods. The MTT tests showed that the extracts of the materials taken between 1 and 21 days were not cytotoxic after their incubation with human fibroblasts, for all the copolymers studied, giving cellular viability values around 100% at all the times, except for the extracts taken at 21 days, for which cell viability was around 90 % (Figure 5.27). Then, we can say that all samples were biocompatible according to the international standard ISO-10993-5, stating cytotoxicity as a reduction in the cellular viability higher than 70%.

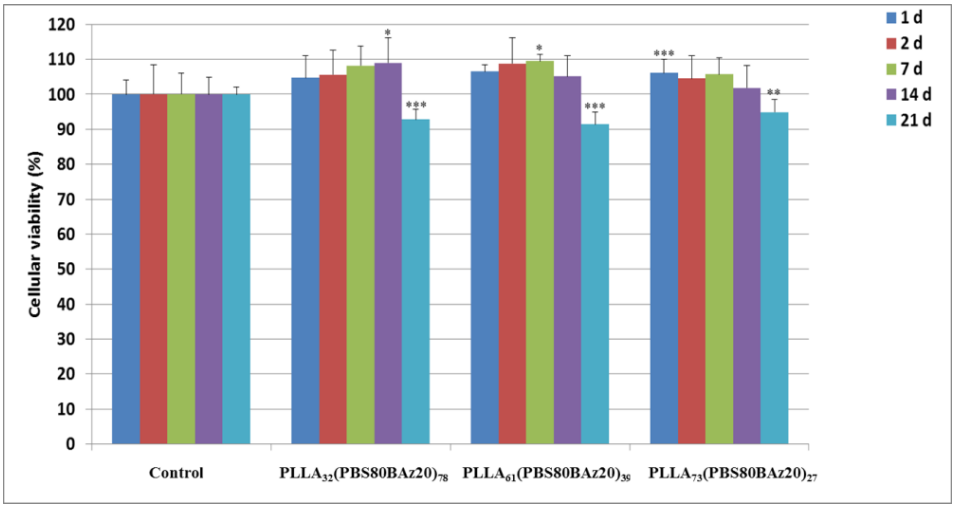

Figure 5.27 MTT assay results of $PLLA_mP(BS80BAz20)_n$ copolymers with human fibroblasts cultures at different time periods. All the results are shown as mean ± SD (n=4). Asterisks depict a significant difference between results of the corresponding sample with respect to control: * $p<0.05$, ** $p<0.01$ and *** $p<0.001$.

Quantitative analysis for cell adhesion and proliferation on copolymers films was carried out by means of the Alamar Blue test. The results were expressed in terms of cellular viability percentage (%) and are shown in Figure 5.28. It can be observed that

the cellular proliferation was higher for $PLLA_{61}(PBS80Baz20)_{39}$ and $PLLA_{73}(PBS80Baz20)_{27}$ copolymers films with respect to $PLLA_{32}(PBS80Baz20)_{68,}$ reaching values around 80% in the 7 first days. This allows us to state that the richest PLLA samples result more attractive for fibroblast. The decrease in cell adhesion with time, more marked after 14 days and for the $PLLA_{32}P(BS80BAz20)_{78}$ copolymer, could be due to the degradation of the film, previously shown in Figure 5.27; this degradation could detach the cells from de surface. In Figure 5.29, an example of the formation of a monolayer on the surface of the copolymers after 17 days of seeding, is given for $PLLA_{61}P(BS80BAz20)_{39}$. In overall, the cell proliferation results showed that these copolymers can be excellent candidates for the preparation of scaffolds for tissue engineering applications.

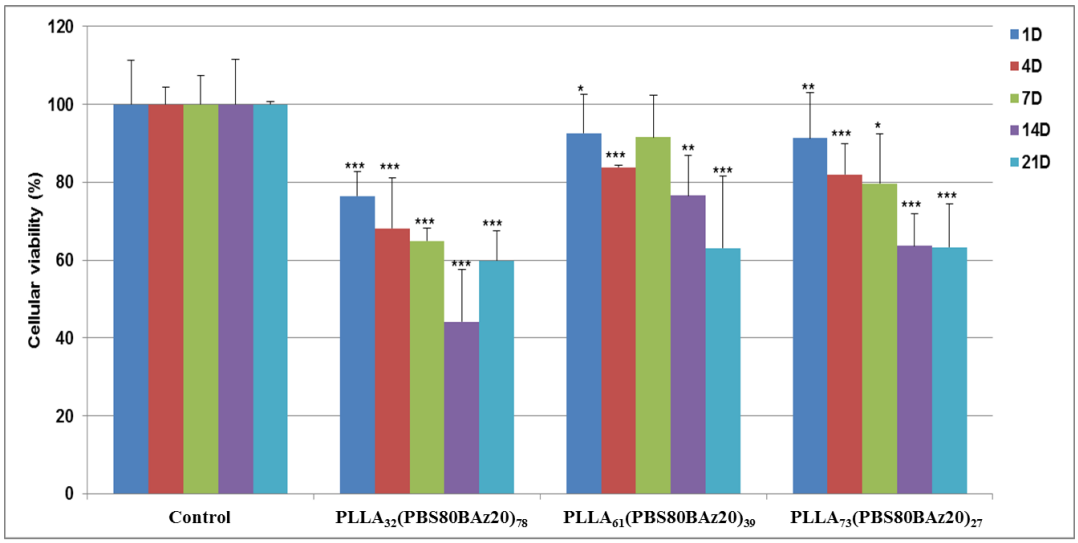

Figure 5.28 Proliferation assay results of $PLLA_mP(BS80BAz20)_n$ copolymers with human fibroblasts cultures. All the results are shown as mean ± SD (n=4). Asterisks depict a significant difference between results of the corresponding sample with respect to control: * $p<0.05$, ** $p<0.01$ and *** $p<0.001$.

Figure 5.29 Optical images (10x) of $PLLA_{61}P(BS80BAz20)_{39}$ film surface with humane fibroblasts after 17 days of seeding.

5.4.6 Nanoparticles characterizations

NPs of selected $PLLA_mP(BS80BAz20)_n$ copolymers were successfully obtained by nanoprecipitation (Fessi *et al.*, 1989). The particle size distributions were obtained by DLS to verify the particles dimension and values of average hydrodynamic diameter (D_h) and the Z-potential are reported in Table 5.22. All the samples presented unimodal distributions with a relatively narrow polydispersity and showed a mean diameter into the nanometric range and a low negative z-potential, indicating a few amount of negative terminal groups.

Table 5.22 NPs characterization data of $PLLA_nP(BS80BAz20)_m$ triblock copolymers.

Sample	D_h (nm)	PDI	Z-potential (mV)
$PLLA_{61}(PBS80Baz20)_{39}$	162	0.200	-14.0
$PLLA_{73}(PBS80Baz20)_{27}$	184	0.301	-9.5

The morphology of the NPs was examined by SEM. Results of NPs analysis shown in Figure 5.30 confirmed the average diameter range for the two polymeric compositions studied, revealed the spherical morphology of the polymeric particles and the absence of particles with irregular forms or aggregates.

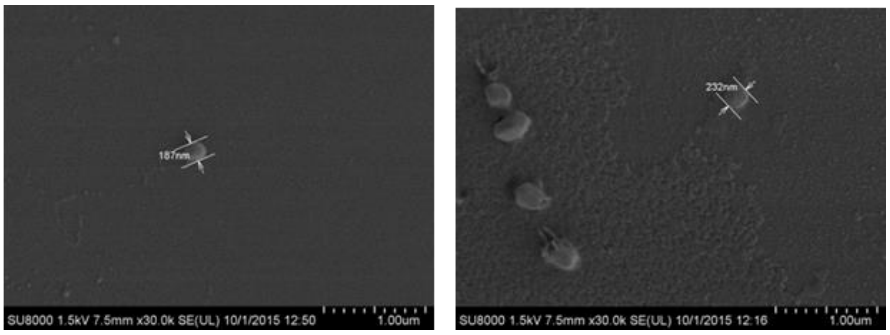

Figure 5.30 SEM image of a) $PLLA_{73}(PBS80Baz20)_{27}$ and b) $PLLA_{61}(PBS80Baz20)_{39}$ NPs. Measurements conducted at 25ºC.

NPs based on these bio-based PLLA copoly(ester-urethane)s can offer very interesting properties for the preparation and application of nanocarries as controlled delivery systems of bioactive principles for tissue engineering and regenerative medicine (Cameron and Shaver, 2011).

5.4.7 Comment on results obtained

Novel fully bio-based poly(lactic acid) copoly(ester-urethane)s characterized by a controlled molecular architecture have been successfully synthesized by a new solvent-free process, by coupling ROP with chain extension reaction. An ad hoc designed prepolymer has been used as initiator.

The synthetic approach used to prepare the polymers under investigation allowed the overcoming of the typical problems of copolymerization, among all, a substantial decrease of the melting temperature when significant amounts of the comonomeric units are introduced along the homopolymer backbone.

The use of two segments (*hard* and *soft*) possessing very different physical properties, permitted to obtain novel materials, with mechanical response that can be tuned simply playing with the mutual ratio of the two blocks. Furthermore, copolymerization revealed a winning strategy to enhance PLLA biodegradation rate under physiological conditions.

Nanoparticles with spherical morphology and adequate hydrodynamic diameter and zeta-potential values were obtained from selected copolymers by the nanoprecipitation

technique. Finally, all the synthetized copolymers were biocompatible and showed good cell adhesion and proliferation of human fibroblasts.

5.5 Cell behavior on 3D electrospun nanofiber mats based on a new PLLA triblock copolymer

Starting from the $PBS_xPCCE_yPNA_z$ A-B-A triblock copoly(ester-urethane)s (described in Chapter 5.4), a 3D mesh-like structure by electrospinning was realized.
Dexamethasone is the most widely used anti-inflammatory steroid drugs, and loaded scaffolds were prepared in order to evaluate the application of these three-dimensional supports in surgeries that present the risk of tissue inflammation after implant application.
The obtained scaffolds stability and dexamethasone release were evaluated in physiological conditions, and the cellular toxicity and proliferation were evaluated using fibroblast of human embryonic skin (HFB), while inflammatory activity was monitored only on murine RAW 264.7 macrophages.

5.5.1 Preparation of 3D mesh-like structure by electrospinning

A 3D-mesh-like structure composed by areas of randomly distributed fibers and areas of aligned fibers was created (Figure 5.31). The use of a PET mesh as a support allow us to obtain scaffolds with a specific geometry. Analysis by SEM showed that the holes of the mesh are mainly formed by random fibers (Figure 5.31 c.1) while the fibers deposited over the ridges of the mesh acquire an aligned disposition perpendicular to the filaments (Figure 5.31 c.2). The diameter of the fibers ranging from 1 µm to 7 µm was produced in both compositions ($PLLA_{32}(BS80BAz20)_{68}$ and $PLLA_{61}(BS80BAz20)_{39}$).

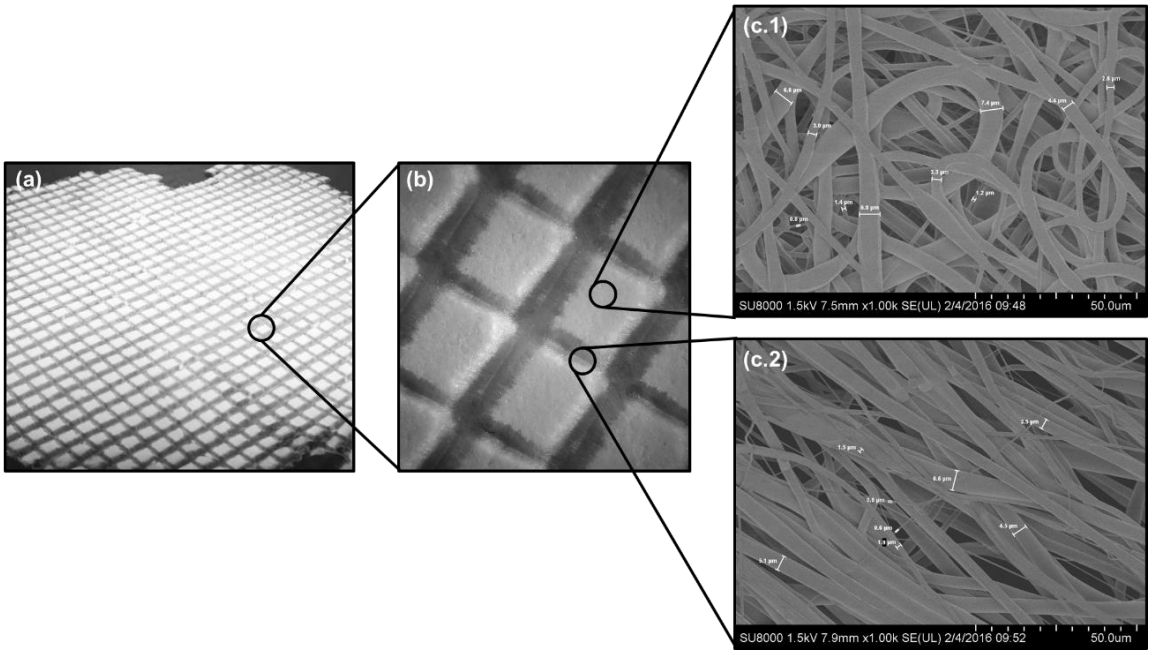

Figure 5.31 (a) Macroscopy view of the electrospun mat; (b) microscopy view of the random and aligned areas; (c) SEM pictures and width measurements of the fibers on the random (c.1) and aligned (c.2) areas.

In the case of dexamethasone loaded mats, the drug was dispersed in the medium before the electrospinning process. SEM pictures show that part of the dexamethasone crystalized on the surface of the fibres (Figure 5.32a). An energy-dispersive X-ray spectroscopy (EDX) microanalysis was carried out in the crystals present on the surface with the purpose of identified the fluorine of the dexamethasone. Figure 5.32c show the results of a EDX analysis, the presence of fluorine in the crystal indicate that it is composed of dexamethasone.

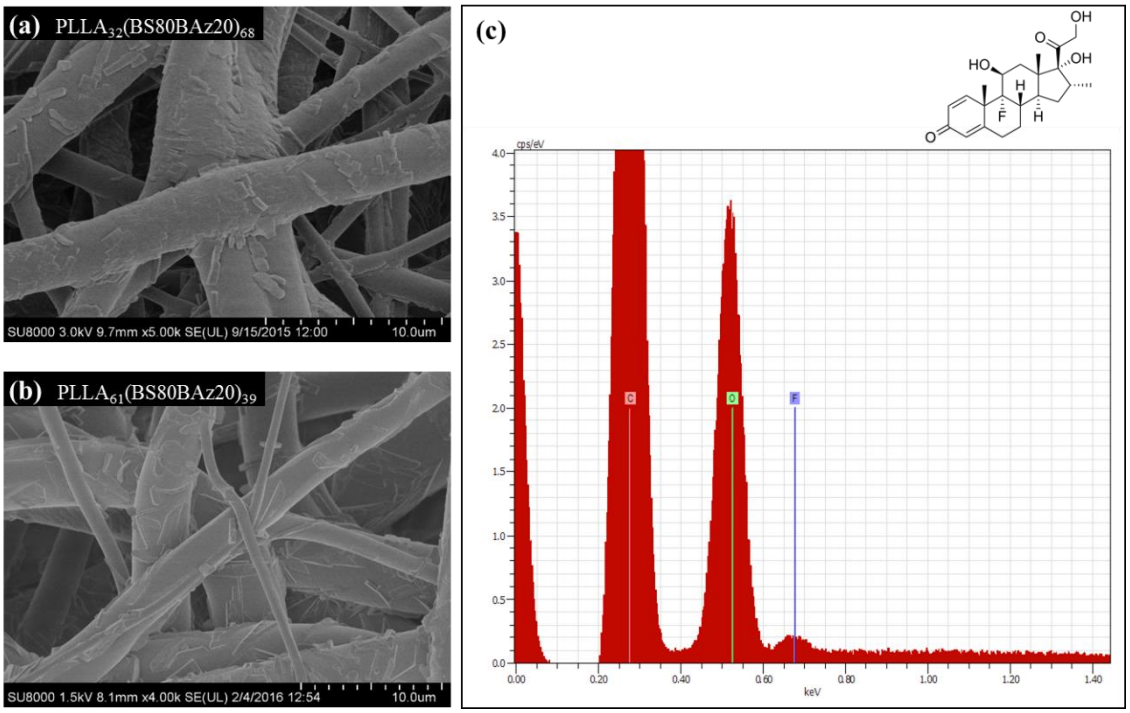

Figure 5.33 (a,b) SEM pictures (c) X-ray spectroscopy (EDX) microanalysis.

5.5.2 Stability and dexamethasone release studies

Figure 5.34a shows the weight loss of the electrospun mats under hydrolytic degradation in physiological conditions (37°C, pH 7.4) at different times.

The degradation of $PLLA_{32}(BS80Baz20)_{68}$ and $PLLA_{61}(BS80Baz20)_{39}$ mats was increasing in time. In the first days the weight loss could be due to loss of residual material in the fibres mat. After the first days, degradation begins to stabilize and the weight loss is due to fibres degradation, as is show in Figure 5.35. In SEM analysis could be observed the degradation of the fibres after 14 and 30 days, highlighting the appearance of erosions in the fibres and partially broken fibres.

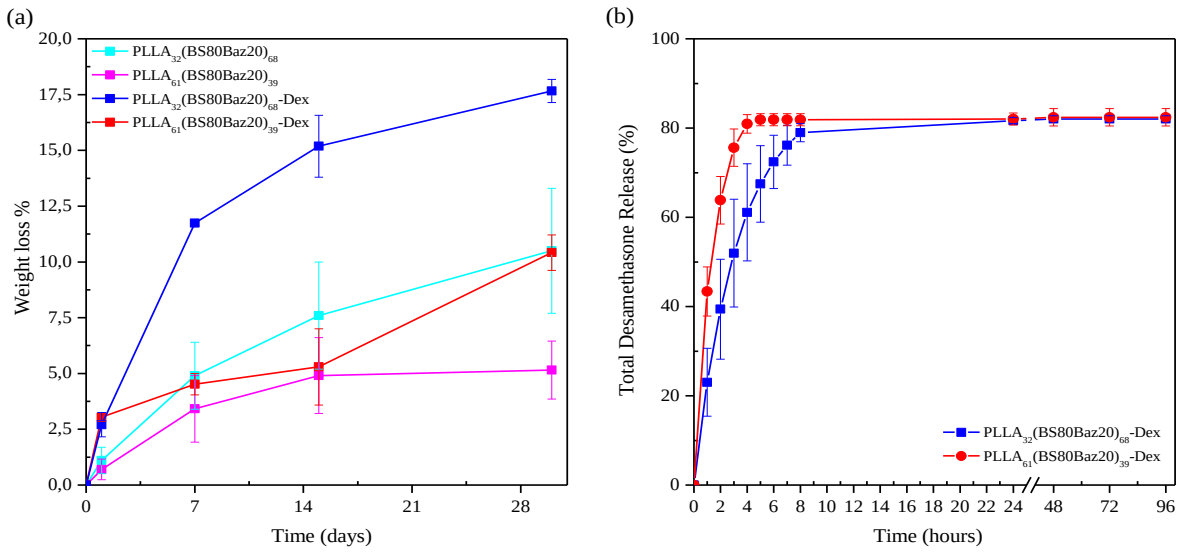

Figure 5.34 (a) Weight loss of the different electrospun mats under hydrolytic degradation and (b) dexamethasone release.

$PLLA_{32}(BS80Baz20)_{68}$-Dex and $PLLA_{61}(BS80Baz20)_{39}$-Dex mats showed a similar behavior. The difference was the higher initial weight loss due to the release of the dexamethasone present on the surface and a relative higher degradation in the time. This is due to the presence of dexamethasone crystals results in erosions and defects in the fibres. In these situation the fibres are more easily degradable, as is showed in Figure 5.35.

The release of dexamethasone was evidenced by SEM (Figure 5.35): dexamethasone crystals were not present in the fibres after few days. Dexamethasone released take place in the first hours (figure 3.54b). An initial burst release happened in the first 6-8 hours. In this time all the dexamethasone entrapped on the surface is released reaching the 80% of the loaded drug. The rest of the drug will be released with the degradation of the fibres.

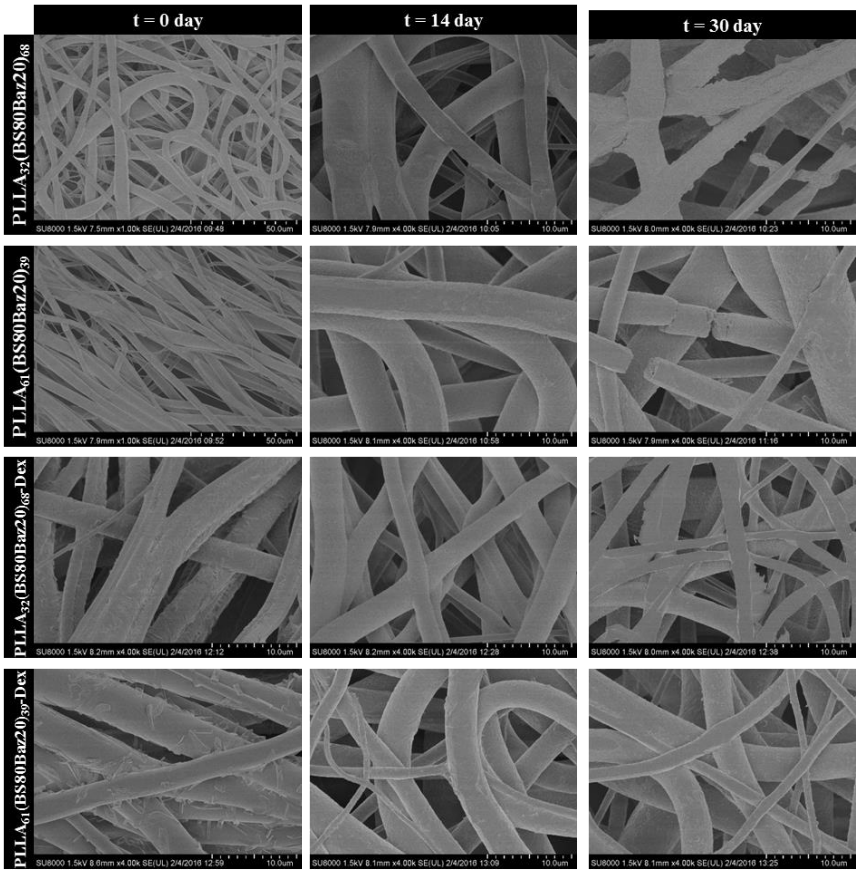

Figure 3.35 SEM monitored degration of $PLLA_m(BS80Baz20)_n$ copolymers with or without Dexamethasone.

5.5.3 Biocompatibility assay

In vitro tolerance of fibers films of $PLLA_{32}(BS80Baz20)_{68}$ and $PLLA_{61}(BS80Baz20)_{39}$ with and without dexamethasone was carried out by means of cellular viability measurements. The MTT assay (Figure 5.36) showed that the electrospun mats without dexamethasone were not cytotoxic after 21 days of incubation, meanwhile the mats that incorporated dexamethasone showed a small decrease in cell viability the first day due to the initial burst release of the drug. Cell viability is recovered after the second day and the film did not show a toxic effect.

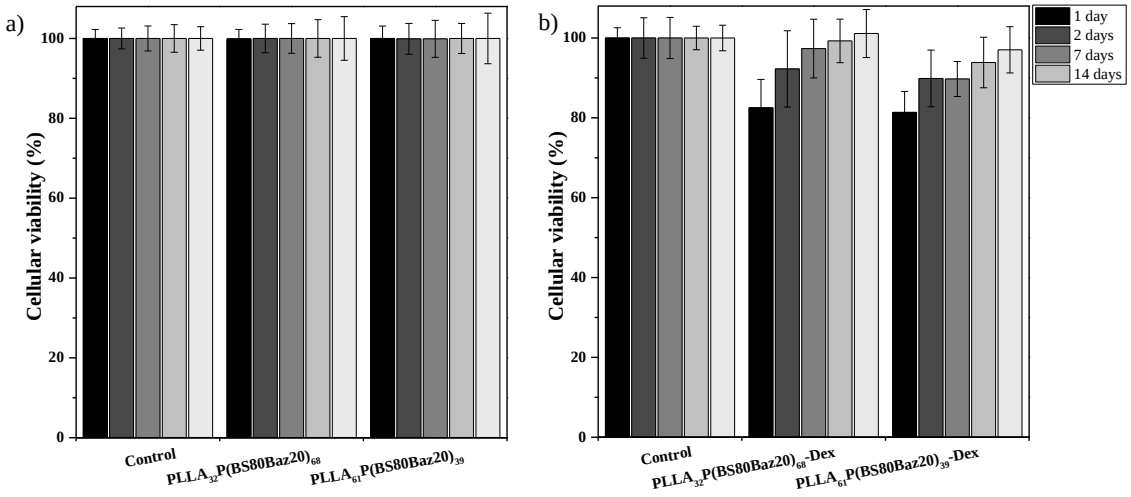

Figure 5.36 MTT assay of $PLLA_m(BS80Baz20)_n$ copolymers (b) with or (a) without Dexamethasone.

The biocompatibility of electrospun mats was also investigated *in vitro* by a cell adhesion and proliferation assay. Different proliferation trends are observed (Figure 5.37). At day 1 of culture, the cell proliferation of the control is higher than that of electrospun mats. It should be considered that cell proliferation can be strongly affected by the structure of the supporting scaffolds.

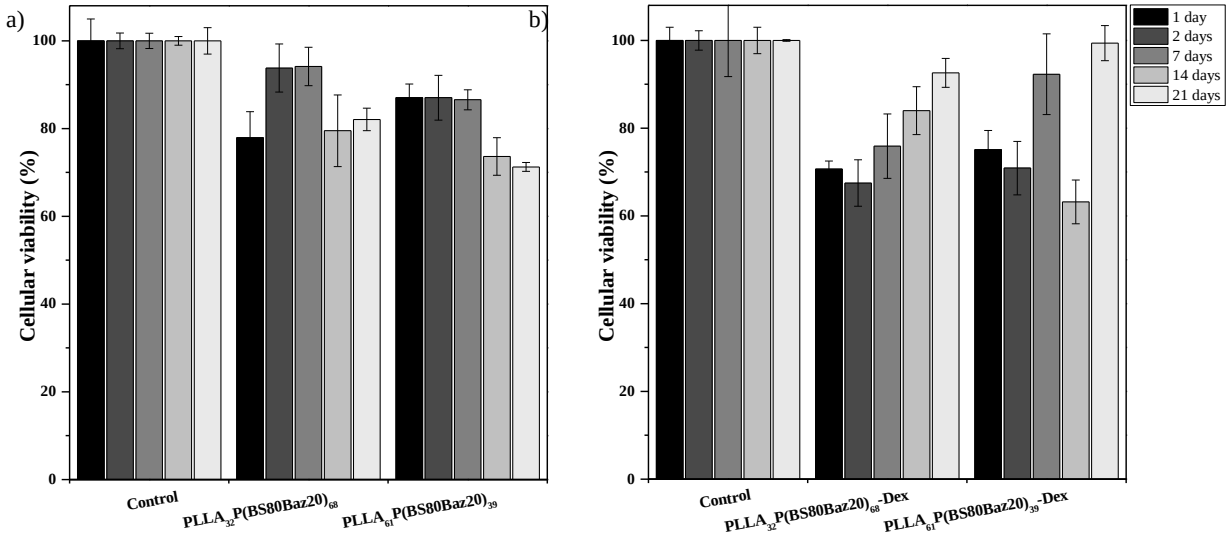

Figure 5.37 Alamar Blue assay of $PLLA_m(BS80Baz20)_n$ copolymers (b) with or (a) without Dexamethasone.

However, after a certain culture time, cell proliferation would result in the complete covering of the electrospun mat and no more space would be available for cells to further proliferate. At 14 and 21 days a decrease in cellular proliferation was observed, it can be related with cellular differentiation processes. This consideration seems to be supported by the trend observed in the SEM analysis (Figure 5.38). At day one of seeding, cells seeded onto the electrospun mat were well adhered and characterized by a flattened morphology. At longer times, cells generated extracellular matrix producing a more compact cellular structure. After 24 days is evident the presence of a monolayer that covers completely the entire polymer fibers surface, confirming the polymers biocompatibility and suggesting that these samples have a great potential as scaffolds for tissue engineering in biomedical applications.

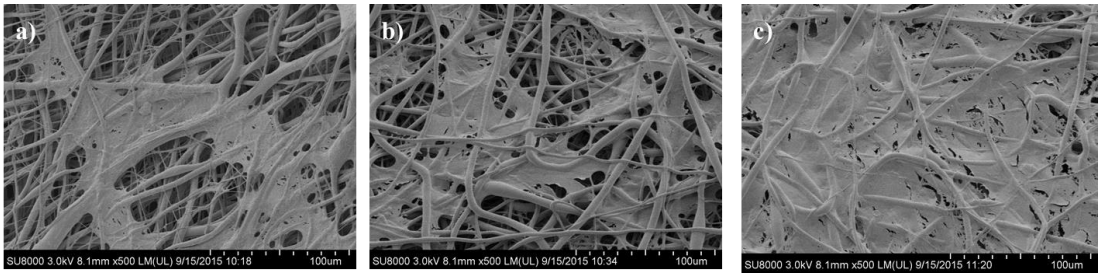

Figure 5.38 SEM analysis of $PLLA_{32}(BS80Baz20)_{68}$: (a) 24 hours cells seeding; (b) 7 days cells seeding; (c) 24 days cells seeding.

5.5.4 Inhibition of macrophage inflammatory response studies

To measure the anti-inflammatory activity of the dexamethasone-loaded mats, a NO inhibitory assay was employed. NO is a mediator and regulator in many pathological reactions, especially in acute inflammatory responses. Pro-inflammatory agents, such as LPS, increase NO production in macrophages through activation of inducible NO synthase (Kojima *et al.*, 2000). The presence of anti-inflammatory drugs such as dexamethasone reduce the inflammatory response. In our case no reduction of the inflammatory response was found with the use of $PLLA_m(BS80Baz20)_n$ electrospun mats. In the case of $PLLA_{32}(BS80Baz20)_{68}$-Dex, the presence of dexamethasone in the

fibres inhibit the inflammatory response without affect the viability of the cells (Figure 5.39)

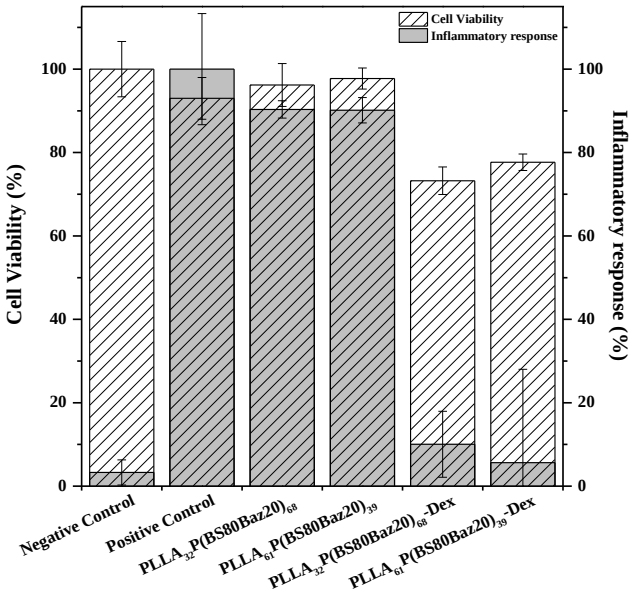

Figure 5.39 Anti-inflammatory assay of $PLLA_{32}(BS80Baz20)_{68}$ with murine RAW 264.7 macrophages.

This results allow the use of this kind of mats for the treatment of diseases involving inflammation process that need to be covered with a biomaterial for full recovery.

5.5.5 Comment on results obtained

The novel fully aliphatic $PLLA_m(BS80Baz20)_n$ copoly(ester-urethane)s characterized previously (Chapter 5.4) have been proven suitable for the realization of 3D mesh-like structure by electrospinning without a decrement in biocompatibility. At the same time, the encapsulation of an anti-inflammatory steroid drugs (Dexamethasone) it was possible. In both cases ($PLLA_m(BS80Baz20)_n$ and $PLLA_m(BS80Baz20)_n$-Dex), after 24 days in culture a cellular monolayer was observed on the surface demonstrating the biocompatibility of the three-dimensional constructs.

Dexamethasone released take place in the first hours: in the first 6-8 hours the 80% of the loaded drug is release. The anti-inflammatory tests shows that these fiber mats can be successfully used in the *in loco* treatment of inflammatory disorders, such as the recovery after surgery.

5.6 Life cycle assessment of PBS tridimensional scaffold

Life Cycle Impact Assessment (LCIA) was performed using IMPACT 2000+ evaluation method. using SimaPro 8.0.4 software, to determine the environmental impacts related to the emissions released and resources consumed in the system under study (Jolliet *et al.*, 2003). Than other methods, more impact categories are covered and more substances are included, but some additions and modifications were implemented to describe the system considered in a more representative manner:

- Land use was estimated by considering the basic indicators of both land occupation and transformation. In the present study Transformation, to forest intensive, normal, Transformation, to forest intensive and Transformation, to arable were introduced.
- Mineral extraction was characterised in consideration of some additional resources, such as silver, gravel, sand, lithium, bromine and water in ground, derived from the category Minerals of Eco-indicator 99 with the same characterization factors (Goedkoop and Spriensma, 2001).
- A radioactive waste category was added. In particular, both this kind of waste and its occupied volume were evaluated considering the same characterization and normalization factors of EPID 2003 method (Potting and Hauschild, 2004). This category allows the possible damage of the electric energy mix, which also includes the electricity generated by nuclear plants, to be taken into account. This latter kind of energy produces radioactive waste, which needs to be safely managed and disposed.

The Ecoinvent 3.1 database was taken as reference to complete the inventory of some chemicals, heat, electricity, transport and waste treatment.

LCIA has been reported by both midpoint and endpoint assessment. The indicators of midpoint analysis are linked to the cause-effect chain (environmental mechanism) of an impact factor. Common exemples include ozone depletion potentials, global warming potentials and photochemical ozone creation (smog) potential. Endpoint indicators are instead linked to the cause-effect chain for all categories of impact, e.g. human health

impacts, in terms of disability adjusted life wears for carcinogenicity, climate change, ozone depletion, or impacts in terms of change in biodiversity (Pini *et al.*, 2014).

5.6.1 LCA Results

A midpoint category interpretation was conducted to evaluate the environmental impact of various substances counted in the life cycle inventory. The impact categories considered are carcinogens, non-carcinogens, respiratory inorganics, ionizing radiation, ozone layer depletion, respiratory organics, aquatic ecotoxicity, terrestrial ecotoxicity, terrestrial acidification, land occupation, aquatic acidification, aquatic eutrophication, global warming, no-renewable energy, mineral extraction, renewable energy, internal costs, carcinogens indoor.

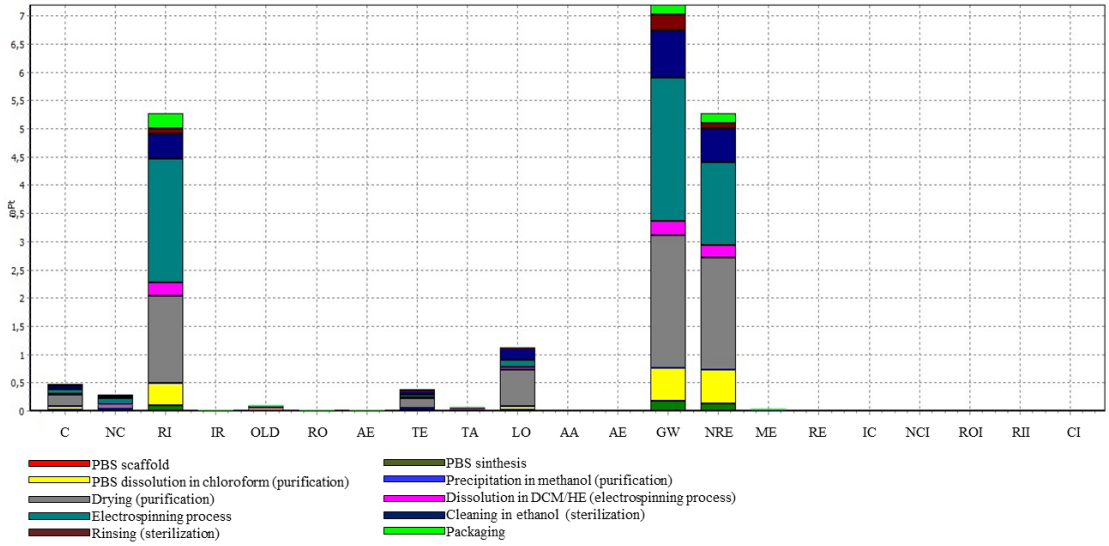

Figure 5.40 Evaluation by impact categories of one scaffold obtained through electrospinning technique from 35 g of purified poly(butylene succinate), where C= Carcinogens; NC= Non-Carcinogens; RI= Respiratory Inorganics; IR= Ionizing Radiation; OLD= Ozone Layer Depletion; RO= Respiratory Organics; AE= Aquatic Ecotoxicity; TE= Terrestrial Ecotoxicity; TA= Terrestrial acid/nutria; LO= Lando occupation; AA= Aquatic acidification; AE= Aquatic eutrophication; GW= Global warming; NRE= No-renewable energy; ME= Mineral extraction; RE= Renewable energy; IC= Internal costs; NCI= Non-Carcinogens indoor; ROI= Respiratory organics indoor; RII= Respiratory inorganics indoor; CI= Carcinogens indoor.

Table 5.23 summarizes the outcomes of the midpoint analysis, while Figure 5.40 highlights that the most significant contribution to the total damage is due to global warming (35.61%, GW), primarily affected by carbon dioxide emission in air (90.99%), which are for the 33.5% belonging to the drying step during purification, in particular for the electric energy consumption. Subsequently, the two major contributes are non-renewable energy (26.07%, NRE) and respiratory inorganics (26.04%, RI). Non-renewable energy is affected by natural gas (50.27%), crude oil (19.70%) and hard coal (15.88%) in which the main contribution is the drying step during purification, and to the uranium (12.54%), mainly due to the dichloromethane used in electrospinning process. Respiratory inorganics is affected by the following emission to the air: 31.71% of particulates <2.5 μm, 30.63% of NO_x, 24.29% of SO_x and 13.10% of particulates >2.5μm and <10μm. In all cases the main contribution is the dichloromethane used in electrospinning process.

Single score damage was 20.203 mPt for one scaffold obtained through electrospinning technique from 35 g of purified poly(butylene succinate). As show in Figure 5.41, the drying after purification (P3) and the electrospinning process (E) are the two mainly responsible contribution for the total damage (34.79% and 32.87%, respectively), followed by the cleaning in ethanol for the sterilization step (11.18%, S1) and the dissolution in chloroform for the purification step (9.05%, P1). These results are probably due to the high needed of solvents in these steps of scaffold production process.

Table 5.23 Characterised LCIA results.

Midpoint results			Endpoint results		
Impact category	**Unit**	**Total**	**Demage category**	**Unit**	**Total**
Carcinogens	kg C_2H_3Cl eq	1.2037	Human health	DALY	4.3585E-05
Non-Carcinogens	kg C_2H_3Cl eq	0.73769			
Respiratory inorganics	kg PM2.5 eq	0.73769			
Ionizing radiation	Bq C-14 eq	621.02			
Ozone layer depletion	kg CFC-11 eq	6.1359E-04			
Respiratory organics	kg C_2H_4 eq	2.7387E-02			
Aquatic ecotoxicity	kg TEG water	2928.8	Ecosystem quality	PDF*m^2*yr	21.492
Terrestrial ecotoxicity	kg TEG soil	649.07			
Terrestrial acid/nutri	kg SO_2 eq	0.88821			
Land occupation	m^2org.arable	14.25			
Aquatic acidification	kg SO_2 eq	0.88821			
Aquatic eutrophication	kg PO_4 P-lim	14.25			
Global warming	kg CO_2 eq	71.228	Climate change	kg CO_2	71.228
Non-renewable energy	MJ primary	800.55	Resources	MJ primary	804.65
Minerals extraction	MJ surplus	4.0974			
Renewable energy	kg	223.64			
Non-carcinogens indoor	kg	5.5299E-08	Human healt indoor	DALY	4.7868E-10
Respiratory organics indoor	kg	2.0017E-04			
Carcinogens indoor	kg	1.863E-05			
			Total damage	**mPt**	**20.203**

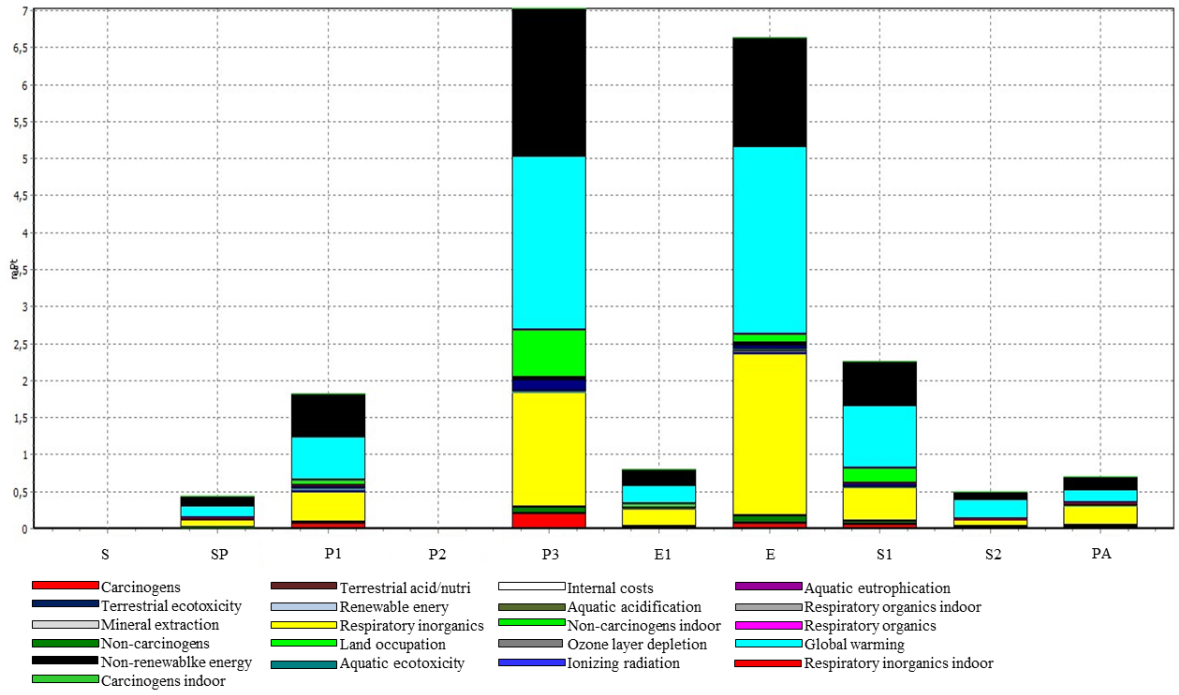

Figure 5.41 Evaluation by single score of one scaffold obtained through electrospinning technique from 35 g of purified poly(butylene succinate), where S= PBS scaffold; SP= PBS synthesis; P1= Dissolution in chloroform (purification); P2= Precipitation in methanol (purification); P3= Drying (purification); E1= Dissolution in DCM/HE (electrospinning process); E= Electrospinning process; S1= Cleaning in ethanol (sterilization); S2= Rising (sterilization); PA= Packaging.

The endpoints analysis (Table 5.23, Figure 5.52) highlights that the total damage worth 20.203 mPt, and affects for 35.61% the Climate change (7.194 mPt), due mainly to CO_2 (64.81%), and in particular the maximum damage is produced by the electrospinning process. Besides, the total damage affects for 30.42% the Human health (6.146 mPt), due to emission in air of particulate <2.5 μm (27.53%), NO_x (26.22%), SO_x (20.79%) and particulate >2.5 μm <10μm (11.22%) during the electrospinning process; for 26.21% the Resources (5.295 mPt), due to natural gas (50.01%), crude oil (19.60%), hard coal (15.80%) and uranium (12.48%), and the maximum damage is produced by the drying after the purification process; for 7.77% the Ecosystem quality (1.570 mPt), due mainly to the occupation forest (65.63%), and in particular the maximum damage is produced by the drying after the purification process; for 3.24E-4% the Human health

indoor, due mainly to the indoor presence of chloroform (48.81%) and methanol (12.88%) during the drying after the purification process.

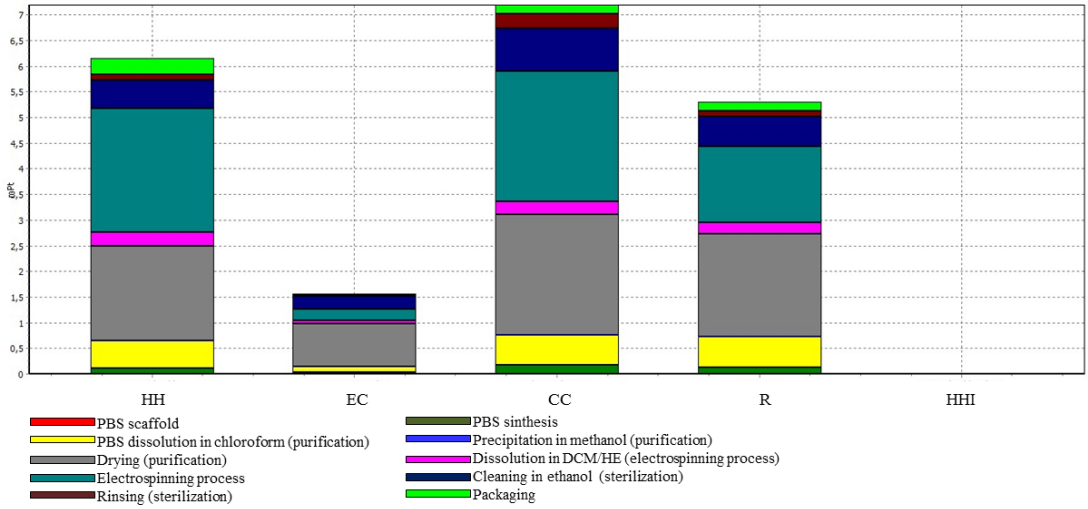

Figure 5.52 Evaluation by damage categories of one scaffold obtained through electrospinning technique from 35 g of purified poly(butylene succinate), where HH= Human health; EC= Ecosystem quality; CC= Climate change; R= Resources; HHI= Human health indoor.

5.6.2 Comment on results obtained

The life cycle analysis of one scaffold obtained through electrospinning technique from 35 g of purified poly(butylene succinate) shows that the total damage is 20.203 mPt and that the most affecting steps are purification (specifically the drying after the purification process, 34.79%) and the electrospinning process (32.87%). In the drying process it shows that the greatest damage comes from the electric energy used for the vapors suction. The choice of a lower flow rate could reduce this damage, as well as the possibility to reduce the hours required for the drying process. During the electrospinning process the maximum damage is due to equipment washing with dichloromethane. The damage due to the use of solvents is among the most important of those due to a chemical process, and could be reduce by regenerating the solvent.

The life cycle analysis highlights also that the damage categories with the highest damage are Climate change (35.61%), followed by Human Health (30.40%) and Resources (26.21%).

Hence, the mass production of studied polymers should be coupled by the detailed study of the manufacturing process, with the aim of improving those steps with a high effect on environmental impact. Such an optimized design in accordance with technical, economic and environmental performance indicators will be the focus of further research.

Chapter 6. Conclusions

The present PhD thesis demonstrated that modification in the poly(butylene succinate) backbone, through the introduction of ether-linkages or by block copolymerization with more amorphous subunits, had a notable and controllable effect on their physico-chemical properties leading to a decrement of chain symmetry and regularity as a result of the presence of co-unit chain segments. An improvement in the surface wettability related to the presence of the hydrophilic comonomeric subunits included is registered, too. In general, the crystallinity decrement and the increasing of the surface wettability affected the degradation rate, making it faster. In addition, in case of plasma surface treatment, there is an increase in hydrophilicity and consequently also the surface wettability increases without degrading the polymers.

In particular, the application of the chain extension strategy allows to obtain high molecular weight polymers with improved flexibility and elasticity, that depend on either the soft/hard ratio in the polymers and by the chemical composition of the soft prepolymer. Moreover, cyclic loading measurements revealed that the elastic behaviour is maintained even after 25 cycles. At the same time, the PBS-based copolymers have proved to be efficient to modify the poly(lactic acid) backbone, a polymer already widely used in the biomedical field and approved from the Food and Drug Administration (FDA), but with high crystallinity and slow degradation rate. The introduction of copolymeric subunits also in this case enhances aforementioned aspects.

All polymers studied have proven biocompatibility *in vitro* with different cell types. As a matter of fact, all the polyesters synthesized are suitable to applications in which is required to provide a support in dynamic conditions, typically in soft tissue engineering, combined with a degradation in non-toxic compounds when the material is no longer necessary, avoiding to resort to surgery to remove the implant after use.

The realization of 3D mesh-like structure by electrospinning allowed to better understand the specific application of these materials in tissue engineering, demonstrating that they are suitable to the cell adhesion and proliferation during time, as well as for the role of carriers for drugs for the *in loco* limitation of the inflammatory response which generally is established after surgery.

The final portion of the work has been focused on the Life Cycle Analysis (LCA) of PBS-based scaffolds, in order to couple technical considerations with an environmental impact study. The idea is to improve the introduction into the market of products with an innovative potential but also a responsible research approach, where the effects on the environment are taken into considerations since the first steps of the design. LCA results show that, given attention paid to material synthesis, the main damage produced by these tridimensional supports is now not due to the materials or workmanship in itself, but by the use of high amount of solvents, which can be reduced through production processes optimization and solvent recovery after use in the industrial mass production that could follow this pioneer study step.

In the industrial production, both copolymerization and chain extension reaction represent a winning strategy to modulate the polymer performances according to the desired application. Both approaches are simple, versatile and cost effective synthetic strategies to obtain a wide range of materials. Further research will be focused on the detailed design of upscalability of the synthesis process here presented, with a particular interest towards biomedical application field.

References

Adomaviciute E., Rimvydas M., The influence of applied voltage on poly(vinyl alcohol) (PVA) nanofibre diameter, *Fibers. Text. East. Eur*., **2007**; 15: 64.

Albertsson A.C., Srivastava R.K., Recent developments in enzyme-catalyzed ring-opening polymerization, *Advanced Drug Delivery Reviews*, **2008**, 60: 1077.

Albertsson A.C., Varma I.K., *Advances in Polymer Science*, Springer-Verlag Berlin Heidelberg, Vol. 157, **2002**.

Albertsson A.C., Varma I.K., Recent developments in ring opening polymerization of lactones for biomedical applications, *Biomacromolecules*, **2003**, 4: 1466.

Almeida L.R., Martins A.R., Fernandes E.M., Oliveira M.B., Correlo V.M., Pashkuleva I., Marques A.P., Ribeiro A.S., Duraes N.F., Silva C.J., Bonifacio G., Sousa R.A., Oliveira A.L., Reis R.L., New biotextiles for tissue engineering: development, characterization and in vitro cellular viability, *Acta Biomater*,, **2013**, 9:8167.

Alves de Silva M.L., Crawford A., Mundy J.M., Correlo V.M., Sol P., Bhattacharya M., Hatton P.V., Reis R.L., Neves N.M., Chitosan/polyester-based scaffolds for cartilage tissue engineering: assessment of extracellular matrix formation, *Acta Biomater*., **2010**, 6:1149.

Andronova N., Albertsson A.C., Resilient bioresorbable copolymers based on trimethylene carbonate, L-Lactide, and 1,5-Dioxepan-2-one, *Biomacromolecules*, **2006**, 7:1489.

Arima Y., Iwata H., Effect of wettability and surface functional groups on protein adsorption and cell adhesion using well-defined mixed self-assembled monolayers, *Biomaterials*, **2007**, 28:3074.

Arphavasin S., Singhatanadgit W., Ngamviriyavong P., Janvikul W., Meesap P., Patntirapong S., Enhanced osteogenic activity of a poly(butylene succinate)/calcium phosphate composite by simple alkaline hydrolysis, *Biomed. Mater*., **2013**, 8: 1.

Auras R., Harte B., Selke S., An overview of polylactides as packaging materials, *Macromol Biosci*, **2004**;4:835.

Auras R., Lim L.T., Selke S.E.M., Tsuji H., Poly(lactic acid): synthesis, structures, properties, processing, and application, *New Jersey: Jhon Wiley & Sons, Inc*, **2010**.

Azim, A., Dekhterman H., Jiang Z., Gross R.A., Candida antarctica lipase B-catalyzed synthesis of poly(butylene succinate): shorter chain building blocks also work, *Biomacromolecules,* **2006**, 7:3093.

Bajpai A.K., Shukla S.K., Bhanu S., Kankane S., Responsive polymers in controlled drug delivery, *Progress in Polymer Science*, **2008**, 33: 1088.

Baker S.C., Rohman G., Southgate J., Cameron N.R., The relationship between the mechanical properties and cell behavior on PLGA and PCL scaffolds for bladder tissue engineering, *Biomaterials*, **2009**, 30: 1321.

Bautista M., Martínez de Ilarduya A., Alla A., Muñoz-Guerra S., Poly(butylene succinate) Ionomers with Enhanced Hydrodegradability, *Polymers*, **2015**, 7:1232.

Bautista M., Martinez de Ilarduya A., Alla A., Munoz-Guerra S., Poly(butylene succinate) Ionomers and Their Use as Compatibilizers in Nanocomposites, *Polymer Composites*, **2015**, 1.

Bechthold I., Bretz K., Kabasci S., Kopitzky R., A Springer, Succinic acid: a new platform chemical for biobased polymers from renewable resources, *Chem. Eng. Technol.*, **2008**, 31:647.

Bikiaris D.N., Papageorgiou G.Z., Achilias D.S., Synthesis and comparative biodegradability studies of three poly(alkylene succinate)s, *Polym Degrad Stabil*, **2006**; 91: 31.

Brandwood A., Noble K.R., Schindhelm K., Influences of stress on biodegradation of novel biomedical polyurethanes, *Adv Biomater*, **1992**, 10: 413.

Bustin S.A., Benes V., Garson J.A., Hellemans J., Huggett J., Kubista M., Mueller R., Nolan T., Pfaffl M.W., Shipley G.L., Vandesompele J., Wittwer C.T., The MIQE guidelines: minimum information for publication of quantitative real-time PCR experiments, *Clin Chem*, **2009**; 55:611.

Candiani G, Riboldi SA, Sadr N, Lorenzoni S, Neuenschwander P, Montevecchi FM, Mantero S., Cyclic mechanical stimulation favors myosin heavy chain accumulation in engineered skeletal muscle constructs, *J Appl Biomater Biom*, **2010**, 8:68.

Cameron D.J.A., Shaver M.P., Aliphatic polyester polymer stars: Synthesis, properties and applications in biomedicine and nanotechnology, *Chemical Society Reviews*, **2011**, 40:1761.

Carothers W.H., Polymers and polyfunctionality, *Trans. Faraday Soc*., **1936**, 32: 39.

Chen H.B., Wang X.L., Zeng J.B., Li L.L., Dong F.X., Wang Y.Z., A novel multiblock poly(ester urethane) based on poly(butylene succinate) and poly(ethylene succinate-co-ethylene terephthalate), *Ind. Eng. Chem. Res.*, **2011**, 50: 2065.

Cheng Y., Deng S., Chen P., Ruan R., Polylactic acid (PLA) synthesis and modifications: a review, *Front Chem China*, **2009**;4:259.

Cohn D., Lando G., Sosnik A., Garty S., Levi A., Novel degradable reverse thermoresponsive multiblock copolymers, *Biomaterials*, **2006**, 27:1718.

Correlo V.M., Boesel L.F., Bhattacharya M., Mano J.F., Neves N.M., Reis R.L., Hydroxyapatite reinforced chitosan and polyester blends for biomedical applications, *Macromol. Mater. Eng*., **2005**, 290:1157.

Correlo V.M., Boesel L.F., Pinho E., Costa-Pinto A.R., Alves de Silva M.L., Bhattacharya M., Mano J.F., Neves N.M., Reis R.L., Melt-based compression-molded scaffolds from chitosan-polyester blends and composites: morphology and mechanical properties, *J. Biomed. Mater. Res*., **2008**, 91: 439.

Costa-Pinto A.R., Salgado A.J., Correlo V.M., Sol P., Bhattacharya M., Charbord P., Reis R.L., N.M. Neves, Adhesion, proliferation, and osteogenic differentiation of a mouse mesenchymal stem cell line (BMC9) seeded on novel melt-based chitosan/polyester 3D porous scaffold, *Tissue Eng. A*, **2008**, 14:1049.

Costa-Pinto A.R., Correlo V.M., Sol P.C., Bhattacharya M., Srouji S., Livne E., Reis R.L., Neves N.M., Chitosan-poly(butylene succinate) scaffolds and human bone marrow stromal cells induce bone repair in a mouse calvaria model, *J. Tissue Eng. Regen. Med*., **2012**, 6:21.

Costa-Pinto A.R., Martins A.M., Castellhano-Carlos M.J., Correlo V.M., Sol P.C., Longatto-Filho A., Reis R.L., Neves N.M., In vitro degradation and in vivo biocompatibility of chitosan poly(butylene succinate) fiber mesh scaffolds, *J. Bioact. Compat. Pol*., **2014**, 29:137.

Costa-Pinto A.R., Vargel I., Correlo V.M., Sol P.C., Faria S.,. Piskin E, Reis R.L.,. Neves N.M, Influence of scaffold composition over in vitro osteogenic differentiation of hBMSCs and in vivo inflammatory response, *J. Biomater. Appl*., **2014**, 28: 1430.

Coutinho D.F., Gomes M.E., Neves N.M., Reis R.L., Development of micropatterned surfaces of poly(butylene succinate) by micromolding for guided tissue engineering, *Acta Biomater*., **2012**, 8:1490.

Coutinho D.F., Pashkuleva I.H., Alves C.M., Marques A.P., Neves N.M., Reis R.L, The effect of chitosan on the in vitro biological performance of chitosan-poly(butylene succinate) blends, *Biomacromolecules*, **2008**, 9:1139.

Denizot F, Lang R., Rapid colorimetric assay for cell growth and survival - Modifications to the tetrazolium dye procedure giving improved sensitivity and reliability, *Journal of Immunological Methods*, **1986**,89:271.

Duda M., Shaw J.S., Life Cycle Assessment, *Social Science And Public Policy –Society*, **1997**, 35:38.

Engler A.J., Sen S., Sweeney H.L, Discher D.E., Matrix elasticity directs stem cell lineage specification, *Cell*, **2006**, 126:677.

Eisenberg A., he Glassy State and the Glass Transition, *Physical properties of polymers*, **1984.**

Fan R.R., Zhou L.X., Li D.X.,. Zhang D.M, Wu M., Guo G., Preparation and characterization of composites based on poly(butylene succinate) and poly(lactic acid) grafted tetracalcium phosphate, J. *Macromol. Sci. Phys*., **2014**, 53: 296.

Fessi H., Puisieux F., Devissaguet J.P., Ammoury N., Benita S., Nanocapsule formation by interfacial polymer deposition following solvent displacement, *International Journal of Pharmaceutics*, **1989**, 55:R1.

Flory P.J.; *J. Am. Chem. Soc*., **1936**, 58: 1877.

Flory P.J.; *J. Am. Chem. Soc*., **1939**, 61: 3334.

Flory P.J.; *J. Am. Chem. Soc*., **1942**, 64: 2205.

Flory P.J.; *J. Chem. Phys.* **1947**, 15: 684.

Flory P.J.; Principles of Polymer Chemistry, Ithaca, NY, 1953.

Fujimaki T., Processability and properties of aliphatic polyesters, 'BIONOLLE', synthesized by polycondensation reaction, *Polym. Degrad. Stabil*., **1998**, 59:209.

Gigli M., Lotti N., Gazzano M., Finelli L., Munari A., Novel eco-friendly random copolyesters of poly(butylene succinate) containing ether-linkages, *React. Funct. Polym*., **2012**, 72:303.

Gigli M., Lotti N., Gazzano M., Finelli L., Munari A., Synthesis and characterization of novel poly(butylene succinate)-based copolyesters designed as potential candidates for soft tissue engineering, *Polym. Eng. Sci*., **2013**, 53: 491.

Gigli M., Negroni A., Soccio M., Zanaroli G., Lotti N., Fava F., Munari A., Influence of chemical and architectural modifications on the enzymatic hydrolysis of poly(butylene succinate), *Green Chem*., **2012**, 14: 2885.

Gigli M., Negroni A., Zanaroli G., Lotti N., Fava F., Munari A., Environmentally friendly PBS-based copolyesters containing PEG-like subunit: effect of block length on solid-state properties and enzymatic degradation, *React. Funct. Polym*., **2013**, 73:764.

Gigli M., Negroni A., Soccio M., Zanaroli G., Lotti N., Fava F., Munari A., Enzymatic hydrolysis studies on novel eco-friendly aliphatic thiocopolyesters, *Polym. Degr. Stab.*, **2013**, 98:934.

Goedkoop M., Spriensma R., The Eco-indicator 99 – A damage oriented method for Life cycle Assessment, *Methodology Report*, Pré Consultants B.V., Amersfoort, **2001**.

Göpferich A., Mechanisms of polymer degradation and erosion, *Biomaterials*, **1996**, 17: 103.

Gourmelon G., Global Plastic Production Rises, Recycling Lags, *Vitalsign*, **2015**.

Gowsika J., Nanthini R., Synthesis, characterization and cytotoxicity of certain itaconic acid based biodegradable aliphatic copolyesters. *J. Chem. Pharm. Res*., **2014**, 6:1452.

Greiner A., Wendorff J.H., Electrospinning: A Fascinating Method for the Preparation of Ultrathin Fibers, *Angewandte Chemie*, **2007**, 46:5670.

Grigoriadou I., Nianias N., Hoppe A., Terxopoulou Z., Bikiaris D., Will J., Hum J., Roether J.A., Detsch R., Boccaccini A.R., Evaluation of silica-nanotubes and strontium hydroxyapatite nanorods ad appropriate nanoadditives for poly(butylene succinate) biodegradable polyester for biomedical applications. *Composites*, 2014, 60:49.

Grima S., Bellon-Maurel V., Feuilloley P., Silvestre F., Aerobic biodegradation of polymers in solid-state conditions: A review, *Journal of Polymers and the Environment*, **2000**, 8: 183.

Gross R.A., Ganesh M., Lu W., Enzyme-catalysis breathes new life into polyester condensation polymerizations, *Trends in Biotechnology*, **2010**, 28: 435.

Gualandi C., Govoni M., Foroni L., Valente S., Bianchi M., Giordano E.D., Pasquinelli G., Biscarini F., Focarete M.L., Ethanol disinfection affects physical properties and cell response of electrospun poly(L-lactic acid) scaffolds, *Eur Polym J*, **2012**; 48:2008.

Gualandi C., Soccio M., Govoni M., Valente S., Lotti N., Munari A., Giordano E., Pasquinelli G., Focarete M.L., Poly(butylene/diethylene glycol succinate) multiblock

copolyester ad a candidate biomaterial for soft tissue engineering: solid-state properties, degradability, and biocompatibility, *J. Bioact. Compat. Pol*., **2012**, 27:244.

Gualandi C., Soccio M., Saino E.,. Focarete M.L, Lotti N., Munari A., Moroni L., Visai L., Easly synthesized novel biodegradable copolyesters with adjustable properties for biomedical applications, *Soft Matter*, 2012, 8:5466.

Guevara I., Iwanejko J., Dembińska-Kieć A., Pankiewicz J., Wanat A., Anna P., Gołabek I., Bartuś S., Malczewska-Malec M., Szczudlik A., Determination of nitrite/nitrate in human biological material by the simple Griess reaction, *Clinica Chimica Acta*, **1998**, 274: 177.

Guo M., Life Cycle Assessment (LCA) of light-weight eco-composites, *Springer Thesis*, **2012**.

Guo W., Zhang Y., Zhang W., Mechanical properties and crystallization behavior of hydroxyapatite/poly(butylenes succinate) composites, *J. Biomed. Mater. Res*., **2013,** 101A:2500.

Guzman D., Chemical Industry awaits for bio-succinic acid potential, *ICIS Chemica Business*, **2012**.

Han S.I., Woong S.W., Kim B.S., Im S.S., A novel polymeric ionomer as potential biomaterial: crystallization behavior, degradation, and in-vitro cellular interactions, *Adv. Funct. Mater*., **2005**, 15:367.

Hao N., Wang Y.B., Zhang S.P., Shi S.Q., Nakashima K.,. Gong Y.K, Surface reconstruction and hemocompatibility improvement of a phosphorylcholine end-capped poly(butylene succinate) coating, *J. Biomed. Mater. Res*., **2014**, 102:2972.

Hariraksapitak P., Suwatong O., Pavasant P., Supaphol P., Effectual drug-releasing porous scaffold from 1,6-isocyanatohexane-extended poly(1,4-butylene succinate) for bone tissue regeneration, *Polymer*, **2008**, 49:2678.

Hench L.L and Polak J.M, Third-Generation Biomedical Materials, *Science*, **2002**, 259:1014.

Hentschel T., Münstedt H., Kinetics of the molar mass decrease in a polyurethane melt: a rheological study, Polymer, **2001**, 42:3195.

Hirotsu T., Tsujisaka T., Masuda T., Nakayama K., Plasma surface treatments and biodegradation of poly(butylene succinate) sheets, *J Appl Polym Sci*, **2000**,78:1121.

Hoffman A.S., The origins and evolution of "controlled" drug delivery systems, *Journal of Controlled Release*, **2008**, 132: 153.

Hollister S.J., Scaffold engineering: a bridge to where?, *Biofabrication*, **2009**, 1: 012001.

Hottle T.A., Bilec M.M., Landis A.E., Sustainability assessments of bio-based polymers, *Polym. Degr. Stabil.*, **2013**, 98:1898.

Hutmacher D.W., Scaffolds in tissue engineering bone and cartilage; *Biomaterials*., **2000**, 21: 2529.

Ikada Y., Tsuji H., Biodegradable polyesters for medical and ecological applications, *Macromol. Rapid Commun.*, **2000**, 21: 117.

ISO 2006a, Environmental management—life cycle assessment—principles and framework. *British Standards Institution*.

Jacquel N., Freyermouth F., Fenouillot F., Rousseau A., Pascault J.P., Fuertes P., Saint-Loup R., Synthesis and properties of poly(butylene succinate): efficiency of different transesterification catalysts, *J. Polym. Sci. A1*, **2011**, 49:5301.

Jager A., Gromadzki D., Jager E., Giacomelli F.C., Kozlowska A., Kobera L., Brus J., Rihova B., El Fray M., Ulbrich K., Stepanek P., Novel "soft" biodegradable nanoparticles prepared from aliphatic based monomers ad a potential drug delivery system, *Soft Matter* , **2012**, 8:4343.

Jager E., Jager A., Chytril P., Etrych T., Rihova B., Giacomelli F.C., Stepanek P., Ulbrich K., Combination chemotherapy using core-shell nanoparticles through the self-assembly of HPM-based copolymers and degradable polyester. *J. Control. Release* , **2013**, 165: 153.

Jeong E.H., Im S.S., Youk J.H., Electrospinning and structural characterization of ultrafine poly(butylene succinate) fibers, *Polymer*, **2005**, 46:9538.

Jérôme C., Lecomte P., Recent advances in the synthesis of aliphatic polyesters by ring-opening polymerization, *Advanced Drug Delivery Reviews*, **2008**, 60: 1056.

Jolliet O.; Margni M.; Charles R., Humbert S., Payet J., Rebitzer G., Rosenbaum R., IMPACT 2002+: a new life cycle impact assessment methodology, **2003**, 8:324.

Kaewkong P., Uppanan P., Thavornyutikarn B., Kosorn W., Janvikul W., Chondrocyte growth and function on HPBS/HA composite scaffolds: static versus dynamic culture, *IPCBEE*, **2012**, 43:11.

Klopffer W., Life Cycle Assesment: from the beginning to the current state, *Environ. Sci. & Pollut*., **1997**, 4:223.

Ko H.C., Milthtorpe, B. K., McFarland, C. D., Engineering thick tissues--the vascularisation problem, *Eur Cell Mater*., **2007**, 14: 1.

Kohn J., Welsh W.J., Knight D., A new approach to the rationale discovery of polymeric biomaterials, *Biomaterials*, **2007**, 28: 4171.

Kojima M., Morisaki T., Izuhara K., Uchiyama A., Matsunari Y., Katano M., Tanaka M., Lipopolysaccharide increases cyclo-oxygenase-2 expression in a colon carcinoma cell line through nuclear factor-κB activation, *Oncogene*, **2000**, 19:1225.

Kosorn W., Thavornyutikarn B., Phumsirl B., Uppanan P., Meesap P., Janvikul W., Hydrolyzed poly(butylene succinate) scaffolds coated with bioactive agent, *J. Metals Materials Minerals*, **2010**, 20:98.

Kun H., Wei Z., Xuan L., Xiubin Y., Biocompatibility of a novel poly(butylene succinate) and polylactic acid blend, *ASAIO J*., **2012**, 58:262.

Lackner M., Chapter Bioplastics - Biobased plastics as renewable and/or biodegradable alternatives to petroplastics, Kirk-Othmer Encyclopedia of Chemical Technology, 6th ed, **2015**.

Lasprilla A.J.R., Martinez G.A.R., Lunelli B.H., Jardini A.L., Filho R.M., Poly-lactic acid synthesis for application in biomedical devices: A review, *Biotechnology Advances* , **2012**, 30: 321.

Legras R, Bailly C, Daumerie M, Dekoninck JM, Mercier JP, Zichy V, Nield E., Crystallization of poly(ethylene terephthalate) induced by organic salts: Model compound study of the mechanism of action of the nucleating agent, *Polymer*, **1986**; 27:109.

Li H., Chang J., Cao A., Wang J., In vitro evaluation of biodegradable poly(butylene succinate) as a novel biomaterial, *Macromo. Biosci.*, **2005** , 5:433.

Li F., Zhao Y., Song T., Core-shell nanofibers: nano channel and capsule by coaxial electrospinning, *Nanofibers*, Book edited by: Ashok Kumar, Chapter 22, **2010**.

Li S.; *Scaffolding in Tissue Engineering*, Taylor & Francis Group, Boca Raton, Ch. 23, **2006**.

Li Y., Thouas G.A., Chen Q.Z., Biodegradable soft elastomers: synthesis/properties of materials and fabrication of scaffolds, *RSC Adv.*, **2012**, 2: 8229.

Lim J.S., Kim J.H., New application of poly(butylene succinate) (PBS) based ionomer as biopolymers: a role of ion group for hydroxyapatite (Hap) crystal formation, *J. Mater. Sci*., **2009**, 44:6398.

Liu Y., He J.H., Yu J.Y., Preparation and morphology of poly(butylene succinate) nanofibers via electrospinning, *Fibers Text. East Eur*., **2007**, 15:30.

Liu J., Jiang Z., Zhang S., Saltzman W.M., Poly(ω-pentadecalactone-co-butylene-co-succinate) nanoparticles as biodegradable carriers for camptothecin delivery, *Biomaterials*, **2009**, 30:5707.

Lloyd A.W., Interfacial bioengineering to enhance surface biocompatibility., *Med. Device Technol.*, **2002**, 13: 18.

Lofgren, A.; Albertsson, A. C.; Dubois, P.; Jerome, R., , *Macromol. Sci. ReV. Macromol. Chem. Phys*., **1995**, 35:379.

Lucas N., Bienaime C., Belloy C., Queneudec M., Silvestre F., Nava-Saucedo J.E., Polymer biodegradation: mechanisms and estimation techniques, *Chemosphere*, **2008**, 73: 429.

Mark H., Whitby G. S., Collected Papers of W.H. Carothers on polymerization, Interscience, New York, **1940**.

Martin I., Wendt D., Heberer M., The role of bioreactors in tissue engineering, *Trends Biotechnol*, **2004**, 22: 80.

Meesap P., Uppanan P., Thavornyutikarn B., Kosorn W., Janvikul W., Surface hydrolysed poly(butylene succinate) microspheres incorporated carboxymethylchitosan scaffolds for cartilage tissue engineering, *J. Metals Materials Minerals* , **2010**, 20:107.

Miyata T., Masuko T., Crystallization behavior of poly(tetramethylene succinate), *Polymer* , **1998**,39:1399.

Mochizuki M., Hirami M., Structural Effects on the Biodegradation of Aliphatic Polyesters, *Polym. Adv. Technol.*, **1997**, 8: 203.

Mohanraj K., Sethuraman S., Krishnan U.M., Development of poly(butylene succinate) microspheres for delivery of levodopa in the treatment of Parkinson's disease. *J. Biomed. Mater. Res.*, **2013**, 10:840.

Mosmann T., Rapid colorimetric assay for cellular growth and survival: Application to proliferation and cytotoxicity assays, *Journal of Immunological Methods*, **1983**;65:55.

Mukai K., Yamada K., Doi Y., Kinetics and mechanism of heterogeneous hydrolysis of poly[(R)-3-hydroxybutyrate] film by PHA depolymerases, *Int. J. Biol. Macromol.*, **1993**, 15: 361.

Müller A.J., Balsamo V., Arnal M.L., Crystallization in Block Copolymers with More than One Crystallizable Block, *Lect. Notes Phys.*, **2007**, 714: 229

Nair L.S., Laurencin C.T., Biodegradable polymers as biomaterials, *Prog. Polym. Sci.*, **2007**, 32: 762.

Nampoothiri K.M., Nair N.R., John R.P., An overview of the recent developments in polylactide (PLA) research, *Biores Technol*, **2010**;101:8493.

Ngamviriyavong P., Patntirapong S., Janvikul W., Arphavasin S., Meesap P., Singhatanadgit W., Development of poly(butylene succinate)/calcium phosphate composites for bone engineering, *Compos. Interface*., **2013**, 21:1.

Nie S., Understanding and overcoming major barriers in cancer nanomedicine, *Nanomedicine-UK*, **2010**, 5: 523.

Niu Y., Cao L., Wei J., Ma Y., Song S., Weng W., Li H., Liu C., Su J., Development of a bioactive composite of nano fluorapatite and poly(butylene succinate) for bone tissue regeneration, *J. Mater. Chem. B*, **2014**, 2: 1174.

Okada M., Chemical syntheses of biodegradable polymers, *Prog. Polym. Sci*., **2002**, 27: 87.

Oliveira T., Correlo V.M., Sol P.C., Costa-Pinto A.R., Malafaya P.B., Salgrado A.J., Bhattacharya M., Charbord P., Neves N.M., Reis R.L., Assessment of the suitability of chitosan/polybutylene succinate scaffolds seeded with mouse mesenchymal progenitor cells for a cartilage tissue engineering approach, *Tissue Eng. A*, **2008**, 14:1651.

Oliveira J.T., Crawford A., Mundy J.L., Sol P.C., Correlo V.M., Bhattacharya M., Neves N.M., Hatton P.V., Reis R.L., Novel melt-processable chitosan-polybutylene succinate fibre scaffolds for cartilage tissue engineering, *J. Biomater. Sci*., **2011**, 22:773.

Papageorgiou G.Z., Bikiaris D.N., Crystallization and melting behavior of three biodegradable poly(alkylene succinates). A comparative study, *Polymer*, **2005**, 46:12081.

Park J.B., Biomaterials Science and Engineering. New York; Plenum Press, **1984**.

Patel N.R., Gohil P.P., A review on biomaterials: scope, applications and human anatomy significance, *International Journal of Emerging Technology and Advanced Engineering*, **2012**, 2: 91.

Park S.J., Lee Y.M., Hong S.K., Release behaviors of porous poly(butylene succinate)/poly(ε-caprolactone) microcapsules containing indomethacin, *Colloid Surface B* , **2006**, 47:211.

Patntirapong S., Singhatanadgit W., Meesap P., Theerathanagorn T., Toso M., Janvikul W., Stem cell adhesion and proliferation on hydrolyzed poly(butylene succinate)/b-tricalcium phosphate composites, *J. Biomed. Mater. Res. A*, **2015**, 103:658.

Pedroso A.G., Rosa D.S., Mechanical, thermal and morphological characterization of recycled LDPE/corn starch blends, *Carbohyd. Polym*., **2005**, 59: 1.

Pinho E.D., Martins A., Araujo J.V., Reis R.L., Neves N.M., Degradable particulate composite reinforced with nanofibres for biomedical applications, *Acta Biomater*. **2009**, 5:1104.

Pini M., Ferrari A.M., Gamberini R., Neri P., Rimini B., Life cycle assessment of a large, thin ceramic tile with advamtageous technological properties, *Int. J. Life Cycle Assess.*, **2014**.

Potting J., Hauschild M., The EDIP 2003 methodology – Background for spatial differentiation in life cycle impact assessment, *Methodology Report*, Danish Environmental Protection Agency, Copenhagen, **2004**.

Rabinovitch E., , *Trans. Faraday Soc.*, **1937**, 33:1225.

Ranella A., Barberoglou M., Bakogianni S., Fotakis C., Stratakis E., Tuning cell adhesion by controlling the roughness and wettability of 3D micro/nano silicon structures, *Acta Biomaterialia*, **2010**, 6:2711.

Reilly G.C., Engler A.J., Intrinsic extracellular matrix properties regulate stem cell differentiation, *J. Biomech*., **2010**, 43:55.

Reneker D.H., Yarin A.L., Fong H., Koombhongse S., Bending instability of electrically charged liquid jets of polymer solutions in electrospinning, *J. Appl. Phys*., **2000**, 87: 4531.

Ribeiro V.P., Ribeiro A.S., Silva C.J., Durães N.F., Bonifácio G., Correlo V.M., Marques A.P., Sousa R.A., Oliveira A.L., Reis R.L., Evaluation of Novel 3D

Architectures Based on Knitting Technologies for Engineering Biological Tissues, *Journal of Donghua University*, **2013**, 5:421.

Riboldi SA, Sampaolesi M, Neuenschwander P, Cossu G, Mantero S., Electrospun degradable polyesterurethane membranes: potential scaffolds for skeletal muscle tissue engineering, *Biomaterials*, **2005**, 26:4606.

Rizvi M.S., Kumar P., Katti D.S., Pal A., Mathematical model of mechanical behavior of micro/nanofibrous materials designed for extracellular matrix substitutes, *Acta Biomater*., **2012**, 8:4111.

Sanchez I.C., Eby R.K., Crystallization of Random Copolymers, *Journal of research of the Notional Bureau of Standards - A. Physics and Chemistry*, **1973**, Vol. 77A, 3: 353.

Schut J.H, Waiting for bio PBS, Plastics Engineering, **2014**.

Schwarz K., Epple M., A detailed characterization of polyglycolide prepared by solid-state polycondensation reaction, *Macromol. Chem. Phys.*, **1999**, 200: 2221

Seppala J., Linko Y.Y., Su T., Photo- and biodegradation of high volume thermoplastics, *Acta Polytech Stand,* **1991**, 198: 10.

Siracusa V., Lotti N., Munari A., Dalla Rosa M., Poly(butylene succinate) and poly(butylene succinate-co-adipate) for food packaging applications: Gas barrier properties after stressed treatments, *Polym. Degrad. Stab*., **2015**, 119:35.

Shirahama H., Kawaguchi Y., Aludin M.S., Yasuda H., Synthesis and enzymatic degradation of high molecular weight aliphatic polyesters, *J. Appl. Polym. Sci.*, 2001, 80:340.

Soccio, Lotti N., Finelli L., Gazzano M., Munari A., Influence of transesterification reactions on the miscibility and thermal properties of poly(butylene/diethylene succinate) copolymers, *Eur. Polym. J.*, **2008**, 44:1722.

Soccio M., Lotti N., Gazzano M., Govoni M., Giordano E., Munari A., Molecular architecture and solid-state properties of novel biocompatible PBS-based copolyesters containing sulphur atoms, *React. Funct. Polym.*, 2012, 72:856.

Staab H.A., Transacylierungen, IV. Reaktionsfähige Heterocyclische Amide von Dicarbonsäuren, *Chem. Ber*., **1957**, 90: 1326.

Stoyanova N., Paneva D., Mincheva R., Toncheva A., Manolova N., Dubois P., Rashkov I., Poly(L-lactide) and poly(butylene succinate) immiscible blends: from electrospinning to biologically active materials, *Mater. Sci. Eng. C* , **2014**, 41:119.

Suchanek W., Yoshimura M., Processing and properties of hydroxyapatite-based biomaterials
for use as hard tissue replacement implants, *J. Mater. Res*., **1998**, 13:94.

Sugihara S., Toshima K., Matsumura S., New strategy for enzymatic synthesis of high-molecular-weight poly(butylene succinate) via cyclic oligomers, *Macromol. Rapid Comm*., **2006**, 27:203.

Sutthiphong S., Pavasant P., Supaphol P., Electrospun 1,6-diisocyanatohexane-extended poly(1,4-butylene succinate) fiber mats and their potential for use as bone scaffolds, *Polymer*, **2009**, 50:1548.

Suyama T., Tokiwa Y., Ouichanpagdee P., Kanagawa T., Kamagata Y., Phylogenetic affiliation of soil bacteria that degrade aliphatic polyesters available commercially as biodegradable plastics, *Applied and Environmental Microbiolology*, **1998**, 64: 5008.

Tallawi M., Rai R., Gleixner M.R., Roerick O., Weyand M., Roether J.A., Schubert D.W., Kozlowska A., El Fray M., Merle B., Goken M., Aifantis K., Boccacini A.R., Poly(glycerol sebacate)/poly(butylene succinate-dilinoleate) blends ad candidate materials for cardiac tissue engineering, *Macromol. Symp*., **2013**, 334:57.

Tallawi M., Zebrowski D.C., Rai R., Roether J.A., Schubert D.W., El Fray M., Engel F.B.,. Aifantis K.E, Boccaccini A.R., Poly(glycerol sebacate)/poly(butylene succinate-dilinoleate) (PGS/PBS-DLA) fibrous scaffolds for cardiac tissue engineering, *Tissue Eng. Pt. C Meth*, **2014**, 20:412.

Tan L., Hu J., Ye S., Wei J., Chen Y., Crystallization and degradation behaviors of poly(butylene succinate)/poly(Z-L-Lysine) composites, *Thermochim. Acta*, **2014**, 575: 279.

Tang J.X., Wu Q.Y., Mesenchimal stem cellular adhesion and cytotoxicity study of random biopolyester scaffolds for tissue engineering, *J. Mater. Sci. Mater. Med*., **2006**, 17:627.

Theron S.A., Zussman E., Yarin A.L., Experimental investigation of the governing parameters in the electrospinning of polymer solutions, *Polyme*r, **2004**, 45: 2017.

Tian H., Tang Z., Zhuang X., Chen X., Jing X., Biodegradable synthetic polymers: preparation, functionalization and biomedical application, *Progress in Polymer Science*, **2012**, 37: 237.

Tserki V., Matzinos P., Pavlidou E., Vachliotis D., Panayiotou C., Biodegradable aliphatic polyesters. Part I. Properties and biodegradation of poly(butylene succinate-co-butylene adipate), *Polym. Degr. Stab.*, **2006**, 91: 367.

Uhrich K.E., Cannizzaro S.M., Langer R.S., Shakesheff K.M., Polymeric systems for controlled drug release, *Chem. Rev*., **1999**, 99:3181.

Ulery B.D., Nair L.S., Laurencin C.T., Biomedical applications of biodegradable polymers, J. *Polym. Sci. Polym. Phys*., **2011**, 49: 832.

Uppanan P., Meesap P., Thavornyutikarn B., Kosorn W., Janvikul W., Study on surface-hydrolyzed poly(butylene succinate)/hydroxyapatite composite scaffolds for cartilage regeneration, *Adv. Sci. Lett.*, **2013**, 19:3070.

Varadarjan S., Miller D.J., Catalytic upgrading of fermentation-derived organic acids, *Biotechnol. Progr*., 1999, 15:845.

Varma I.K., Albertsson A.C., Rajkhowa R., Srivastava R.K., Enzyme catalyzed synthesis of polyesters, *Prog. Polym. Sci*., 2005, 30: 949.

Vert M., Aliphatic Polyesters: Great Degradable Polymers That Cannot Do Everything, *Biomacromolecules*, **2005**, 6:538.

Vert M., Degradable and bioresorbable polymers in surgery and in pharmacology: beliefs and facts, *J. Mater. Sci. – Mater. Med*., **2009**, 20: 437.

Von Burkersroda F., Schedl L., Göpferich A., Why degradable polymers undergo surface erosion or bulk erosion, *Biomaterials*, **2002**, 23: 4221.

Wang H., Ji J., Zhang W., Wang W., Zhang Y., Wu Z., Zhang Y., Chu P.K., Rat calvaria osteoblast behavior and antibacterial properties of O_2 and N_2 plasma-implanted biodegradable poly(butylene succinate), *Acta Biomater*., **2010**, 6:154.

Wang L.C., Chen J.W., Liu H.L., Chen Z.Q., Zhang Y., Wang C.Y., Feng Z.G., Synthesis and evaluation of biodegradable segment multiblock poly(ether ester) copolymers for biomaterial applications, *Polym. Int*., **2004**, 53:2145.

Wang, S.Y., Lan X.Y., Xiao J.H., Yang J.C., Kao Y.T., Chang S.T., Antiinflammatory activity of Lindera erythrocarpa fruits, *Phytotherapy Research*, **2008**, 22:213.

Wang H., Ji J., Zhang W., Jiang J., Wu Z., Pu S., Chu P.K., Biocompatibility and bioactivity of plasma-treated biodegradable poly(butylene succinate), *Acta Biomater*., **2009**, 5:279.

White A.A., Best S.M., Hydroxyapatite-carbon nanotube composites for biomedical applications: a review, *Int. J. Appl. Ceram. Tec*., **2007**, 4:1.

Williams D.F., On the mechanisms of biocompatibility, *Biomaterials*, **2008**, 29: 2941.

Wu F., Huang C.L., Zeng J.B., Li S.L., Wang Y.Z., Synthesis and characterization of segmented poly(butylene succinate) urethane ionenes containing secondary amine cation. *Polymer*, **2014**, 55:4358.

Wu C.S., Hsu Y.C., Liao H.T., Yen F.S., Wang C.Y., Hsu C.T., Characterization and biocompatibility of chestnut shell fiber-based composites with polyester, *J. Appl. Polym. Sci*., **2014**, 131: 1.

Xiao L., Wang B., Yang G., Gauthier M., Poly(Lactic Acid)-Based Biomaterials: Synthesis, Modification and Applications, Biomedical Science, *Engineering and Technology*, **2012**, Chapter 11.

Xu J., Guo B.H., Poly(butylene succinate) and its copolymers: research, development and industrialization, *Biotechnol. J*., **2010**, 5:1149.

Yagihara T., Matsumura S., Enzymatic synthesis and chemical recycling of novel polyester-type thermoplastic elastomers, *Polymers*, **2012**, 4:1259.

Yang J., XTian W., Li X.Q., Li X., Cao A., Novel biodegradable aliphatic poly(butylene succinate)s bearing functionalizable carbonate building blocks: II. Enzymatic biodegradation and in vitro biocompatibility assay, *Biomacromolecules*, **2004**, 5:2258.

Yarin A.L., Koombhongse S., Reneker D.H., Bending instability in electrospinning of nanofibers, *J. Appl. Phys*., **2001**, 89: 3018.

Yildirim ED, Ayan H, Vasilets VN, Fridman A, Guceri S, Sun W., Effect of dielectric barrier discharge plasma on the attachment and proliferation of osteoblasts cultured over poly(Îµ-caprolactone) scaffolds, *Plasma Processes and Polymers*, **2008**,5:58.

Yolles, S.; Eldridge, J. E.; Woodland, Sustained delivery of drugs from polymer drug mixtures, *J. H. R. Polymer News*, **1971**, 1:9.

Yoo E.S, Im S.S., Melting behavior of poly(butylene succinate) during heating scan by DSC, *J. Polym. Sci. Pol. Phys*., **1999**, 37:1357.

Yoshii E., Cytotoxic effects of acrylates and methacrylates: Relationships of monomer structures and cytotoxicity, *Journal of Biomedical Materials Research*, **1997**,37:517.

Zhan D., Chang J., Zang Y., Fabrication of fibrous poly(butylene succinate)/wollastonite/apatite composite scaffolds by electrospinning and biometric process, *J. Mater. Sci. Mater. Med*., **2008**, 19:443.

Zhang S.P., Wang L.L., Yang S.,. Gong Y.K, Improved Biocompatibility of phosphorylcholine end-capped poly(butylene succinate), *Sci. China*, **2013**, 56:174.

Zenz C.R., Conference on Biomaterials, For Genomics and Bioinformatics, 2008.

Zhu X., Chen J., Scheideler L., Altebaeumer T., Geis-Gerstorfer J., Kern D., Cellular reactions of osteoblasts to micron- and submicron-scale porous structures of titanium surfaces, *Cells Tissues Organs*, **2004**, 178:13.

Zimmermann H., Grassie N, editors, Developments in Polymer Degradation, *Applied Science Publishers*, **1984**, 5.

Supplementary informations

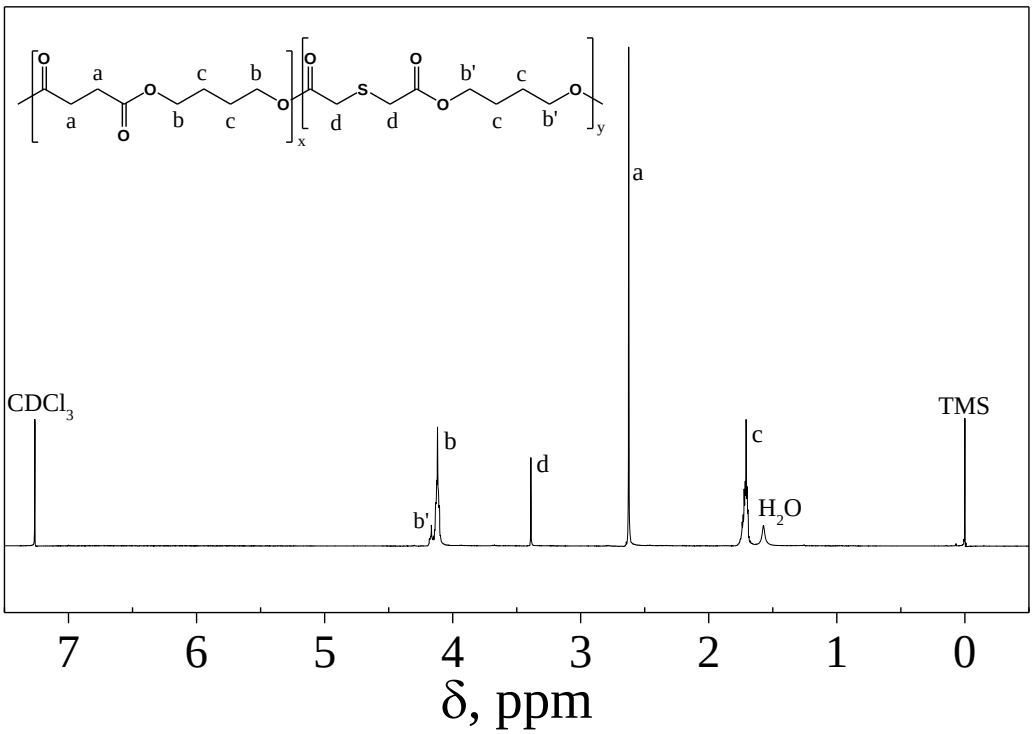

Figure S1 [1]H-NMR spectra of P(BS85BTDG15) with resonance assignments.

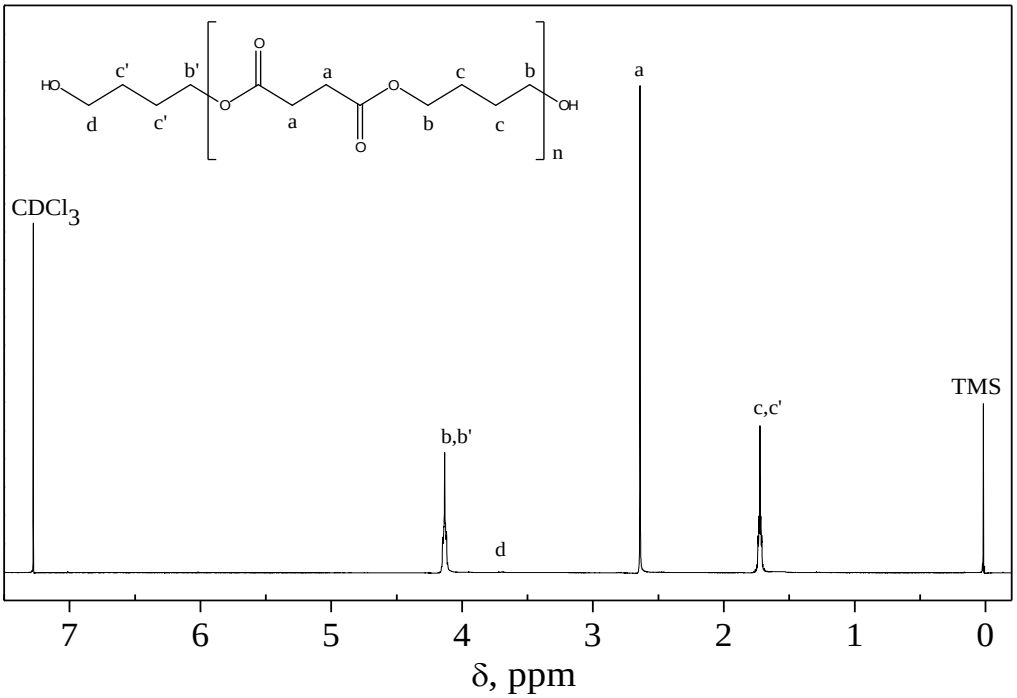

Figure S2 [1]H-NMR spectrum of PBS-OH with resonance assignments.

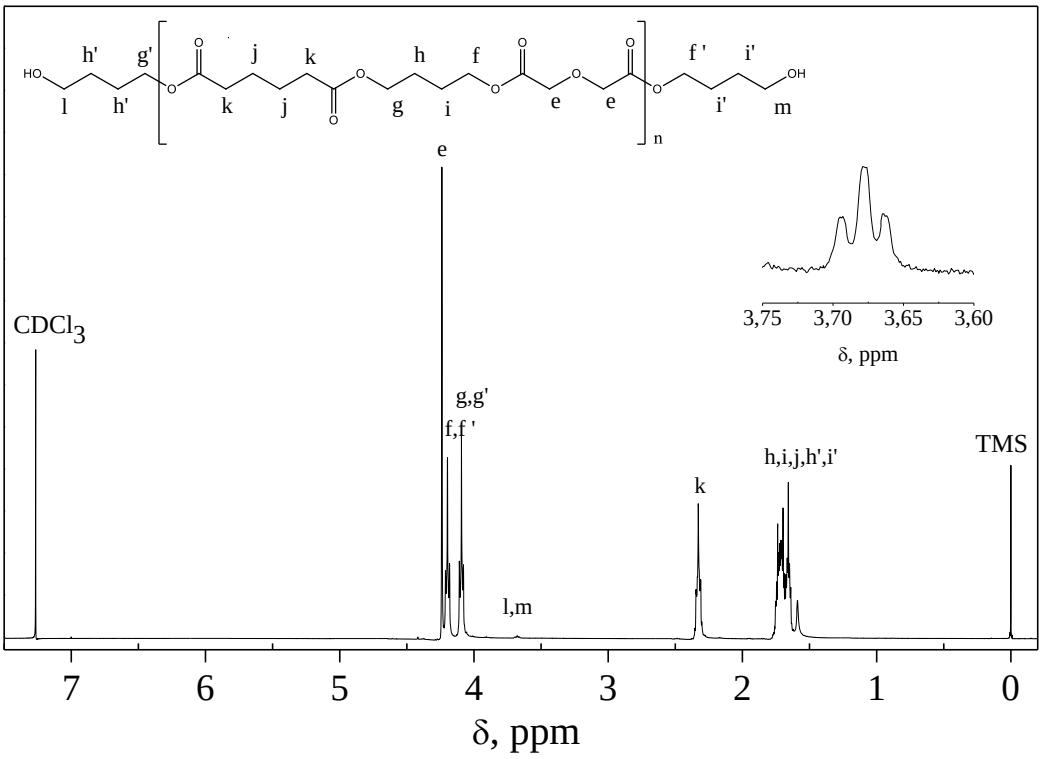

Figure S3 ^{1}H-NMR spectrum of P(BA50BDG50)-OH with resonance assignments and enlargement of the section presenting the terminal groups.

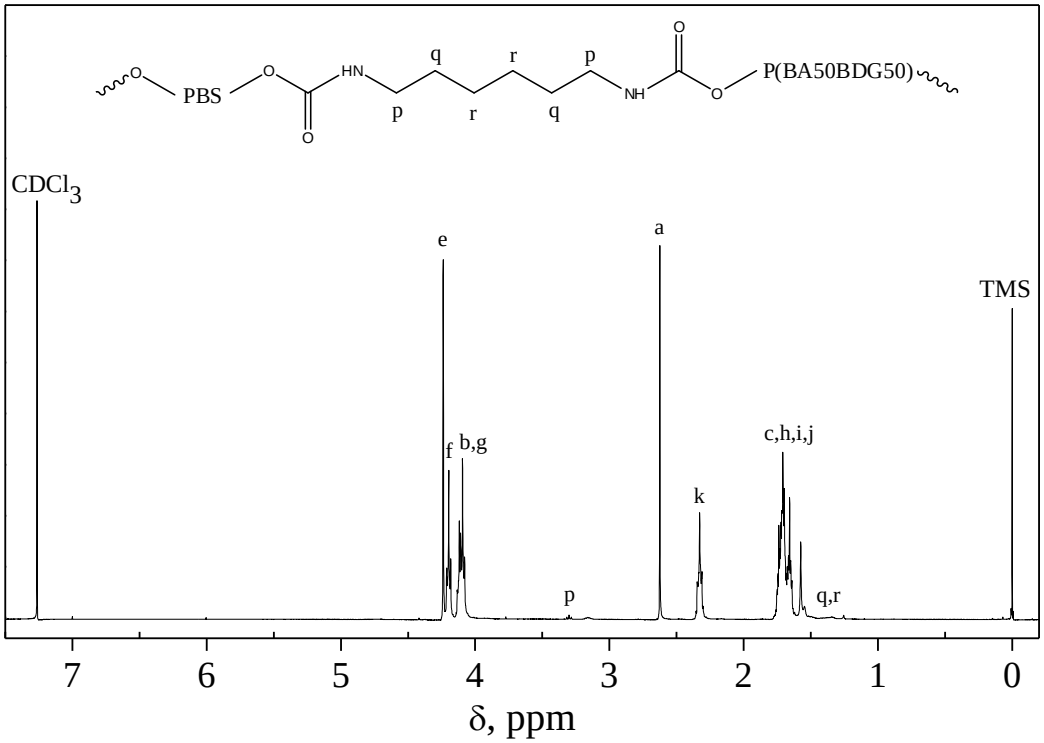

Figure S4 ^{1}H-NMR spectrum of $PBS_{30}P(BA50BDG50)_{70}$ multiblock copolymer with resonance assignments.

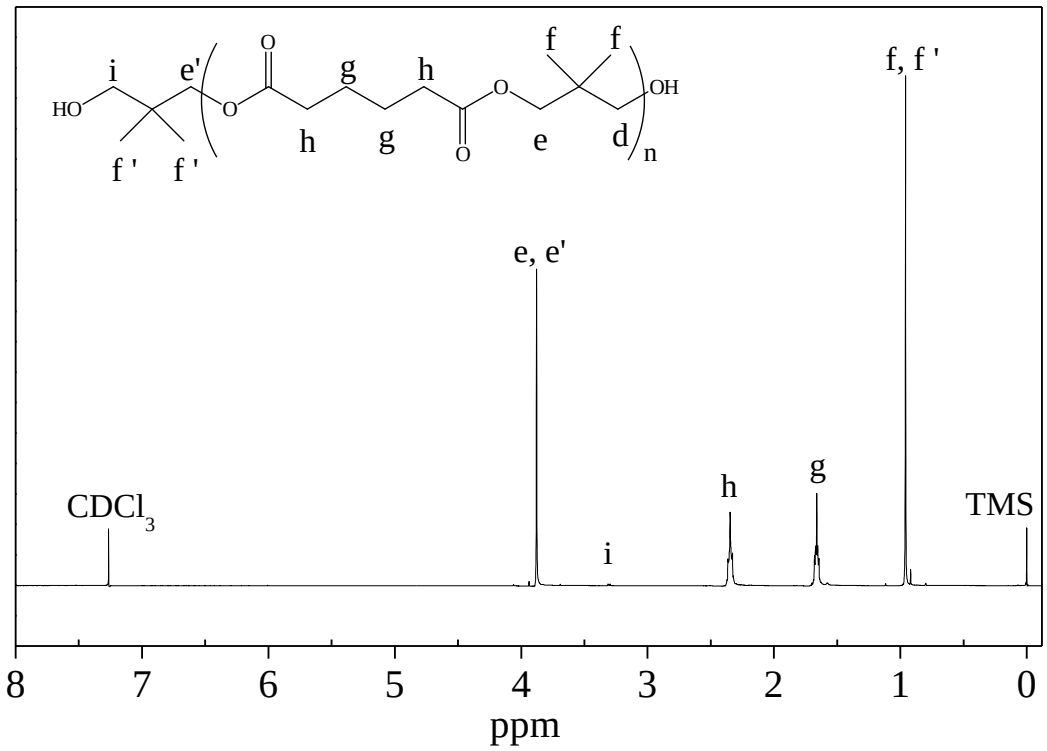

Figure S5 [1]H-NMR spectrum PNA-OH with resonance assignments.

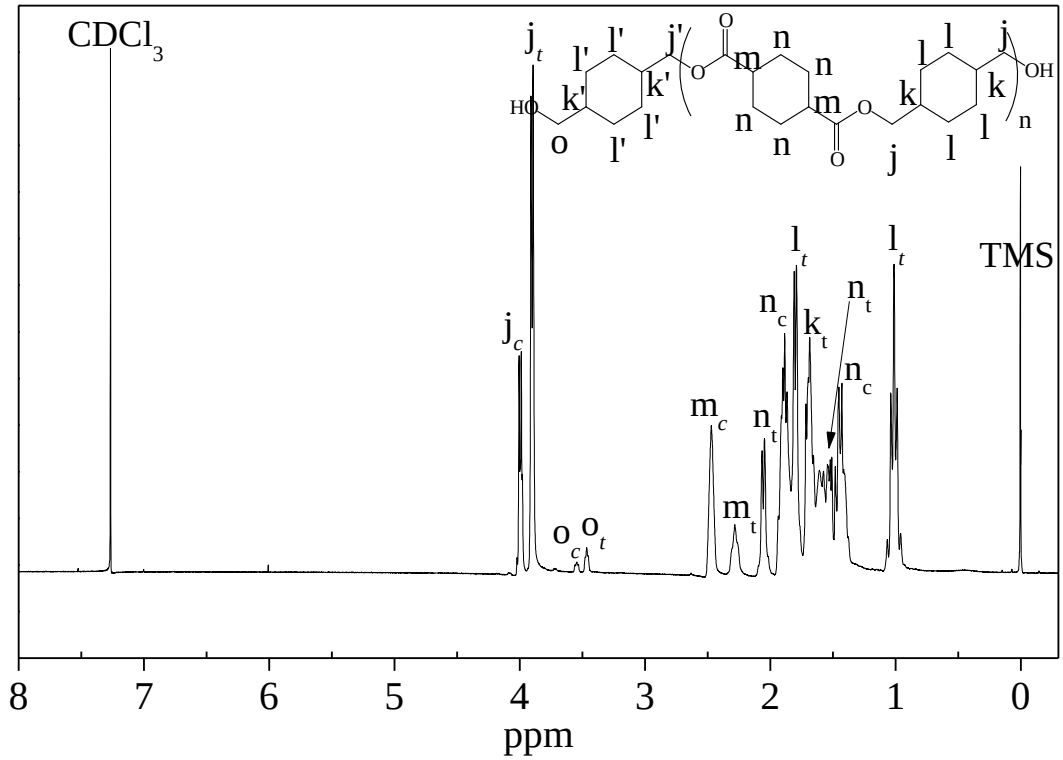

Figure S6 [1]H-NMR spectrum PCCE-OH with resonance assignments.

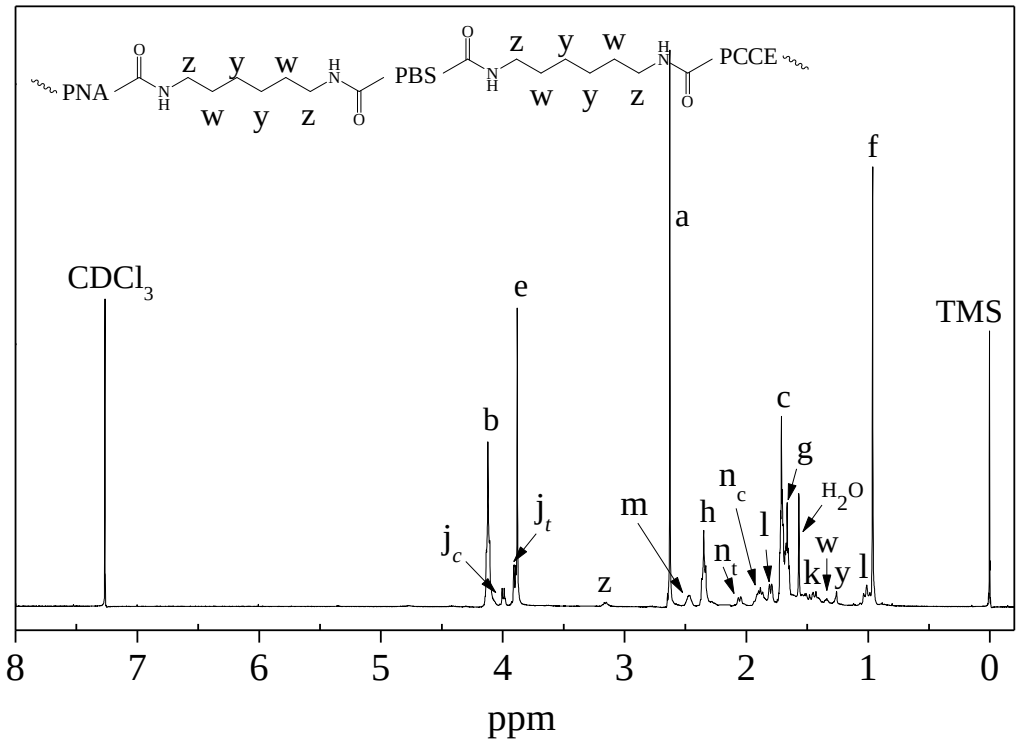

Figure S7 ^{1}H-NMR spectrum of PBS50PCCE10PNA40 multiblock copolymer with resonance assignments.

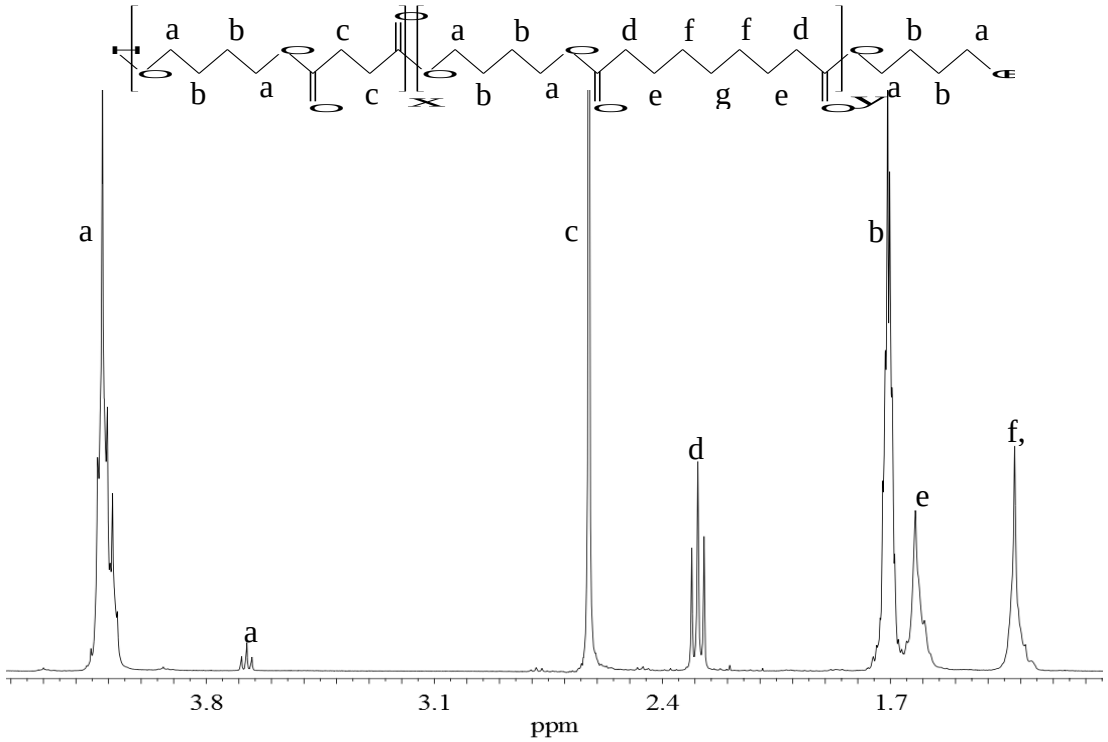

Figure S8 ^{1}H-NMR spectrum of the low molecular weight random copolymer P(BS80BAz20) with resonance assignments.

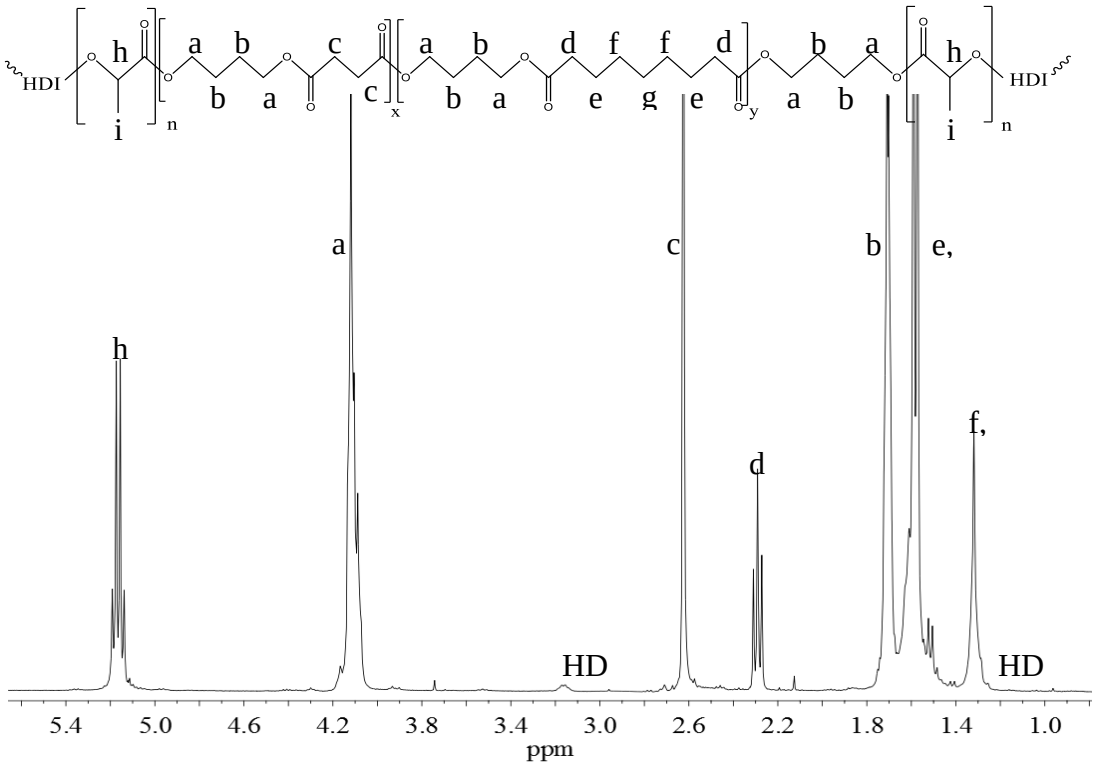

Figure S9 ^{1}H-NMR spectrum of $PLLA_{32}P(BS80BAz20)_{68}$ triblock copolymer with the corresponding resonance assignments.

Publications

The following list of publications collects all papers produced during the doctoral period, both those strictly relating to relevant topics to thesis work, and those referred to the further research projects which the candidate has participated during the doctoral program

1. M. Fabbri, M. Gigli, R. Gamberini, N. Lotti, M. Gazzano, B. Rimini, A. Munari. Hydrolysable PBS-based poly(ester urethane)s thermoplastic elastomers. *Polymer Degradation and Stability,* **2014**, 108:223.
2. M. Fabbri, M. Gigli, M. Costa, M. Govoni, P. Seri, N. Lotti, E. Giordano, A. Munari, R. Gamberini, B. Rimini, G. Neretti, A. Cristofolini, C. A. Borghi. The effect of plasma surface modification on the biodegradation rate and biocompatibility of a poly(butylene succinate)-based copolymer. *Polymer Degradation and Stability*, **2015**, 121:271.
3. M. Fabbri, M. Soccio, M. Gigli, G. Guidotti, R. Gamberini, M. Gazzano, V. Siracusa, B. Rimini, N. Lotti, A. Munari. Design of fully aliphatic multiblock poly(ester urethane)s displaying thermoplastic elastomeric properties. *Polymer*, **2016**, 83:154.
4. M. Gigli, M. Fabbri, N. Lotti, R. Gamberini, B. Rimini, A Munari. Poly(butylene succinate)-based polyesters for biomedical applications: a review. *European Polymer Journal*, **2016**, 75:431.
5. M. Fabbri, M. Soccio, M. Costa, N. Lotti, M. Gazzano, V. Siracusa, R. Gamberini, B. Rimini, A. Munari, L. García-Fernández, B. Vázquez-Lasa, J. San Román. New fully bio-based PLLA triblock copolymers as potential candidates for soft tissue engineering. Accepted in *Polymer Degradation and Stability*, **2016**.
6. M. Fabbri, L. García-Fernández, M. Soccio, N. Lotti, B. Vázquez-Lasa, J. San Román. Cell behavior on 3D electrospun nanofiber mats based on a new PLLA triblock copolymer. Pending to submission to *Biomaterials*.

7. M. Fabbri, S. Spinoso, A.M. Ferrari, P. Neri, R. Gamberini, N. Lotti, A. Munari, B. Rimini. Life cycle assessment of poly(butylene succinate) scaffold for biomedical applications. Pending to submission to *Industrial & Engineering Chemistry Research*.

Scientific contributions to national and international congresses

1. M. Fabbri, R. Gamberini, M. Gigli, N. Lotti, B. Rimini. Biodegradable PBS-based aliphatic polyesters for biomedical applications: a comparative analysis in a life cycle thinking perspective. In proceeding of XVIII Summer School "Francesco Turco" - A challenge for the future: the role of industrial engineering in a global sustainable economy, Senigallia (Italy), 11^{th}-13^{th} September 2013.
2. M. Fabbri, M. Gigli, R. Gamberini, N. Lotti, M. Gazzano, B. Rimini, A. Munari. Novel PBS-based fully aliphatic thermoplastic elastomers. In BIOPOL 2013 - 4^{th} International Conference on Biodegradable and Biobased Polymers, Rome (Italy), 1^{st}-3^{th} October 2013.
3. M. Fabbri, M. Gigli, M. Govoni, P. Seri, N. Lotti, E. Giordano, A. Munari, R. Gamberini, B. Rimini, G. Neretti, A. Cristofolini, C.A. Borghi. The effect of plasma surface modification on biodegradation rate and biocompatiblity of a poly/butylene succinate)-based copolymer. In POC 2014 - 15^{th} International Conference on Polymers and Organic Chemistry, Timisoara (Romania), 10^{th}-13^{th} June 2014.
4. N. Lotti, M. Fabbri, R. Gamberini, A. Monaco, L. Visai, M. Gazzano, B. Rimini, A. Munari. New biodegradable PBS-based copolyesters containing ionic groups as potential candidates for nanodrug delivery. In SIB 2014 - Congresso Società Italiana Biomateriali, Palermo (Italy), 2^{nd}-4^{th} July 2014.
5. M. Fabbri, N. Lotti, R. Gamberini, M. Vercellino, L. Visai, M. Gazzano, B. Rimini, A. Munari. New biodegradable PBS-based copolyesters as potential candidates for nanodrug delivery. In BiPoCo 2014 - 2^{nd} International Conference

on Bio-based Polymers and Composites, Visegrad (Ungary), 24th-28th August 2014.

6. N. Lotti, M. Fabbri, M. Gazzano, M. Govoni, E. Giordano, L. Finelli, R. Gamberini, B. Rimini, A. Munari. Novel biodegradable and biocompatible poly(butylene/triethylene succinate) random copolyesters with adjustable properties for tissue engineering. In AICIng 2014 - Congresso Associazione Italiana di Chimica per l'Ingegneria, Lecce (Italy), 14th-17th September 2014.
7. M. Fabbri, Application of Life Cycle Assessment metodology on poly(butylene succinate) synthesis. In 2nd Technical Seminary - Contribution of Department of Sciences and Methods for Engineering to the development of Life Cycle Assessment (LCA) for the management of environmental sustainability, Reggio Emilia (Italy), 18th February 2015.
8. M. Fabbri, B. Vázquez-Lasa, M. Soccio, N. Lotti, R. Gamberini, J. San Román, A. Munari, B. Rimini. Biodegradable PLLA-based copolyesters as potential candidates for antioxidants nanocarriers. In BIOPOL 2015 - 5th International Conference on Biodegradable and Biobased Polymer, San Sebastian-Donostia (Spain), 6th-9th October 2015.
9. M.Soccio, M.Fabbri, M.Costa, N.Lotti, M.Gazzano, V.Siracusa, R.Gamberini, B.Rimini, A.Munari. New PLA-based triblock coplymers as potential candidates for soft tissue engineering. In BIOPOL 2015 - 5th International Conference on Biobased and Biodegradable Polymers, San Sebastian-Donostia (Spain), 6th-9th October 2015.

Participation to Congresses

1. XVIII Summer School "Francesco Turco" - A challenge for the future: the role of industrial engineering in a global sustainable economy, Senigallia (Italy), 11th-13th September 2013.
2. BIOPOL 2013 - 4th International Conference on Biodegradable and Biobased Polymers, Rome (Italy), 1st-3th October 2013.

3. Polymers from renewable resources and biodegradable polymers, Bologna (Italy), 29th November 2013.
4. XXXV School "Mario Farina" – Characterization of Polymeric Materials, Gargnano (Italy), 18th-24th May 2014.
5. POC 2014 - 15th International Conference on Polymers and Organic Chemistry, Timisoara (Romania), 10th-13th June 2014.
6. BiPoCo 2014 - 2nd International Conference on Bio-based Polymers and Composites, Visegrad (Ungary), 24th-28th August 2014
7. BIOPOL 2015 - 5th International Conference on Biodegradable and Biobased Polymer, San Sebastian-Donostia (Spain), 6th-9th October 2015.

Experiences abroad

Institute of Polymer Science and Technology, Spanish National Research Council (CSIC), Madrid (Spain), April 2015 – October 2015.

Acknowledgments

Sono passati poco più di otto anni da quando ho mosso il primo passo all'interno del mondo universitario, in una tiepida e soleggiata giornata autunnale. Ed oggi, il primo giorno di primavera, compirò l'ultimo passo di questa lunga camminata, quello che mi porterà alla conclusione del percorso. E ad un nuovo inizio, ancora inaspettato.
Questi ultimi tre anni, che a volte mi sono parsi tanti (troppi!) ed altre volte una piccola manciata, hanno visto il susseguirsi di molti cambiamenti, più o meno importanti, ognuno dei quali ha contribuito a formarmi e permesso di affermarmi per quella che sono, nel bene e nel male. E se sono riuscita ad arrivare fino qui, fino all'ultima pagina della tesi di dottorato, un grande merito va a tutte le persone che mi sono state accanto durante il percorso, che esso fosse o meno tortuoso.
La mia gratitudine è tutta, infinitamente, per voi.

Il ringraziamento più grande va una volta ancora al mio papà, che tenacemente mi ha supportata e sopportata, rivelandosi come sempre il pilastro portante della mia vita. Ed alla mia sorellina Elena: solo lei sa riempire di spensieratezza anche le notti più buie.
Un grazie immenso, poi, alle mie zie Fabrizia e Luisa, che seguono appassionate le mie peripezie in ogni parte del globo, ed a Sofia che, idealista, "minaccia" di seguire le mie orme nel mondo della chimica a passi di danza.

E' doveroso ringraziare le Professoresse Bianca Rimini e Rita Gamberini per avermi dato l'opportunità di continuare la mia formazione con il dottorato, il Professor Andrea Munari e la Professoressa Nadia Lotti per avermi accolta nel loro gruppo di ricerca, nonché la Professoressa Anna Maria Ferrari e l'Ingegner Paolo Neri per il supporto preziosissimo negli studi LCA.
Matteo, per gli insegnamenti iniziali. Laura per averli divisi con me e per il suo saper sempre portare la serenità. Michelina, per l'aiuto dell'ultimo anno e le conversazioni in spagnolo origliate. Giulia, per l'eterna allegria.
Michela, per essere stata prima amica e poi collega. Senza di lei in questi tre anni sarebbero mancate la maggior parte delle gioie.
Lucia e Grazia, per i caffè nelle mattine di inverno e le chiacchiere a tutte le ore. Micaela, per i viaggi temerari. Claudio, per il disordine, e Maria Barbara, per l'ordine. Stefano, tutti i

ragazzi del gruppo Fava e gli “infiltrati” Matteo e Daniele, per gli aperitivi e i sorrisi. Vilma, perché senza di lei sarei stata perduta.
Luca, Francesco ed Elisa, per la leggerezza delle giornate a Reggio Emilia, le montagne di caffè, e il GiustoSpirito.
Tutti gli studenti che ho avuto l’onore di seguire, perché nonostante i grattacapi sono stati la soddisfazione più grande.

Un ringraziamento particolare va a Blanca Vazquez e Julio San Roman, per avermi accolta per sette mesi nel loro gruppo, permettendomi di vivere un’esperienza di formazione professionale e personale meravigliosa.
E per avermi permesso di tornare arricchita da amicizie nuove. Alvaro, con i suoi brontolii e la passione per la montagna. Sergio, fonte di ogni presa in giro e “docente” di parolacce. Raquel, dall’infinita dolcezza.
Angela, l’amica che spero di conservare per sempre. Anna, e le chiacchiere sedute sul pavimento.

Non posso non ringraziare anche gli amici di sempre, quelli vicini e quelli partiti per andare lontano, perché senza di loro sarebbero mancate molte sfumature al verde della vita.
Alice, Simone, Maria Chiara, Dino, Chiara, Ansa, Lucio, Valerio, Martina, Gabri, Roma, Guglielmo, Carbo, Ballero, Kiri, Francesca, Marzio, Agnese, Alice, Davide: grazie.
Andrea, che ha portato una tremola luce nel buio più cupo.
Gli Irriducibili, perché anche se stiamo diventando grandi e le nostre strade sono costrette ad allontanarsi, quando siamo assieme è sempre come essere tra i corridoi del Fantini.
Valentina, che è sempre rimasta la mia metà, e mi ha insegnato con pazienza a puntare al bello del mondo.

Giulio, grazie per avermi mostrato la Strada, tenendomi per mano.